Techno-economic Feasibility of a Solar Assisted Coal Power Plant

Prepared by:

Anthony Govender

GVNANT002

Department of Mechanical Engineering

University of Cape Town

Supervisor:

Professor Kevin Bennett

Co-supervisor:

Dr Wim Fuls

September 2014

Submitted to the Department of Mechanical Engineering at the University of Cape Town in partial fulfilment of the academic requirements for a Master of Science degree in Mechanical Engineering

Key Words: Eskom, Power Station, Parabolic Trough Collector, Linear Fresnel Reflector, Central Receiver, Solar augmentation

Abstract

The use of solar heat in conventional coal-fired power plants has been demonstrated to reduce the coal consumption of the plant. A reduction in the amount of coal that is burnt by the power plant, means that less greenhouse gases are emitted by the power plant. Hence, the plant has a smaller impact on global warming. Countries such as Australia and the USA have implemented this concept of adding solar heat to a coal-fired power plant.

This study investigates if solar heat addition to the power station in Mpumalanga, South Africa, is technically and economically feasible. The power station is one of the largest coal-fired power stations in Eskom. Two solar heat integration options were examined in this study i.e. the use of solar heat to heat feedwater or to produce superheated steam. A market assessment of concentrated solar power (CSP) technologies was performed to establish the maximum water/steam conditions (temperature and pressure) that can be produced by each CSP technology. The CSP technologies assessed were the parabolic trough collector (PTC), the linear Fresnel reflector (LFR) and the central receiver (CR). By using the results of the market assessment, a suitable CSP technology was selected for each integration option. The technical capabilities of each plant area of the power station, such as the boiler, turbines, feedwater pump etc., was also assessed by reviewing original equipment manufacturer (OEM) data sheets.

The solar field size of each integration option was determined through an iterative method, such that none of the technical capabilities of the power station were exceeded once solar heat was added. The annual hourly heat output of each solar field was thereafter predicted by using the System Advisor Model (SAM). The annual hourly heat output of each solar field was then used with a thermodynamic model of the power station (referred to as the VirtualPlant^{TM} model), to calculate the hourly project benefits. The hourly benefits are coal savings, greenhouse gas emission reduction, solar electricity etc. The capital expenditure (CAPEX) and operating expenditure (OPEX) of each integration option was calculated by using cost models provided in SAM. The benefits and costs of each integration option were used in an economic life-cycle assessment (LCA) model, to determine the most economically feasible integration option.

It was found that the integration options that produced high-temperature steam have the highest integration effectiveness, such as the steam supply to the high-pressure turbine etc. The LCA revealed that the supply of steam, by using the LFR, to the highest pressure feedwater heater (HPH6), is the most economical option. This is because the LFR technology has the lowest CAPEX and fixed OPEX cost amongst the 3 CSP technologies. This integration option has a discounted payback period of 14,6 years and a real Levelised cost of electricity (LCOE) of R1.64/kWh$_e$.

Declaration

I, Anthony Govender, hereby declare the work contained in this dissertation to be my own. All information which has been gained from various journal articles, text books or other sources has been referenced accordingly. I have not allowed, and will not allow, anyone to copy my work with the intention of passing it off as their own work or part thereof.

Signed by candidate

_____

Anthony Govender

September 2014

To my brothers, Jude and Mark . . .

Acknowledgements

- To Him, for giving me the ability to persevere and to do this research.
- To my parents and my two brothers. Thank you for always supporting and encouraging me.
- To Mr Nielen Toerien, Engineering Manager at Eskom, for providing me with the opportunity, time and resources to undertake this project.
- To Professor Kevin Bennett and Dr Wim Fuls, my supervisors at the University of Cape Town, for their guidance and support in this project.
- To Mr Gary De Klerk, Chief Engineer at Eskom Group Technology, for providing the research topic and valuable technical advice in this project.

Table of Contents

List of Figures

List of Tables

List of Nomenclature

General symbols

Symbol	Description	Unit
D	Annual depreciation allowance	ZAR
d	Annual discount rate	%
G	Annual Greenhouse Gas emissions	tCO_{2eq}/year
T	Annual income tax	ZAR
L	Annual loan repayment	ZAR
R	Annual revenue	ZAR
h	Enthalpy	kJ/kg
$\dot{E}$	Hourly electricity power output	MW_e
E	Hourly electricity production	MWh_e
m	Mass flow rate	Kg/s
Q	Solar heat	MW_t

Greek symbols

η	Efficiency	%
ε	Emission factor	Kg/GJ

Acronyms and Abbreviations

ASME	American Society of Mechanical Engineers
CT	Annual Carbon Tax
BFP	Boiler Feedwater Pump
CAPEX	Capital Expenditure
CCS	Carbon Capture and Storage
CLFR	Compact Linear Fresnel Reflector
CSP	Concentrated Solar Power
CEP	Condensate Extraction Pump
DA	Deaerator
DoE	Department of Energy of South Africa
DC	Direct Cost
DNI	Direct Normal Irradiation
DSG	Direct Steam Generation
DPB	Discounted Payback Period
LCA	Economic Life-Cycle Assessment
EPC	Engineer-Procure-Construct
GSC	Gland Steam Condenser
GWP	Global Warming Potential
GHG	Greenhouse Gas
HR	Heat rate
HTF	Heat Transfer Fluid

HPH	High-Pressure Feedwater Heater
HPT	High-Pressure Turbine
CS	Hourly Coal Savings
ER	Hourly Green House Gas Emission Reduction
ISCC	Integrated Solar Combined Cycle
IPT	Intermediate-Pressure Turbine
LCOE	Levelised Cost of Electricity
LFR	Linear Fresnel Reflector
LPH	Low-Pressure Feedwater Heater
LPT	Low-Pressure Turbine
NERSA	National Energy Regulator of South Africa
NREL	National Renewable Energy Laboratory of the United States Department of Energy
NCV	Net Calorific Value
NPV	Net Present Value
OPEX	Operating Expenditure
OEM	Original Equipment Manufacturer
PTC	Parabolic Trough Collector
AI	Power plant Actual Carbon Intensity
BI	Power plant Benchmark Carbon Intensity
REFIT	Renewable Energy Feed-In-Tariff
SPB	Simple Payback Period
SCA	Solar Collector Assembly
SEGS	Solar Energy Generating Systems
ST	Solar Tower
ZAR	South African Rand
SARS	South African Revenue Service
TES	Thermal Energy Storage
TLCC	Total Life Cycle Cost
TMY	Typical Meteorological Year
USD	United States Dollar

1. Introduction

Climate change is driven by the emissions of greenhouse gases (GHG) into the atmosphere [1].The major GHG is carbon dioxide, as carbon dioxide is identified as the single most anthropogenic (caused by human activity) GHG in the atmosphere [2]. Carbon dioxide is produced by the combustion of fossil fuels, such as coal, natural gas etc. [3].

The GHG emissions from fossil fuelled power plants can be mitigated by applying zero- or low carbon emitting technologies, such as carbon capture and storage (CCS) systems and /or renewable energy technologies [4].However, the retrofitting of CCS to coal-fired power plant units has a major drawback, as CCS can reduce unit efficiency by up to 7 to 12 percentage points [5, 6]. A loss in unit efficiency will result in a reduced unit power output [6].

In South Africa (SA), the electricity generation sector produces approximately 40 % of the GHGs emitted in SA, making it the single largest emitter of GHGs in SA [7]. The electricity utility of SA, Eskom, generates 96 % of the country's electricity requirements [8].Most of Eskom's electricity, 92.8 %, is produced from its coal-fired power stations [9]. Thus, from a country perspective, focus should be drawn towards reducing the GHG emissions of Eskom's coal-fired power stations i.e. by reducing Eskom's coal usage.

The Government of SA has realised the need to diversify its electricity mix and has planned, through the Integrated Resource Plan for Electricity, that 52.4 % of the installed electricity capacity by 2030 is from energy sources other than coal [10]. This plan will assist in mitigating climate change. The Eskom renewable energy projects such as the 100 MW_e Sere wind farm and the 100 MW_e Upington CSP power plants are part of this plan [11].

In line with global practices to reduce GHG production and taking into consideration that solar radiation levels in SA are amongst the highest in the world [12], it was decided to evaluate the possibility of augmenting solar heat to an existing Eskom coal-fired power station, to offset coal usage. Thus, this study investigates the technical and economic feasibility of augmenting solar heat to the power station, a coal-fired power station in Mpumalanga, South Africa.

1.1 The problem statement

The research hypothesis: "The addition of solar heat to the power station, is an economically and technically feasible solution to the mitigation of GHG emissions"

Hence, the purpose of this study is to investigate if the addition of solar-derived heat to the power station, a coal-fired power plant, is both technically and economically viable.

1.2 The importance and benefits of this study

The addition (augmentation) of solar heat to a coal-fired power plant for electricity production has the following primary and secondary benefits.

1.2.1 Primary benefits

a) The addition of solar heat to the existing coal-fired power plant will offset coal consumption, and consequently reduce the annual GHG production of the coal-fired power plant. The carbon intensity of electricity production[1] from the existing coal-fired power plant will thus be reduced.

b) A reduction in the carbon tax payable by the coal-fired power plant to government will occur, as a result of a lower carbon intensity of electricity production.

c) The electricity capacity of the coal-fired power plant can be increased, through the addition of solar heat to the power plant [13] . This benefit will provide support to the electricity grid of South Africa during power shortages.

1.2.2 Secondary benefits

a) The augmentation of a renewable energy source such as solar energy to a coal-fired power plant is potentially a cost effective solution to increase the electricity production from renewable technologies in Eskom, as compared to constructing stand-alone concentrated solar power (CSP) plants.

b) The existing infrastructure of a coal-fired power station is utilized, thus creating cost-reduction opportunities for electricity generation from solar heat i.e. the power block, the steam condenser, the main steam piping, the grid connections and the balance of plant [14].

[1] Carbon intensity of the coal-fired power plant is the amount of GHGs produced per a unit of electricity generated.

1.3 Objectives of this study

To investigate as to whether the concept of augmenting solar heat to the power station is both technically and economically feasible, the research questions listed below arose. Answering these research questions are the objectives of this study.

1.3.1 Research questions

a) What are the possible options to integrate solar heat into the regenerative Rankine power cycle of the power station?

b) Which CSP technology(s) are applicable to the possible solar heat integration options?

c) What are the technical capabilities of the infrastructure of the power station?

d) What are the economic benefits and expenses associated with solar heat addition to the power station?

e) Are these economic benefits sufficient to recover the associated expenses over the life time of the project?

1.3.2 Research outline

To answer the above listed research questions, the following steps were undertaken:

a) A site assessment of the power station for available land and annual solar resource.

b) A review of the methods that are used to integrate solar heat into the regenerative Rankine power cycle.

c) An assessment of the CSP technologies on the market and their maximum producible water/steam conditions (temperature and pressure).

d) The selection of applicable CSP technology (s) for each solar heat integration option.

e) A review of original equipment manufacturer (OEM) data to establish the technical capabilities of the power station.

f) The determination of the maximum solar field size of each integration option by using a Power plant model of the power station together with the technical capabilities of the power station i.e. this step forms the technical feasibility assessment of each integration option.

g) Prediction of the heat rate reduction[2] of the power station, which is produced by each solar heat integration option, by using the Power plant model of the power station.

h) By using the heat rate reduction produced by each integration option, the annual coal savings, solar electricity production etc. were calculated for each solar heat integration option.

i) An economic life-cycle assessment of each solar heat integration option.

1.4 The coal-fired power station

Figure 1: The power station [15]

1.4.1 Plant description

The power station, shown in Figure 1, is a base-load coal-fired power plant located in Witbank, Mpumalanga. The power station consists of 6 units; each rated at 600 MW_e (gross), with an overall net station capacity of 3450 MW_e. The power station operates on a sub-critical regenerative Rankine power cycle, which consists of a steam boiler, a turbine and generator set, a steam condenser and a feedwater heating plant. A process flow diagram of a single unit of the power station is illustrated in Figure 2.

[2] Heat rate is the amount of energy required from coal to produce a single unit of electricity [20].

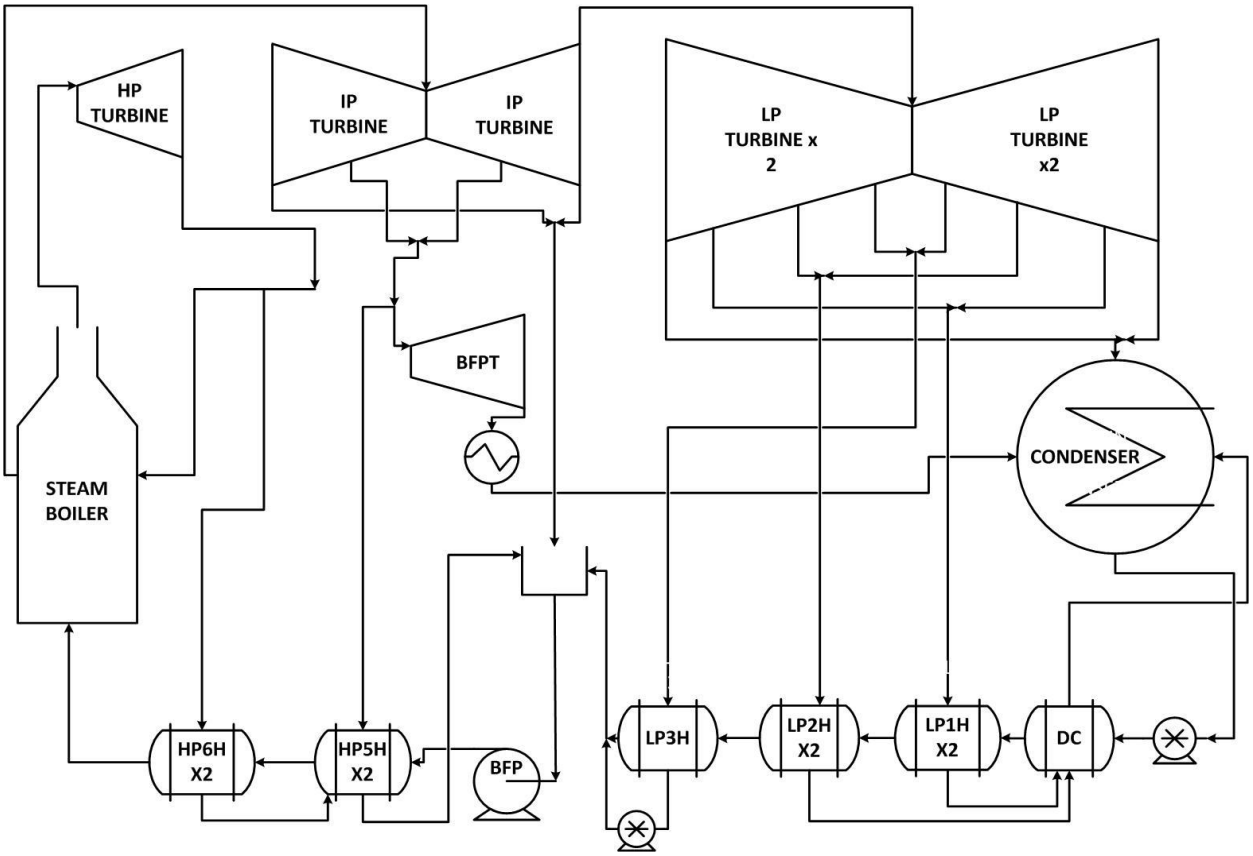

Figure 2: A process flow diagram of a single unit of the power station.

The turbine plant consists of a single-flow high-pressure turbine (HPT), a reheat double-flow intermediate-pressure turbine (IPT) and two double-flow low-pressure turbines (LPT). The turbine plant is manufactured by GEC Turbine – Generators Ltd. The steam to the turbine plant is provided by the once-through single-reheat Benson boiler. The boiler plant is manufactured by STEINMÜLLER.

The main steam condenser is of a double vacuum wet-cooled design, with a natural-draft cooling tower. The main steam condenser is manufactured by Hamon Sobelco. The feedwater heating plant has a high-pressure section and a low-pressure section. The high-pressure feedwater heating section consists of two parallel trains of high-pressure feedwater heaters (HPH), with two heaters per a train. The low-pressure feedwater heating section consists of a deaerator (DA), a single low-pressure heater (LPH) and two parallel trains of low-pressure feedwater heaters, with two heaters per a train. The feedwater heating plant is manufactured by James Brown, Hammer Ltd and Hamon Sobelco. The boiler feedwater pump (BFP) which is driven by the boiler feed pump steam turbine (BFPT), pressurizes the flow of feedwater to the inlet of the steam boiler. The BFP is manufactured by SULZER.

1.4.2 Report layout

A review of literature related to solar aided power generation is presented in chapter two, which also lists the possible solar heat integration options and available CSP technologies. The research methodology is explained in further detail in chapter three. The validation of the thermodynamic model of the power station and the validation of the economic life-cycle assessment model are both presented in chapter four. The results from both the thermodynamic model and the economic model are presented in chapter 5 and are discussed in chapter 6. The conclusions of this research work and recommendations for future work, forms the final chapter of this report.

2. Literature Review

The following chapter begins by discussing the efficiency benefit of a solar-fossil plant versus a stand-alone CSP plant and the various possible solar heat integration options at a conceptual level. This is followed by the three applicable CSP technologies to solar augmentation and their technical capabilities. The chapter closes with operational practices of a solar-coal plant, a brief overview of the solar resource in SA, and the cost of power generation in SA.

2.1 The solar-fossil power plant

A fossil-power plant which is augmented with solar heat, is referred to in this study, as a solar-fossil power plant. The solar-fossil power plant converts solar energy[3] to electricity more efficiently, via a conventional regenerative Rankine power cycle, than the stand-alone solar power plant [16].

A second great advantage of the solar-fossil power plant is that it utilizes the existing plant infrastructure such as the turbine-generator, the main steam condenser, the water/steam piping etc. of the fossil-power plant. This creates cost reduction opportunities for electricity generation from solar heat. [16]

An early example of the solar-fossil plant concept are some of the Solar Energy Generating System (SEGS) power plants, which use natural gas as a supplementary heat source [17].The more recent application of this concept is the integration of solar heat into the combined cycle power plant (ISCC). E.g. The Martin Next Generation plant in Florida (the largest ISCC plant in operation, 75 MW_e) uses the Parabolic Trough Collector (PTC) technology to supply steam to the heat recovery steam generator of a gas turbine [18].

An example of a coal-fired power plant which has solar heat addition, would be Liddell Power Station (rated at 2000 MW_e) in New South Wales. Liddell Power Station is the world's first solar-coal fired power station. Liddell Power Station uses 9 MW_t of solar steam, which is generated by the AREVA Compact Linear Fresnel Reflector (CLFR) technology, to replace the bled steam to the feedwater heaters. [19]

[3] The solar energy referred to is of low to medium temperature. Higher solar energy temperatures produce higher thermal efficiencies in stand-alone solar power plants. [16]

2.1.1 The solar-fossil plant versus the stand-alone solar plant

It was mentioned in section 2.1 that the use of solar heat in a conventional fossil-power plant, has an associated efficiency benefit. This efficiency benefit will be illustrated by the results of a study conducted by Hu et al. [16]. The study compared the benefit of augmenting solar heat to a subcritical and supercritical power plant, against the benefit of using solar heat in a stand-alone solar plant.

Solar heat at three different temperatures, 90 ^{o}C, 215 ^{o}C and 260 ^{o}C, were used in each of the three power plants. The results of the study are presented in Figure 3. The results show that the 'solar heat to power efficiency'[4] in the subcritical and supercritical power plants is much greater than the 'solar heat to power efficiency' in the stand-alone solar power plant.

This is because the maximum operating temperature of the subcritical and supercritical power cycles, are greater than the temperature of the solar heat source. Hence, the subcritical and supercritical power plants have a greater thermal efficiency than the stand-alone solar plant, and can thus convert solar heat to electricity more efficiently. It was also noted that the higher solar heat source temperatures produced a greater 'solar heat to power efficiency'. [16]

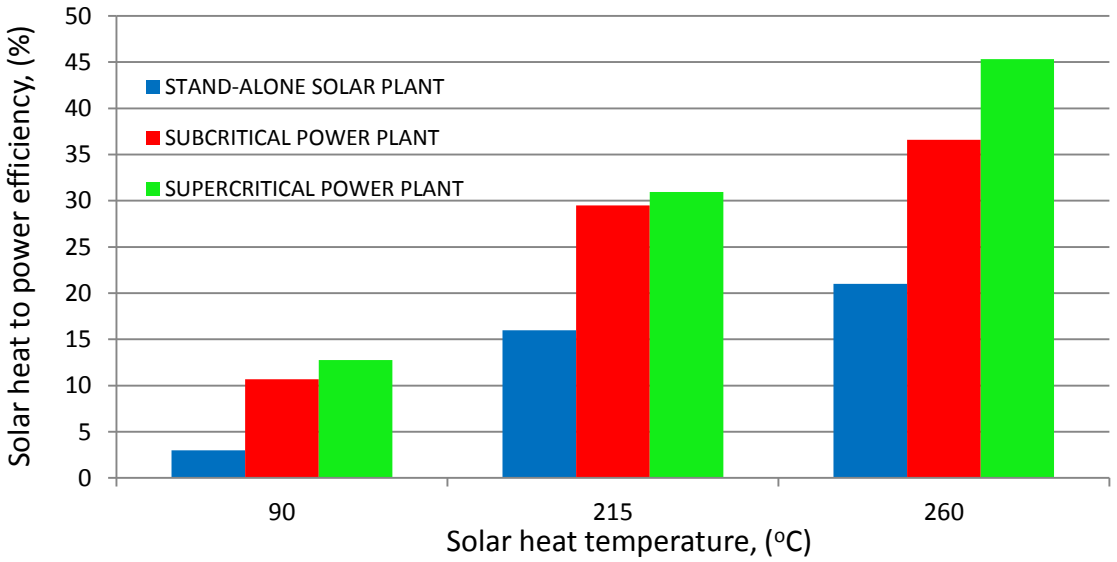

Figure 3: Comparison of the solar heat to power efficiency in different power cycles. [16]

[4] The 'solar heat to power efficiency' is = (increased power output) / (solar heat input + change in boiler reheating load). [16]

2.1.2 The operating modes of the solar-fossil plant

The solar heat addition to the fossil-power plant can either be used to operate the plant at rated capacity and hence save fuel, this is called the “Fuel-saving mode”, or the solar heat can be used to operate the plant at above rated capacity, this is called the “Power-boosting mode” [13] . The two operating modes of a solar-fossil plant are illustrated in Figure 4.

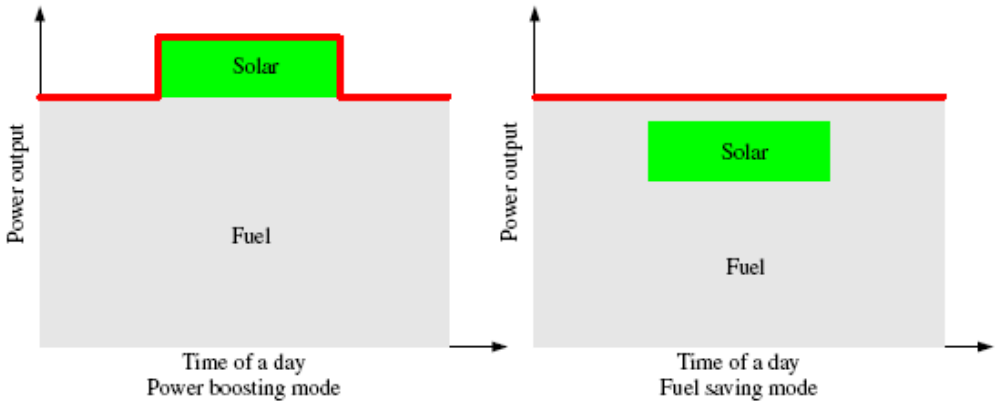

Figure 4: The operation modes of a solar-fossil power plant [13]

During both the Fuel-saving and the Power-boosting plant operation modes, the amount of heat required from coal per a MW_e output is reduced, because of the solar heat addition to the fossil-power plant. A reduction in the coal consumption of the fossil-power plant effectively reduces the heat rate of the fossil-power plant. Heat rate is a performance measure of the fossil-power plant. The heat rate of the fossil-power plant is defined as the amount of energy (from coal) that is required to produce a single kilowatt hour of electricity [20]. Heat rate has the units of kJ/kWh_e.

If the amount of solar energy that is augmented to the fossil-power plant is also included in the determination of heat rate, the overall heat rate would remain essentially unchanged. In this case the definition of heat rate is the ratio of total energy input (coal + solar) to the electrical energy output.

For the purposes of this study, the original definition as is defined for pure fossil plants is used. The solar energy is therefore omitted from the determination of the fossil-power plant heat rate, as solar energy is a “free” heat source. This allows the heat rate reduction of the fossil-power plant (due to coal savings) to be calculated.

2.2 The Rankine power cycle

The Rankine cycle is essentially composed of a boiler, a turbine, a condenser and a pump, as illustrated in Figure 5. There are four processes which occur in the ideal Rankine cycle (refer to Figure 5) i.e. [21]:

Point 5-1: Isentropic compression of water by the pump.

Point 1-3: Heating of water in the boiler (to produce steam) at constant pressure.

Point 3-4: Isentropic expansion of steam in the turbine.

Point 4-5: Heat rejection in the condenser at constant pressure.

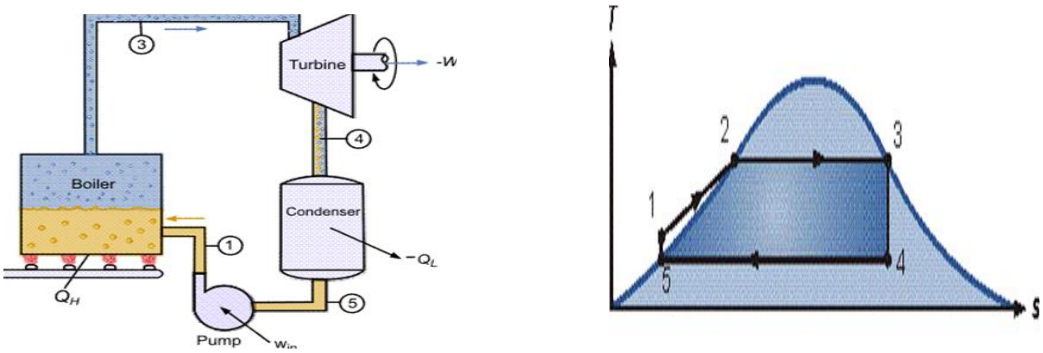

Figure 5: The Rankine cycle (left), and the T-s diagram of the ideal Rankine cycle. [22]

There are ways to increase the performance of the Rankine cycle, such as, by raising the inlet steam temperature to the turbine. The inlet steam temperature to the High-P turbine is increased by superheating the steam to the High-P turbine, and the inlet steam temperature to the Low-P turbine is increased by reheating the exhaust steam from the High-P turbine. The process of superheating and reheating the inlet steam to the turbines is illustrated in Figure 6. [21]

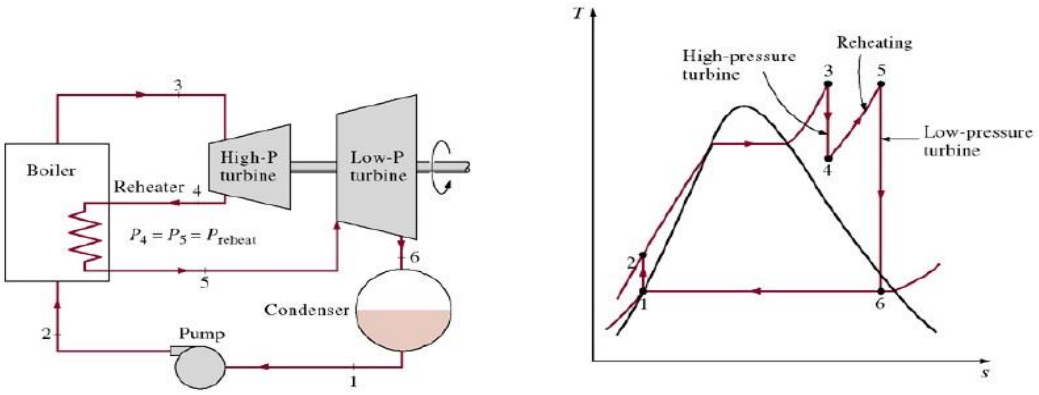

Figure 6: The ideal reheat Rankine cycle (left), and the T-s diagram of the ideal Rankine cycle. [21]

2.3 Solar heat integration methods

There are various methods of integrating solar heat into the regenerative Rankine power cycle. The choice of a particular solar heat integration method depends on, the technical ease of integration into the regenerative Rankine power cycle and the associated cost.

A comprehensive study conducted by R.J. Zoschak and S.F. Wu, on the use of solar heat in a fossil-power plant, suggested the following solar heat integration options [23] :

1) Feedwater heating.
2) Production of saturated and superheated steam.
3) Reheating of steam.
4) Preheating of inlet combustion air to boiler.

2.3.1 Feedwater heating

The boiler feedwater is normally heated in a feedwater heater by bled steam extracted from the turbines. One way to introduce the solar heat is to bypass some of the feedwater to a solar heater. This process is illustrated in Figure 7.

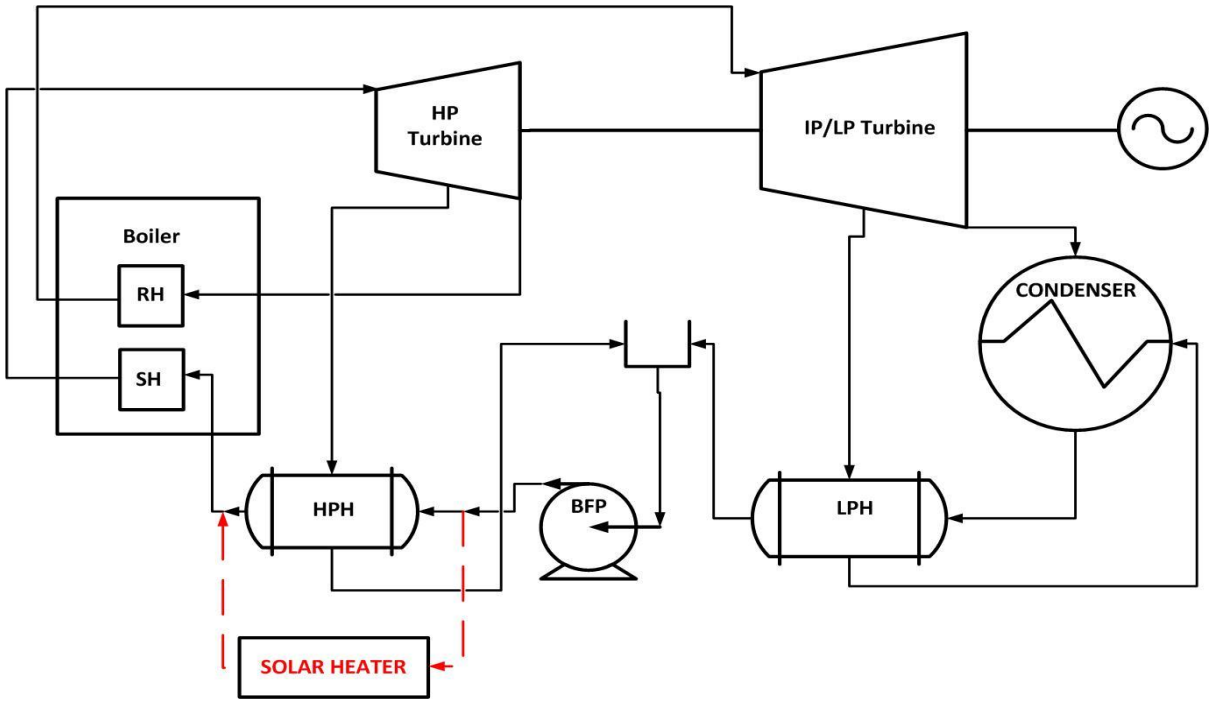

Figure 7: The bypassing of a high-pressure feedwater heater (HPH) to the solar heater: (LPH) low-pressure feedwater heater, (RH) boiler reheater, (SH) boiler superheater. Adapted from [23].

The consumption of bled steam, for feedwater heating, is thus reduced. The saved bled steam expands through the turbine, producing additional turbine power. The maximum additional turbine power that can be produced, during the Power-boosting mode, is dependent on the reserve power capacity of the turbine. During the Fuel-saving mode, the turbine power remains constant and the total boiler steam flow is reduced.

The bypassed feedwater may be heated indirectly in an oil/water heat exchanger which receives hot thermal oil from the solar field, or the bypassed feedwater may be heated directly by flowing through the solar field [24]. The indirect method of heating is preferred for the bypassing of the high-pressure feedwater heaters, as the high-pressure feedwater flow may create leaks if diverted to the solar field [24]. In addition, the installation of high-pressure pipework to and from the solar field would create a very costly project.

An alternative method of feedwater heating is accomplished by, completely or partially replacing the bled steam flow to the feedwater heater, with steam that is produced by the solar plant [19].This 2nd method of feedwater heating will also be investigated in this study.

Feedwater heating using solar heat has been implemented at the Unit 2 of the coal-fired Cameo Power Station (rated at 49 MW_e net[5]) in the USA, which uses PTC technology to generate a 4 MW_t solar heat source [25] .The solar heat addition to Unit 2 of Cameo Power Station, saves 0.39 kg/s of bled steam which produces 0.3 MW_e of additional generator power, and effectively reduces the heat rate of the plant by 195 kJ/kWh_e (1.33 %) [25].

A study conducted on a subcritical power station found that the use of solar heat to bypass a high-pressure feedwater heater results in a greater benefit, when compared to using the same solar heat to bypass a low-pressure feedwater heater [26]. An important point to note is that the HPH bled steam temperature is greater than the LPH bled steam temperature. A concluding remark of the study is “This is due to the higher temperature that corresponds to the higher quality of energy (exergy)” [26].

[5] Net power generation is the gross power from the generator terminals less the plant auxiliary power consumption i.e. power required for the boiler feedwater pump, boiler air fans etc.

2.3.2 Production of saturated and superheated steam

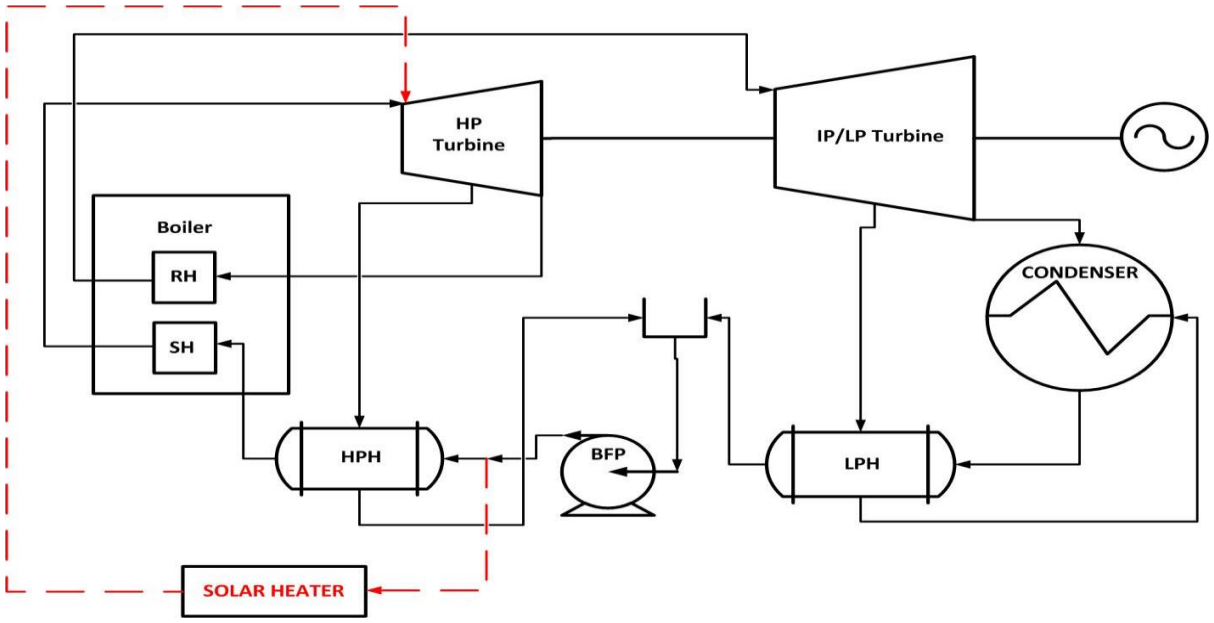

Figure 8: Superheated steam supply from the solar steam generator to the HP turbine inlet. Adapted from [23].

This solar heat integration option produces saturated or superheated steam, with the use of a solar steam generator. The solar steam generator heats high-pressure feedwater flow, which is bypassed from the discharge of the boiler feedwater pump, to saturated or superheated steam conditions. This is illustrated in Figure 8.

The pressure of the generated steam is controlled by a pressure regulating valve, to the required pressure set point. The steam generated by the solar steam generator can be supplied to the turbine plant areas such as the HP turbine, the IP/LP turbine, the boiler feed-pump turbine etc. The temperature, pressure and the flow rate of the steam supplied to these plant areas must be within the technical capabilities set by the respective Original Equipment Manufacturer (OEM). This particular solar heat integration option, illustrated in Figure 8, partially bypasses the feedwater flow of the high-pressure feedwater heaters (hence saving bled steam), and also, partially bypasses the flow of the SH section of the fossil-boiler (resulting in a direct reduction in coal consumption).

The coal-fired Kogan Creek Power Station (rated at 750 MW_e) in Australia, uses the AREVA Compact Linear Fresnel Reflector (CLFR) technology for the superheating of boiler feedwater to supply steam to the IP turbine inlet [27] . The solar heat addition to Kogan Creek Power Station increases the plant's electricity generation capacity by 44 MW_e (5.8 %) and also reduces the plant's annual GHG emissions by 35600 tons [28] .

2.3.3 Reheating of steam

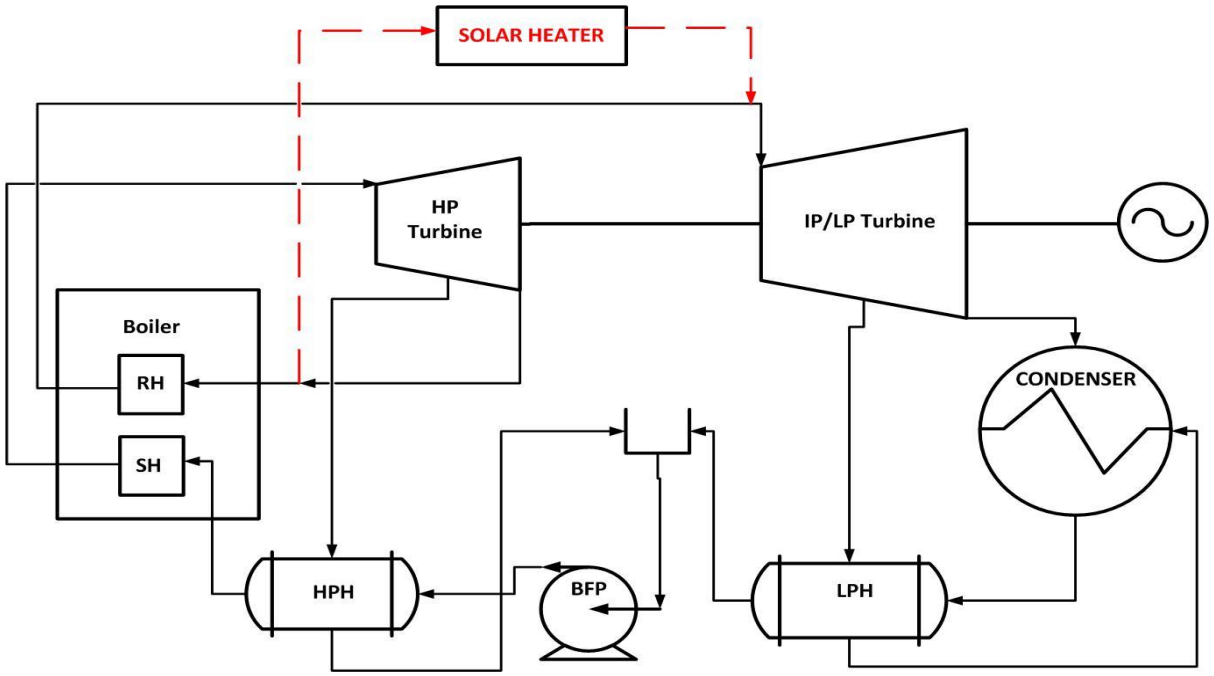

Figure 9: Reheating of steam using solar heat. Adapted from [23].

This solar heat integration option heats steam to the required steam temperature of the IP/LP turbine inlet. The steam which is heated, by the solar heater, is bypassed from the boiler reheater inlet. This is illustrated in Figure 9.

The reheat steam flow, which has a high specific volume and temperature, requires large piping diameters to be transported to and from the solar heater and the power plant [23]. This piping requirement creates an expensive installation [23]. This type of solar heat integration option can also pose many technical challenges, in routing large diameter steam piping through the existing power plant.

The boilers at the power station are of a single-pass design, and have convective reheating sections (the reheater tube bundles are heated by convective heat transfer) which are always exposed to the full flow of the high temperature flue gases. Thus, the bypassing of a portion of the reheater inlet steam flow to the solar heater may result in excessive reheater spraywater usage to control the boiler reheater steam outlet temperature. The excessive usage of reheater spraywater has a detrimental effect on plant heat rate. This type of solar heat integration may also cause overheating of the reheater tube bundles, resulting in boiler tube leaks.

Thus, based on the adverse plant impacts associated with this integration option, the use of solar heat for steam reheating will not be considered in this study.

2.3.4 Preheating of inlet combustion air to boiler

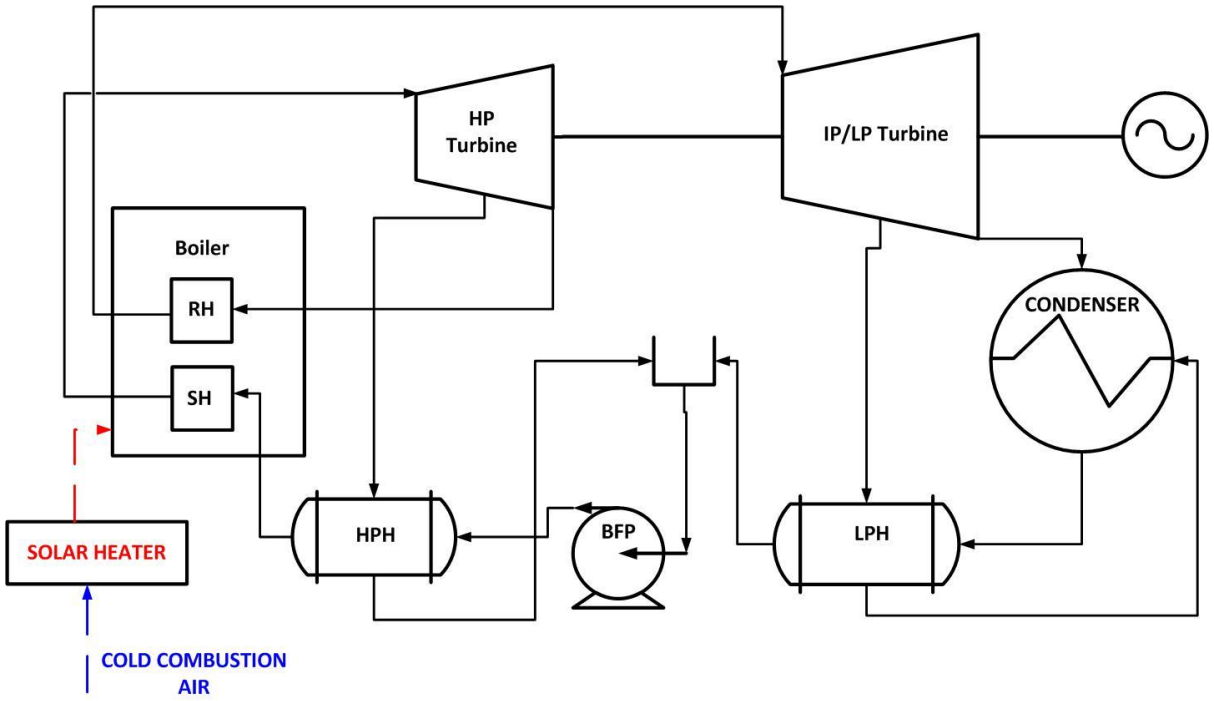

Figure 10: Preheating of the boiler inlet combustion air using solar heat. Adapted from [23].

This integration option uses solar heat to raise the temperature of the combustion air which enters the boiler. The concept of using solar heat to preheat inlet combustion air to the boiler is depicted in Figure 10. However, all of Eskom's coal-fired power stations have boiler air heaters, which serve to also heat the inlet boiler combustion air.

The boilers at the power station have an air heater installed in the exit flue gas path of the boiler (most coal boilers have this arrangement). The boiler air heater transfers the heat from the hot exit flue gases to the boiler inlet combustion air. Combustion air is the air required for the complete combustion of the pulverised coal in the boiler furnace. This is a method of recovering waste heat from the hot exit flue gases of the boiler plant, and thus increases the boiler thermal efficiency. The hot inlet combustion air is also required for stable boiler combustion.

If a solar air heater is installed in a boiler which has an air heater (i.e. bypassing the existing boiler air heater), it would imply that the heat from the hot exit flue gases is lost to the environment. This retrofit would reduce the boiler efficiency. [23]

Hence, based on this reason, this integration option will not be considered in this study.

2.4 Concentrated solar power (CSP) technologies

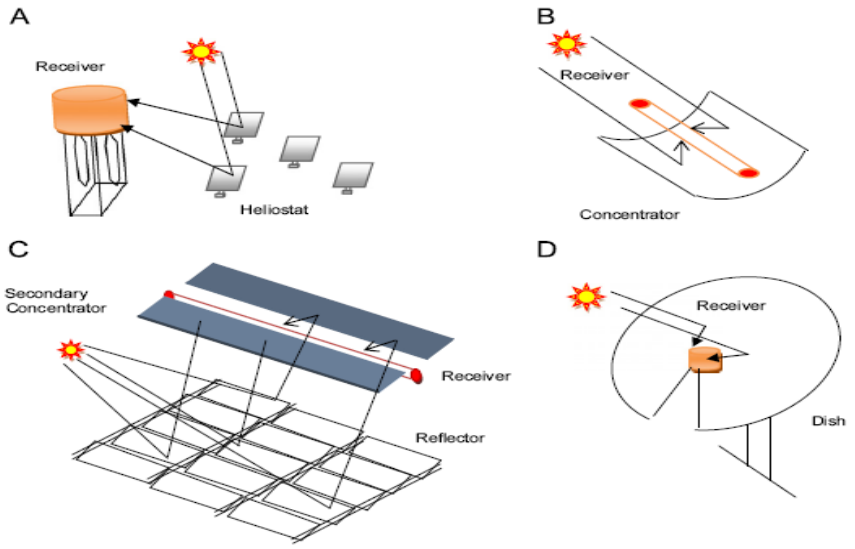

Figure 11: Basic concept of the four CSP technologies : (A) Central Receiver, (B) Parabolic Trough Collector, (C) Linear Fresnel Reflector, (D) Dish Engine. [29]

Concentrated solar power (CSP) technologies operate by concentrating the Direct Normal Irradiation (DNI) from the sun. DNI is the fraction of the total solar irradiation from the sun which is not diffused (by clouds, dust etc.) and reaches the surface of the earth as a beam. CSP technologies that concentrate DNI to either a point or a line are termed point-focus and line-focus concentrators respectively, this is illustrated in Figure 11. [30]

DNI is required to be concentrated in order to produce high temperatures, which are needed for efficient power generation. For example, a non-concentrating collector can produce temperatures below 200 ^{o}C [31]. In comparison, the Central Receiver (a CSP technology) can produce temperatures up to 565 ^{o}C (salt temperature) [32].

Currently, there exists four types of CSP technologies on the market [33] :

a) The Parabolic Trough Collector (PTC) (Line-focus concentrator)
b) The Central Receiver (CR) (Point-focus concentrator)
c) The Linear Fresnel Reflector (LFR) (Line-focus concentrator)
d) The Dish Engine (Point-focus concentrator)

The Dish Engine is not considered in this study, as it is not suitable for hybrid applications but rather for stand-alone electricity generation.

2.5 The Parabolic Trough Collector

2.5.1 Description

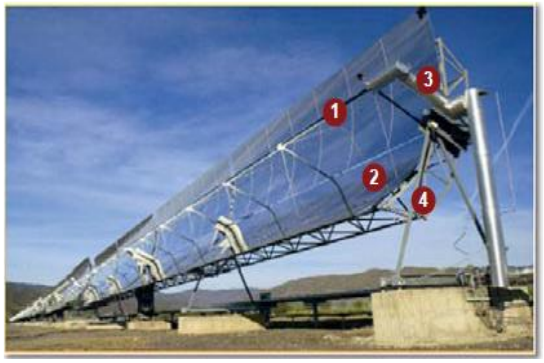

1:Reciever 2:Parabolic mirror
3:Ball joints 4:Support structure

A:External glass B:Expansion bellow
C:Glass-to-metal seal D:Internal pipe

Figure 12: The parabolic trough collector (left) and heat collection element. [34]

The Parabolic Trough Collector (PTC), as shown in Figure 12, consists of parabolic mirror facets, a heat collection element (HCE) located at the focal line of the collector and a metal support structure.

2.5.2 System operation

The PTC assembly is usually aligned on a North-South axis and tracks the position of the sun, using single axis tracking, from East to West. The reflective surface of the parabolic mirrors reflect incident DNI to the focal line of the collector. The HCE (the receiver tube), which is located at the focal line, absorbs and transfers the thermal energy of the concentrated solar radiation to the heat transfer fluid, which flows through the HCE. This is illustrated in Figure 11. This process of heat absorption increases the temperature of the heat transfer fluid. [30]

2.5.3 Heat transfer fluids

The heat transfer fluids (HTF) that are commonly used in the HCE of the PTC are [35] :

1. Thermal oil.
2. Molten salt.
3. Water/steam.

The thermal oil is a well-proven HTF, which is used in most of the Solar Energy Generating Systems (SEGS) PTC power plants. The thermal oil is commonly known as Therminol VP-1. The thermal oil is

capable of operating stably at a maximum temperature of 400 ^{o}C, above which it begins to degrade. Typically, the solar field outlet oil temperature is approximately 390 ^{o}C. [30].The hot thermal oil is normally used in a steam generator to produce superheated steam, of pressures up to 100 bar [36].

The molten salt, as the HTF, can achieve much higher operating temperatures, between 450 ^{o}C - 500 ^{o}C, but does have a high freezing point temperature of 220 ^{o}C. The high freezing point temperature requires that anti-freeze protection be fitted to the HTF system. This additional feature drives up costs and operating & maintenance requirements. [37]

Water can also be used as a HTF, to generate hot water/steam directly from the solar field, referred to as direct steam generation (DSG), without the use of an oil/water heat exchanger. The achievable outlet temperature of the solar field, with water as the HTF, is greater than 400 ^{o}C. However, the use of high-pressure water as a HTF requires expensive hydraulic piping components. [30]

2.5.4 Thermal energy storage

The excess thermal energy in the thermal oil and in the molten salt HTF can both be stored, for long periods of time. However, steam cannot be stored for long periods [36].The thermal energy storage (TES) medium can be the same as the HTF used or it can be a different medium. Salt is typically used as the heat storage medium because it is cheaper than thermal oil [37]. The use of TES lowers the cost of electricity production and improves the availability of the solar plant [38].

TES is not necessary for this project because during the hours of low solar resource, coal serves as the 'back-up' energy source. However, it would be wise to select technology options which have TES capabilities, as this introduces additional "flexibility" into the system. Thus, TES will only be considered in this study if it creates an additional project benefit. For E.g. for the qualification of a special electricity tariff from the National Energy Regulator of South Africa (NERSA) etc.

In summary, thermal oil will be used as the HTF for the PTC technology, when applied to the two solar heat integration options that are applicable to this project i.e. feedwater heating and the production of superheated steam. Thermal oil is selected over the other mentioned HTFs because it is the most well proven HTF.

2.6 The Central Receiver

2.6.1 Description

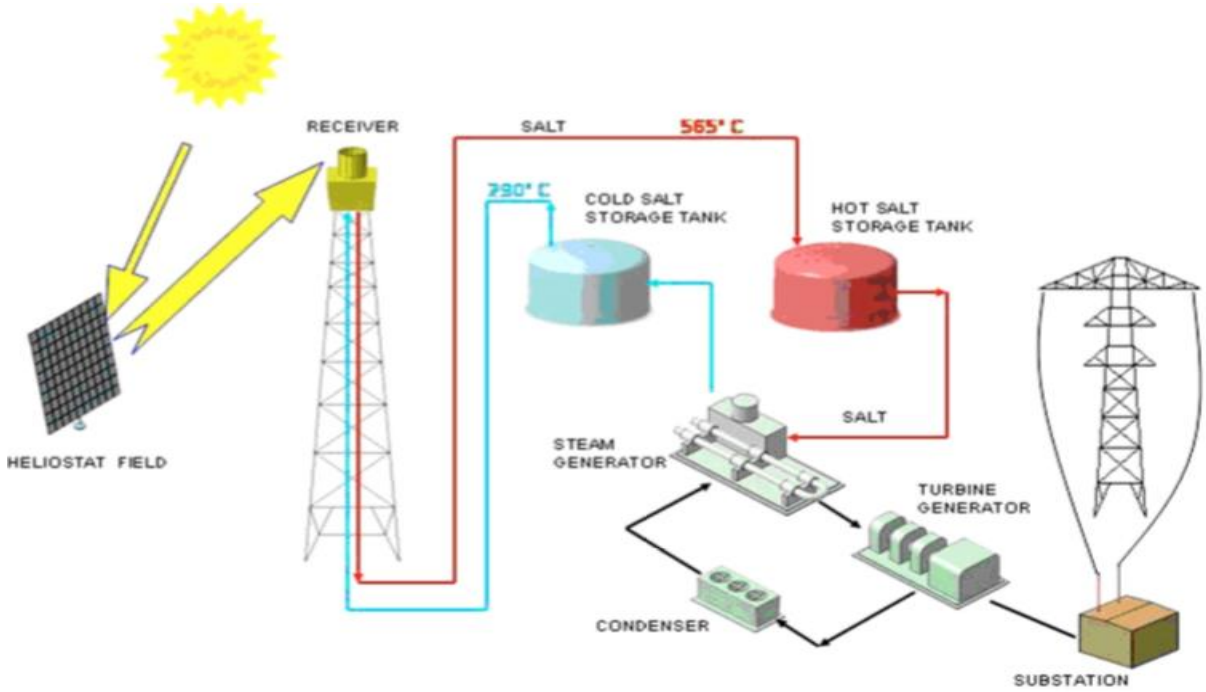

Figure 13: The solar TRES plant [32]

The Central Receiver (CR) plant, illustrated in Figure 13, consists of a field of reflective mirrors (the heliostat field), a receiver which is located on the top of a tower, thermal energy storage tanks and a steam generator. The turbine generator, condenser etc. are available in the existing coal-fired power plant. The Solar Two CR power plant in operation is illustrated in Figure 14.

Figure 14: Solar Two Central Receiver (Source: NREL). [35]

2.6.2 System operation

The mirrors of the heliostat field track the position of the sun, using two-axis tracking, and reflect the incident DNI from the sun onto the receiver. The receiver is located on the top of a tower. The temperature of the HTF inside the receiver is raised, when the HTF absorbs the high radiation energy which is reflected on the receiver. The excess heat energy that is produced during the day is stored in the thermal energy storage tanks. [29]

2.6.3 Heat transfer fluids

The three most commonly used HTF mediums in the CR system are [39]:

1. Molten salt (Referred to as the Molten Salt solar tower).
2. Water/steam (Referred to as the Direct Steam solar tower).
3. Air.

Air as an HTF is been tested in small scale plants and was thus not considered in this study [39].Water/steam can also be used as the HTF, to produce superheated steam in the receiver, but no commercial storage options are available for superheated steam [36]. Steam in its saturated state can be stored, but is limited to short times (<10 min) [36] . The direct steam solar tower will thus not be considered in this study.

Molten salt as the HTF is used for the heating of water, to produce superheated steam. Molten salt has an operating temperature of 565 ^{o}C and is returned to the receiver at approximately 290 ^{o}C [32]. The superheated steam pressure can range up to 160 bar [36].

The molten salt, which is thus used as the HTF in this study, has a chemical composition of 60% $NaNO_3$ & 40% KNO_3.

2.6.4 Thermal energy storage

The excess thermal energy that is produced by the receiver can be stored as high temperature molten salt in storage tanks. The molten salt storage tanks are capable of long time storage, typically 10-12 hours.

In summary, the molten salt solar tower is thus considered in this study because, it can provide adequate thermal energy storage, if required. The molten-salt solar tower is only considered to be applied to the solar heat integration option which produces superheated steam, because it is not practical to use a salt temperature of 565 ^{o}C to heat feedwater in the range of 50 ^{o}C – 250 ^{o}C.

2.7 The Linear Fresnel Reflector

2.7.1 Description

Figure 15: The NOVATEC Linear Fresnel Reflector system at Puerto Errado 1 in Spain. [40]

The Linear Fresnel Reflector (LFR) system, as shown in Figure 15, consists of a fixed elevated linear heat receiver, which is located above an array of flat or slightly bent mirrors strips [41]. A process flow diagram of a particular LFR system is illustrated in Figure 16.

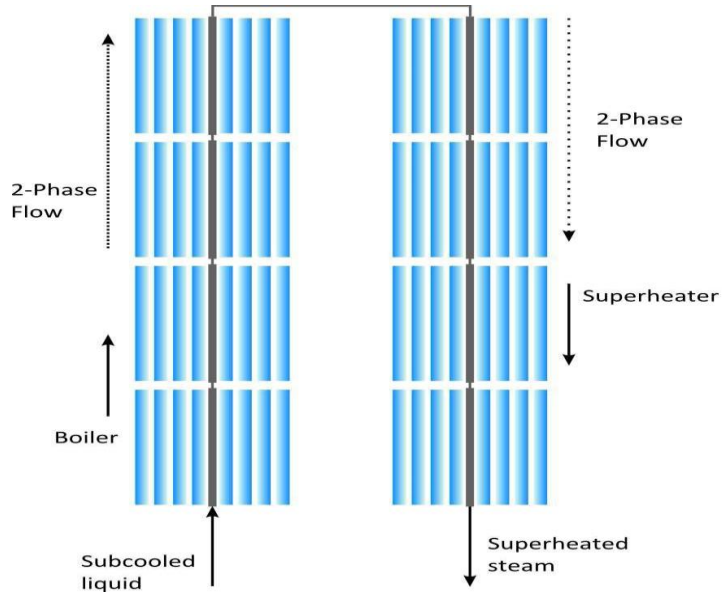

Figure 16: The once-through Linear Fresnel Reflector solar boiler. [42]

2.7.2 System operation

The flat (slightly bent) mirrors track the position of the sun, using single axis tracking, and reflect incident DNI onto the elevated linear heat receiver. The heat receiver absorbs the reflected radiation and transfers the absorbed heat to the HTF that flows through the heat receiver. The heat absorbed by the HTF, raises the HTF temperature. [43, 41]

2.7.3 Heat transfer fluids

Water has always been selected, from the beginning, as the HTF for LFR systems, which allows for direct steam generation (DSG) from the solar field [43].The use of water as the HTF, simplifies the system because no additional heat exchangers are required [43].The LFR system can produce steam at a high-temperature and pressure. For example, a leading LFR manufacturer, Novatec, has developed a LFR system, called the "Supernova collector", which can produce superheated steam at 500 ^{o}C @ 100 bar [44, 45].

In recent years, molten salt was introduced as an HTF for LFR systems. For example, AREVA solar, also a leading LFR manufacturer, developed a molten salt CLFR system, which can achieve a salt temperature of 550 ^{o}C. [46]

However, water is only considered as the HTF for the LFR system because, the software program which is used in this study to model the performance of the LFR system, can only use water as the HTF. The performance models of all 3 CSP technologies are discussed in chapter 3.

2.7.4 Thermal energy storage

The steam produced by the LFR system cannot be stored, because there is no commercial storage option for superheated steam. Steam accumulators can be used as a storage option for saturated steam, however all of the solar heat integration options in this study which require steam, need superheated steam. [47]

In summary, the LFR will be considered for both solar heat integration options i.e. feedwater heating and the production of superheated steam.

2.8 Comparison of CSP technologies

The Table 1 below contains a summary of the properties of each CSP technology discussed.

Table 1: Comparison of the CSP technologies

Technical Parameter	Unit	CSP technology		
		Parabolic Trough	**Molten Salt Tower**	**Linear Fresnel Reflector**
Concentration ratio[6] [36]	-	70-80	>1000	>60
Absorber/Receiver	-	Mobile	Fixed	Fixed
Heat storage (medium)	-	Yes (molten salt)	Yes (molten salt)	No storage
HTF	-	Therminol VP-1	Molten salt	Water
HTF conditions	^oC/ bar	390 ^oC	565 ^oC	500 ^oC / 100 bar
Max steam conditions	^oC/ bar	380 ^oC / 100 bar	535 ^oC / 160 bar	500 ^oC / 100 bar

2.9 Summary of integration options and CSP technologies

The applicability of each solar heat integration option to the power station, and the applicability of each CSP technology to each solar heat integration option, is summarized in Table 2.

Table 2: Summary of solar heat integration options and CSP technologies.

Integration option	Applicable to the power station? (Yes/No)	CSP technology applicable to integration option? (Yes/No)		
		Parabolic Trough	**Molten Salt Tower**	**Linear Fresnel Reflector**
Feedwater heating	Yes.	Yes.	No-HTF temperature not suitable for feedwater heating.	Yes.
Steam production	Yes.	Yes.	Yes.	Yes.
Steam reheating	No-many adverse plant impacts.	-	-	-
Air preheating	No-the power station has an air heater.	-	-	-

[6] Concentration ratio is defined as the area of the collector aperture divided by the surface area of the receiver [124].

2.10 Solar resource In South Africa

South Africa has an excellent solar resource, which is amongst the highest in the world [12]. The regions in the Northern Cape of SA, as illustrated in Figure 17, receives the highest annual DNI in the country. There are plans to use the solar resource in these regions for electricity generation. For example, Eskom has planned to construct a 100 MW_e CSP plant near Upington in the Northern Cape [48] .

The site of the power station, which is in Witbank, Mpumalanga, receives less DNI than the site of Upington. This is clear from Figure 17.The Upington site receives approximately 25 % more DNI than the site of the power station, as tabulated in Table 3. This difference in solar resource makes the construction of a stand-alone CSP plant in Mpumalanga less feasible than in the Northern Cape. Hence, the reason for this study, which investigates the techno-economic feasibility of solar heat augmentation to the power station.

Table 3: Annual weather data (Source: Meteonorm)

Weather condition	Unit	Location	
		The power station	**Upington**
Direct normal irradiation (DNI)	kWh/m^2	2240.1	2801
Daily peak DNI	W/m^2	651	942

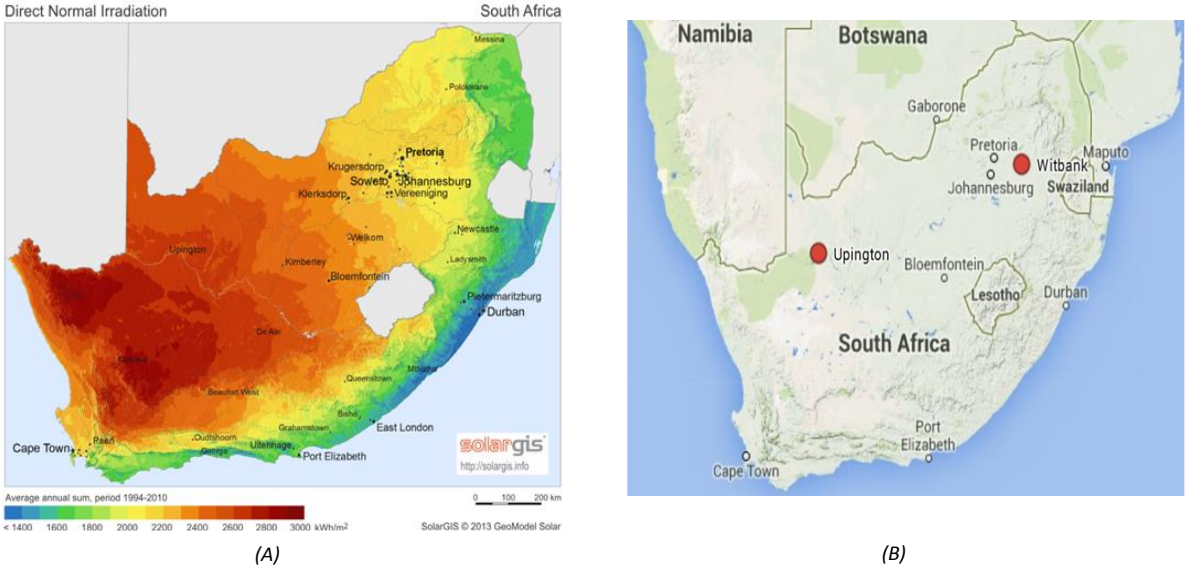

(A) *(B)*

Figure 17: (A) The average annual sum of DNI (1994-2010) of South Africa [49] , (B) A map of South Africa indicating the location of Upington and Witbank [50].

2.12 Solar – coal plant daily operation

The following section describes the typical daily operation of the solar field and the coal-fired power plant, as demonstrated by Cameo Power Station [25]. The Unit 2 of Cameo Power Station uses the PTC technology to heat boiler feedwater. A picture of Cameo Power Station with its PTC field, is presented in Figure 18. [51]

Figure 18: Cameo Power Station and its PTC solar field. [51]

a) Daily operation

The solar field begins operating by the starting of the HTF pumps, only once the DNI reached a critical value (approximately 200 W/m^2). The PTC assemblies then began to track the position of the sun through the day, and were stowed once the DNI fell below the critical value.

The solar heat collected by the HTF was transferred to the unit, through a heat exchanger, only once the following requirements were met:

1. The unit was operating stably.

The implication of this requirement for the power station is that solar heat is to be transferred to the unit, at loads > 45 % MCR[7] (270 MW_e). During loads < 270 MW_e, the units at the power station do not operate stably. This requirement reduces the risk of a unit trip.

[7] MCR is the maximum continuous rating of the unit, i.e. 600 MW_e.

2. There was a sufficient temperature difference (> 3^{o}C) between the outlet HTF of the solar field and the flow exiting the feedwater heater. This requirement guaranteed that heat was transferred from the HTF to the feedwater and not vice versa.

In this study, a 10 ^{o}C and 30 ^{o}C temperature difference (between the HTF and the outlet steam/water) is specified for the PTC and the CR systems respectively, during normal plant operation. This is noted in Table 1.

b) The effect of cloud cover

During the day, cloud cover which blocked the direct sunlight caused the heat output of the solar field to be reduced. The cloud cover also produced fast transients in HTF temperature, because of the limited thermal inertia of the system. However, the temperature transients had little impact on the operation of the Unit 2 of Cameo Power Station, because the solar field is small (4 MW_t ~ 1 MW_e) in comparison to the size of the Unit 2 (49 MW_e net). I.e. a 2 % solar share[8].

The units of the power station are rated at 575 MW_e net, and the expected maximum solar field size is 30 MW_e (this is discussed in section 3.8). I.e. a 5.2 % solar share. Although the maximum solar share expected in this study is also small, the complete effect of cloud over on the solar field system and the power station, should be assessed by transient heat modelling. However, this investigation is beyond the scope of this study.

[8] Solar share is defined, in this study, as the solar MW_e'S produced relative to the net unit output.

2.13 The cost of power generation in SA

Coal-fired power plants are one of the cheapest electricity generation technologies in South Africa, because these power plants have the lowest 'overnight capital cost' and produce the lowest Levelised cost of electricity (LCOE), as indicated in Table 4. The figures in Table 4 are sourced from the updated Integrated Resource Plan (IRP) for Electricity in South Africa (2010-2030) [10].

On the other hand, electricity generation from CSP in South Africa is far more expensive. For example, a PTC power plant (with 3 hrs TES) which is implemented in Upington, would produce an LCOE of R1.58/kWh$_e$, which is approximately 2.7 times the LCOE of a coal-fired power plant.

There are other technologies which produce cheaper electricity than CSP power plants, a good example are nuclear power plants. Nuclear power plants have an 'overnight capital cost' which is more than twice that of coal-fired power plants, however these power plants do produce a LCOE which is competitive with coal-fired power plants. This is because nuclear power plants have lower operating & maintenance and lower fuel costs than coal-fired power plants in SA [10].

Table 4: The costs (in 2012 Rands) of different power plant technologies in SA [10].

Power plant technology	**Overnight capital cost (R/kW$_e$)**	**Levelised cost of electricity (R/kWh$_e$)**
Conventional coal-fired with FGD[9]	21572	0.58
Nuclear	46841	0.69
Central receiver with 3 hrs TES	37577	1.43
Parabolic trough with 3 hrs TES	40438	1.58

The high cost of electricity generation from CSP technologies is one of the reasons for the low deployment of these technologies. This is illustrated in Table 5. To date, the PTC technology has the largest operational capacity, amongst all other CSP technologies, in the world. This is because, the PTC technology is the most mature CSP technology, and together with an operational experience exceeding 25 years, it creates low risk for investors [52].

Table 5: Operational capacity of CSP power plants in the world [53].

CSP technology	**Operational capacity (MW$_e$)**
Linear Fresnel reflector	89
Central receiver	436
Parabolic trough collector	3200

However, it has been shown that the CR technology has the ability to produce lower-cost electricity than the PTC technology. This is because the CR technology can reach higher temperatures than the

[9] Flue gas desulphurization

PTC technology, and hence the power cycle of the CR technology operates with a higher efficiency than the power cycle of the PTC technology. [54] .The cost data from the IRP, which is tabulated in Table 4, also shows that the cost of the CR technology is cheaper than the PTC technology.

The LFR technology is relatively new to the commercial CSP market. For example the world's first commercial LFR power plant, Puerto Errado 2 in Spain which has a capacity of 30 MW_e, began operation in 2012 [55]. The LFR technology does have cost advantages over the CR and the PTC technologies, as it uses flat mirrors and uses water as an HTF. The LFR technology can also achieve higher temperatures than the conventional PTC technology, thus it would be a strong competitor in this study.

3. Research Methodology

3.1 Methodology overview

The purpose of this study, as mentioned in section 1.1, is to investigate if the addition of solar heat to the power station is technically and also economically feasible. The main intention of the project, as mentioned earlier, is to reduce the GHG emissions from the power station.

At the beginning of this study, 1 of the first questions that one would ask is, what are the possible methods that can be used to integrate solar heat to the power station? This is the 1st research question, as mentioned in section 1.3.1. This question has already been answered in the Literature review, in section 2.3. The answer is, solar heat can only be integrated to the power station by using two possible methods i.e. feedwater heating and by supplying superheated steam.

The question which would follow next is, which CSP technology (s) are applicable to these solar heat integration options? This is the 2nd research question, as mentioned in section 1.3.1. This question was answered in two steps. The first step was to conduct a CSP technology market assessment. This assessment was to determine the maximum producible water/steam conditions (temperature and pressure) from each available CSP technology. This technology market assessment has already been done, which is also part of the Literature review, in section 2.4.

The 2nd step, in answering research question 2, would be to compare, the operating conditions of each feedwater heater or turbine plant area, with the producible water/steam conditions from each available CSP technology. If the maximum producible water/steam conditions from a particular CSP technology, can meet or exceed, the operating conditions of a feedwater heater or turbine plant area, then that particular CSP technology is applicable to that integration option.

a) Technical feasibility assessment

The addition of solar heat to the power station, either by feedwater heating or supplying superheated steam, will produce changes in the process flow of the Rankine cycle of the power station. The process flow condition at any point in the Rankine cycle, is expressed in terms of a mass flow rate (kg/s), temperature and pressure.

The technical feasibility assessment, of this study, establishes if these changed process flow conditions, exceed the technical capabilities of the infrastructure of the power station. This assessment raised the 3rd research question, what are the technical capabilities of the infrastructure of the power station? This question can be answered by using one of two methods.

The first method would be, to practically test each plant component of the power station, to determine its technical capabilities. This method is time consuming and it may require that the plant be taken off load in order to conduct tests. The second method would be, to source the technical capabilities of each plant component, from its Original Manufacturer (OEM). The latter method was chosen, because data sheets from OEMs which specify plant capabilities, are readily available in the Eskom Library.

The next step in the technical feasibility assessment was to, predict the process flow changes, which will occur when solar heat is added to the Rankine cycle of the power station. Through much thought it was realised that the best possible way, to predict these process flow changes, was by using a model of the Rankine cycle of the power station. Hence, a thermodynamic model of the Rankine cycle of the power station was developed and validated. This model was developed by using a software programme (which is discussed later) and is referred to in this study as, the VirtualPlant^{TM} model.

The VirtualPlant^{TM} model was used in the technical feasibility assessment, as follows. Firstly the model was configured with a solar heat integration option, which supplies a given amount of solar heat to the Rankine power cycle of the power station. Thereafter the model was simulated to generate full load (600MW$_e$), and the process flow conditions were noted. If the technical capabilities of the plant were exceeded, then the amount of solar heat supplied by the integration option was reduced, and the model was simulated again to note the new process flow conditions. This process was repeated until the technical capabilities of the plant were met (equalled).

Indirectly, this process of iteration determined the maximum amount of solar heat that can be supplied by a particular integration option. This maximum amount of solar heat, is referred to as the 'design point solar heat' of that particular integration option. However, if the 'design point solar heat', exceeds the equivalent of 30 MW$_e$ (this is discussed in section 3.8), it is further reduced.

b) Economic feasibility assessment

The economic feasibility assessment of a commercial-scale project, such as this project, has always been of major importance. It is one of the factors that determine if a commercial- scale project gets the go ahead or not.

To perform a comprehensive economic analysis of a project, it would require taking into consideration the project's costs (including taxes) and benefits, over each year of the life of the project [56].This analysis gave rise to the 4th and 5th research questions (as mentioned in section 1.3.1) such as, what are the economic costs and benefits associated with this project?, and do these project benefits outweigh the project costs over the life of the project?.

The project's costs (capital and operating expenditure) were calculated by using cost models. These cost models were developed by the National Renewable Energy Laboratory (NREL) of the United States Department of Energy, with support from organisations such as WorleyParsons Group Inc. and Sandia National Labs. These models are available in NREL's System Advisor Model (SAM). [57, 58]

SAM was initially developed, in 2005, to be used by the United States Department of Energy's Solar Energy Technologies Program. Since SAM was released to the public, in 2007, it is been used by project developers, policy makers, researchers etc. to evaluate renewable energy projects. [59].Thus, based on the extensive use of SAM, by the solar industry, it was chosen to be used in this study.

The main economic benefit for this project is the production of solar electricity. The procedure to calculate the annual solar electricity production, is similar to the procedure to calculate annual GHG reduction and coal savings. Essentially, each of these benefits would have to be calculated for each of the 8760 hours of the year. The reason for this would become clear in the discussion that follows.

As explained in section 2.1.2, the coal consumption (boiler load) of the power plant will reduce due to the addition of solar heat. The heat rate of the power plant will thus also reduce. Heat rate is a common term used in the Power Industry, and it gives an indication of how efficiently the power plant is burning coal. It was thus decided to express the reduction in boiler load, as a reduction in plant heat rate, as this would make the results more meaningful. The calculation of the heat rate reduction of the power station, is thus the first step towards calculating the 3 project benefits mentioned.

A project benefit (such as coal savings) is calculated, as explained below. The VirtualPlant^{TM} model was set up to produce a generator load of, for example 600 MW_e. The model was then simulated for two scenarios. The 1st scenario had no solar heat supplied to the power cycle whilst maintaining 600 MW_e. The 2nd scenario had solar heat supplied to the power cycle whilst also maintaining 600 MW_e. The difference in the boiler loads (which is expressed as a heat rate reduction) from these two scenarios, was used to calculate the coal savings.

However, the solar resource is not constant during the day, and it also varies through the year. Because a smaller solar heat input to the power cycle would create a smaller heat rate reduction, the coal savings had to be calculated for each of the 8760 hours of the year. An implication of the annual hourly calculation steps, was that the heat output from the solar field also be modelled for each hour of the year. This was done by using SAM, as SAM has this modelling capability.

As mentioned, the procedure to calculate the annual solar electricity production from the solar field and the annual reduction in GHGs, are similar to this.

There are additional economic benefits that are applicable to this project, that are offered by some national departments of SA, such as The Department of Energy (DoE), The South African Revenue Service (SARS) etc.

The final stage of the economic feasibility assessment was to use the projects costs and benefits in a project life cycle assessment. The life cycle assessment was performed according to methods explained in [56], these methods are also used in SAM. The life cycle assessment calculates economic measures such as the discounted payback period (DPB), the levelised cost of electricity (LCOE) etc. of the project.

c) Summary of Research Methodology

1) Research the possible methods that can be used, to integrate solar heat to the power station.
2) List the specific plant areas of the power station, which can be supplied with solar heat. Also include the operating conditions of these plant areas.
3) Perform a CSP technology market assessment, to determine the maximum producible water/steam conditions from each available CSP technology.
4) Select a CSP technology (s) that can be used to supply solar heat, to each plant area that is listed in point 2. This process will create a list of solar heat integration options which are specific to the power station.
5) Source the technical capabilities of each plant component of the power station, from OEM data sheets.
6) Develop and validate a thermodynamic model of the Rankine cycle of the power station. This model will be referred to as the VirtualPlant^{TM} model.

For each solar heat integration option of the power station:

a) Determine, by using the VirtualPlant^{TM} model, the maximum amount of solar heat that can be supplied, without exceeding the technical capabilities of the power station.
b) Determine the annual hourly, solar heat output of the solar field, by using SAM.
c) Using the annual hourly solar heat output from the solar field, determine the annual hourly heat rate reduction of the Rankine cycle of the power station.
d) By using the annual hourly heat rate reduction, determine the annual project benefits such as solar electricity production, GHG reduction and coal savings.
e) Determine the projects costs by using cost models from SAM.
f) Perform an economic life cycle assessment based on the project's costs and benefits.

Also included in the methodology of this study is:

- An assessment of the available land & annual solar resource (DNI) at the power station.

- A formulation of the daily operation modes of the power station. I.e. defining which times of the day, to operate the power station on the Fuel-saving mode and Power-boost mode.

3.2 Site assessment for the power station

The starting point of the project, was to assess the site around the power station, for:

1. Available land
2. Solar resource

The land assessment would determine the amount of land area that is available for the solar field, and also the location of the land. The location of the land plays an important role in deciding which 1 of the 6 units of the power station would receive the solar heat. The solar resource assessment would be used to design the solar field(s) of each integration option, and also to predict the hourly heat output of the solar field(s) of each integration option.

3.2.1 Land assessment

An aerial view of the power station and its surroundings was obtained from Google Earth. A land area was selected for the solar field, by taking into consideration its environmental conditions, its distance from the power station and its accessibility. The area of the land was also estimated by using Google Earth.

3.2.2 Solar resource assessment

The solar resource can be assessed by using ground measurements or satellite derived data. Although ground measurements are more accurate than satellite data, it is an expensive and time consuming method of assessing the solar resource. Thus, satellite derived data was selected to be used in this study, because it does provide accurate results and is relatively cheap. [60]

The Meteonorm Software, which is widely used by the solar industry, was used to create a weather file for the site of the power station. Meteonorm creates weather files based on satellite and weather station data. The weather file contains the expected DNI resource available for each of the 8760 hours of the year. This file was used in SAM, to predict the annual hourly solar field heat output.

3.3 Solar heat integration options for the power station

A solar heat integration option, as explained, is a method that is used to add solar heat to the regenerative Rankine power cycle. As discussed in chapter 2 section 2.3, there are four methods that can be used to integrate solar heat into the regenerative Rankine power cycle. However only the solar heat integration options that are applicable to the power station, will be considered in this study.

The solar heat integration options that are applicable to the power station are:

1. Feedwater heating

There are two methods employed to heat feedwater, with the use of solar heat:

Method 1: A portion of the feedwater flow to a feedwater heater is bypassed to the solar plant, which heats the bypassed feedwater flow to the required temperature.

Method 2: The bled steam flow to a feedwater heater, which is normally extracted from a turbine, is replaced partially or completely by steam which is produced by the solar plant.

2. Superheated steam supply

A portion of the high-pressure feedwater flow from the discharge of the boiler feedwater pump, is bypassed to the solar plant. The solar plant heats the bypassed feedwater flow to the required steam temperature, and regulates the steam pressure to the required pressure set point. The steam which is produced by the solar plant is supplied to the relevant turbine plant areas. E.g. the HP or IP turbine inlet etc. The steam produced can also be supplied to the feedwater heaters, to replace bled steam i.e. this refers to Method 2 of feedwater heating.

3.4 Operating conditions of feedwater heaters and turbines

It is required to list the specific plant areas of the power station which can be supplied with solar heat, along with their operating conditions. This would imply, to list all the feedwater heaters and turbine plant areas of the power station, with their respective operating conditions. This information is used in selecting a CSP technology (s) which can be used to supply solar heat, to each feedwater heater or turbine plant area. The operating conditions are sourced from an OEM heat-balance-diagram (HBD) of the Rankine cycle of the power station, at full load conditions (600 MW_e).

3.4.1 Feedwater heating plant

The Rankine cycle of the power station has 6 feedwater heaters i.e. 5 closed-type feedwater heaters and 1 open-type feedwater heater. In a closed-type feedwater heater the bled steam flow and the feedwater flow do not mix. In an open-type feedwater heater, the bled steam flow is allowed to mix with the feedwater flow. The closed-type feedwater heaters at the power station, consist of low-pressure heaters (LPH) and high-pressure heaters (HPH).Thus, the list of closed-type feedwater heaters at the power station is, LPH1, LPH2, LPH3, HPH5 and HPH6. The deaerator (DA) is the open-type feedwater heater.

It was found that, Method 1 of feedwater heating, applies to all of the feedwater heaters, except the DA, because the DA is an open-type feedwater heater. It was also found that Method 1 can only be applied to LPH1 and LPH2, as a pair. This is because LPHs 1 & 2 are of a duplex design (they are both contained in a single shell), hence they cannot be bypassed individually. Method 2 of feedwater heating, applies to all of the feedwater heaters, except LPHs 1 & 2. This is because the LPHs 1 & 2 are located within the neck of the main condenser, hence solar steam cannot be supplied to them. The operating conditions of all the feedwater heaters, during full load operation of the power station, are listed in Table 6.

Table 6: Operating conditions of the feedwater heaters during full load operation

Feedwater heater	Bled steam temperature & pressure °C (MPa)	Inlet feedwater temperature & enthalpy °C (kJ/kg)	Outlet feedwater temperature & enthalpy °C (kJ/kg)	Feedwater mass flow rate & pressure kg/s (MPa)
Low-pressure heater 1 (LPH1)	59 (0.02)	42.6 (179.3)	57.4 (241.1)	372.8 (2)
Low-pressure heater 2 (LPH2)	84 (0.06)	57.4 (241.1)	81.7 (342.7)	372.8 (2)
Low-pressure heater 3 (LPH3)	118 (0.11)	81.7 (342.7)	101.1 (424.2)	372.8 (2)
Deaerator steam inlet (DA)	243 (0.38)	-	-	23.6
High-pressure heater 5 (HPH5)	372 (1.2)	145.2 (626)	188.4 (811.1)	491.2 (22)
High-pressure heater 6 (HPH6)	330 (3.9)	188.4 (811.1)	247 (1073.2)	491.2 (22)

3.4.2 Turbine plant

The Rankine cycle of the power station has 4 turbine plant areas i.e. the high-pressure (HP) turbine, the intermediate-pressure (IP) turbine, the low-pressure (LP) turbine and the boiler feedwater pump turbine (BFPT). The superheated steam which is produced by the solar plant, can be supplied to all of these turbine plant areas.

The operating conditions of all the turbine plant areas, during full load operation of the power station, are listed in Table 7. The feedwater conditions at the boiler feedwater pump (BFP) discharge are also include in Table 7.

Table 7: Operating conditions of the turbine plant during full load operation

Turbine plant area	**BFP discharge temperature & enthalpy °C (kJ/kg)**	**Inlet steam temperature & enthalpy °C (kJ/kg)**	**Inlet steam mass flow rate & pressure kg/s (MPa)**
High-pressure (HP) turbine	145.2 (626)	535 (3395.4)	491.2 (16)
Intermediate-pressure (IP) turbine	145.2 (626)	535 (3528.0)	439.9 (3.65)
Low-pressure (LP) turbine	145.2 (626)	243 (2949.7)	365.6 (0.41)
Boiler feedwater pump turbine (BFPT)	145.2 (626)	377 (3211.8)	19.1 (1.21)

3.5 CSP technology selection

Each solar heat integration option requires a CSP technology to collect solar heat, which is delivered to the power station. The selection of a CSP technology(s) for a particular integration option is done by, comparing the operating conditions of the feedwater heater or turbine plant area, with the maximum producible water/steam conditions from each available CSP technology. If the maximum producible water/steam conditions from a CSP technology, can equal or exceed, the operating conditions of a feedwater heater or turbine plant area, then that particular CSP technology is applicable to that integration option. In some instances more than one CSP technology is applicable to a particular integration option. The maximum producible water/steam conditions from each CSP technology are presented in Table 1, but are also listed here for convenience. The PTC, CR and the LFR can produce maximum steam conditions of 380 ^{o}C (10 MPa), 535 ^{o}C (16 MPa) and 500 ^{o}C (10 MPa) respectively.

The PTC technology is applicable to all of the solar heat integration options, but is not applicable to the supply of superheated steam to the HP and the IP turbine. This is because the PTC technology cannot produce the steam temperature of 535 ^{o}C, which is required by the HP and the IP turbine. The steam temperature from the PTC technology is limited to 380 ^{o}C.

The LFR technology is applicable to all of the feedwater heating options, but is not applicable to the Method 1 of feedwater heating for the HPHs. This is because the feedwater flow through the HPHs has a pressure range of 18-22 MPa, and the LFR technology cannot heat water which has a pressure greater than 10 MPa. The LFR technology also cannot supply steam to the HP and the IP turbine, because it cannot produce the required steam of the HP and the IP turbine. The steam temperature from the LFR technology is limited to 500 ^{o}C.

The molten salt solar tower technology is only applicable to the supply of superheated steam to the HP and the IP turbine. Although it is theoretically possible to heat feedwater by using the molten salt solar tower, it would not be practical to use molten salt @ 565 ^{o}C to produce feedwater temperatures in the range of 50 ^{o}C - 250 ^{o}C. Hence, the molten salt solar tower was not applied to the feedwater heating options. Similarly, the molten salt solar tower was not consider for the supply of superheated steam to the LP turbine and the BFP turbine, because these plant areas require low steam temperatures of 243 ^{o}C - 377 ^{o}C respectively.

Table 8 and Table 9, summarize the applicable CSP technology(s) for each solar heat integration option, along with the type of heating employed by each CSP technology. If the feedwater is used as the HTF of the CSP technology, this is referred to as Direct heating. If an alternative HTF is used in the CSP technology, this is referred to as Indirect heating.

Examples of feedwater heating and superheated steam supply integration options are presented in Figure 19 and Figure 20 respectively.

Table 8: Summary: Applicable CSP technology (s) for each feedwater heating integration option

Integration option	**CSP technology- applicability (Yes/No)**		
Feedwater heating (M1=method 1, M2=method 2)	**Parabolic Trough Collector**	**Linear Fresnel Reflector**	**Molten Salt Solar Tower**
LPH 1&2 (M1)	Yes (Indirect)	Yes (Direct)	No
LPH 3 (M1)	Yes (Indirect)	Yes (Direct)	No
LPH 3 (M2)	Yes (Indirect)	Yes (Direct)	No
DA (M2)	Yes (Indirect)	Yes (Direct)	No
HPH 5 (M1)	Yes (Indirect)	No	No
HPH 5 (M2)	Yes (Indirect)	Yes (Direct)	No
HPH 6 (M1)	Yes (Indirect)	No	No
HPH 6 (M2)	Yes (Indirect)	Yes (Direct)	No

Table 9: Summary: Applicable CSP technology (s) for each superheated steam supply integration option

Integration option	**CSP technology- applicability (Yes/No)**		
Superheated steam supply	**Parabolic Trough Collector**	**Linear Fresnel Reflector**	**Molten Salt Solar Tower**
HP turbine	No	No	Yes (Indirect)
IP turbine	No	No	Yes (Indirect)
LP turbine	Yes (Indirect)	Yes (Direct)	No
BFP turbine	Yes (Indirect)	Yes (Direct)	No

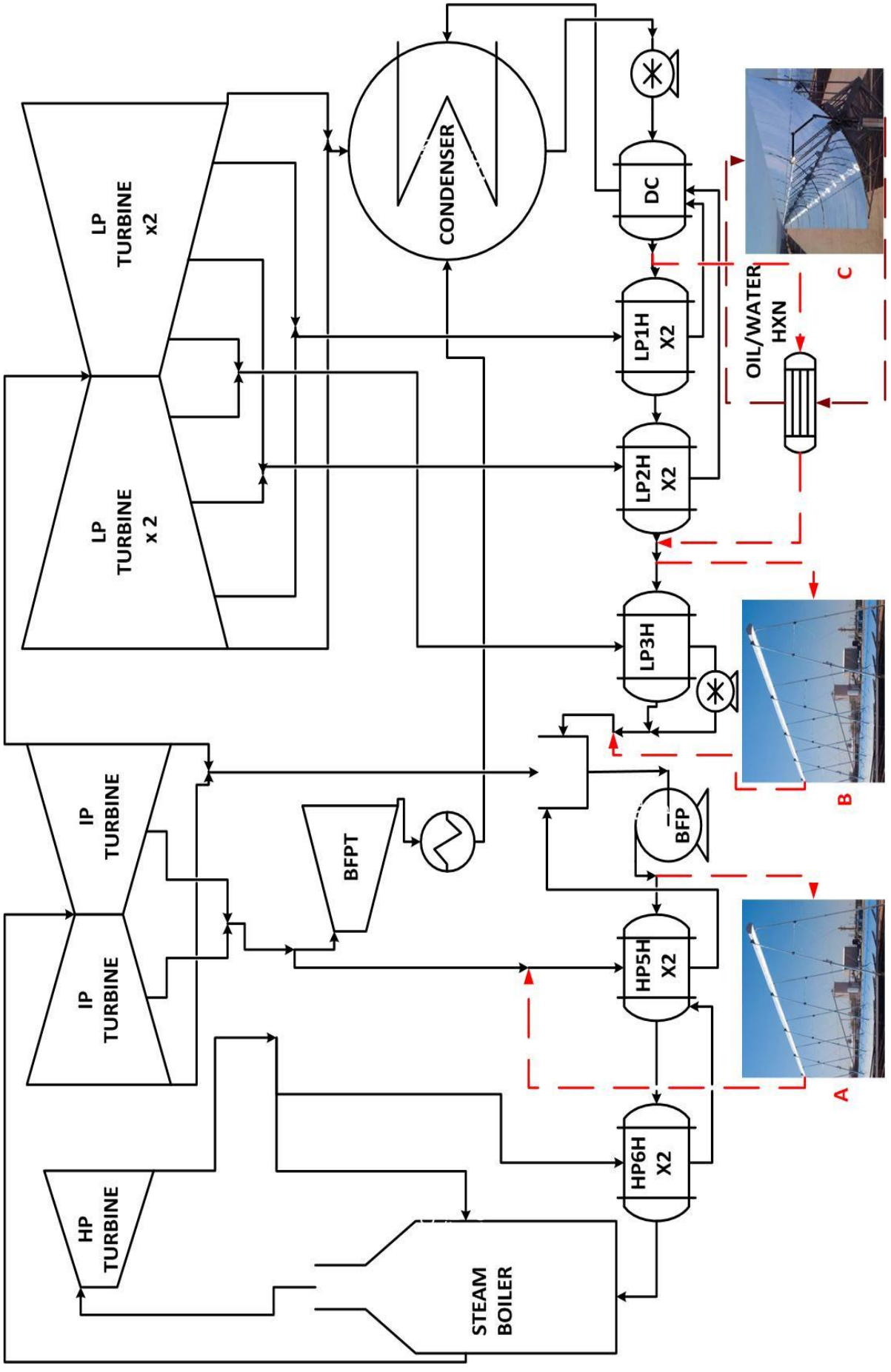

Figure 19 : Examples of Feedwater heating integration options. A: Bled steam supply to HPH5 using the LFR (Method 2), B: Bypassing of LPH3 using the LFR (Method 1), C: Bypassing of LPH1&2 using the PTC (Method 1). [121, 122]

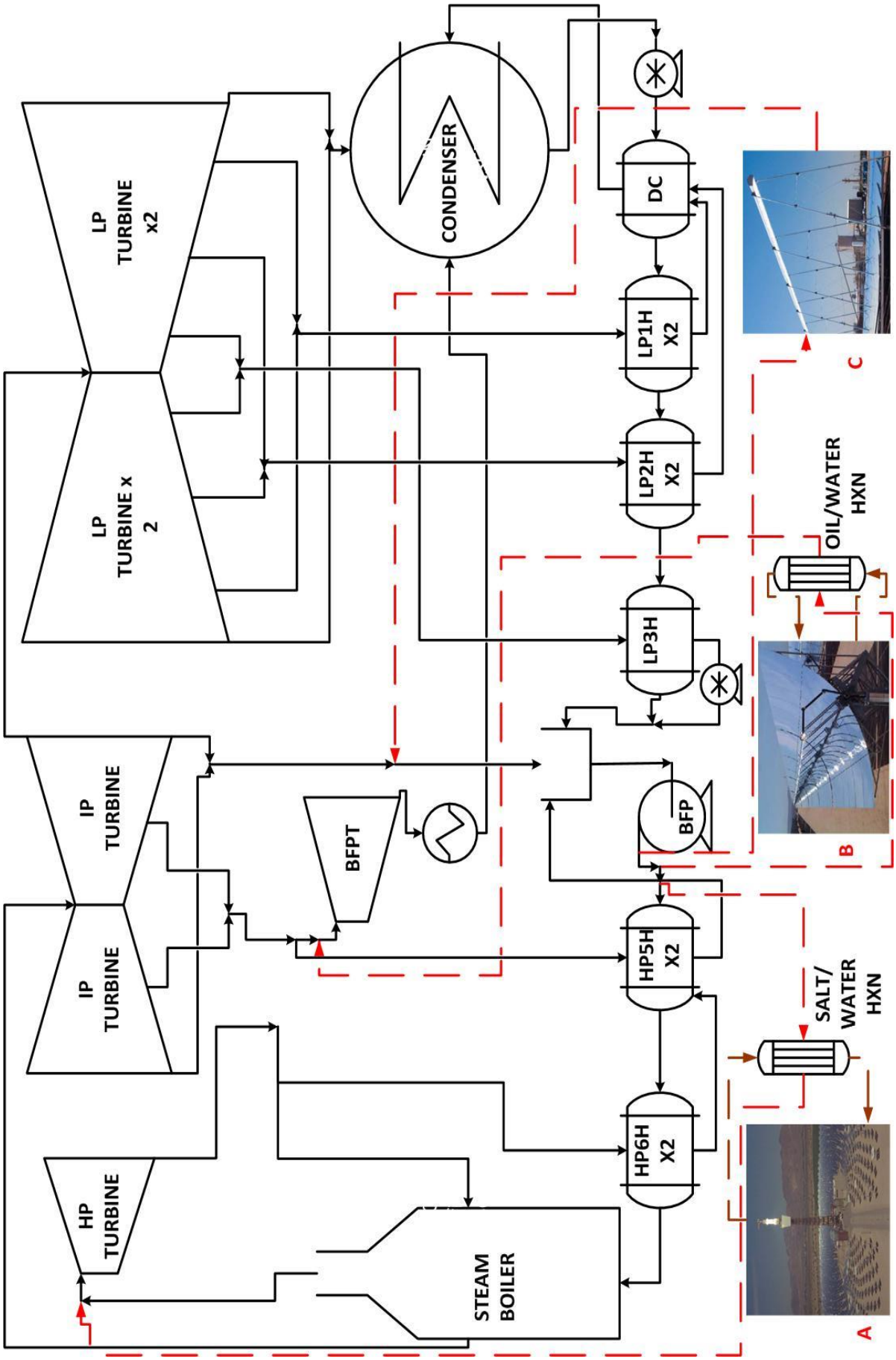

Figure 20: Examples of Superheated steam supply integration options. A: Steam supply to the HP turbine inlet using the CR, B: Steam supply to the BFPT inlet using the PTC, C: Steam supply to the DA inlet using the LFR. [121, 122, 35]

3.6 Plant technical capabilities

It is required to list the technical capabilities of each plant component of the Rankine cycle of the power station. This information is used, with the VirtualPlant™ model, to determine the maximum amount of solar heat that can be supplied by each integration option. The technical capabilities of each plant component are sourced from:

a) Original equipment manufacturer (OEM) data sheets.
b) Heat balance diagrams (HBD) that were developed by using the results from the acceptance tests of the power station.

The technical capabilities of the following plant areas were examined:

a) The boiler
b) The HP, IP and LP turbines
c) The main steam condenser
d) The boiler feedwater pump (BFP)
e) The BFP turbine
f) The condensate extraction pump (CEP)

A summary of the technical capabilities of the above plant areas, is provided in Table 10.

Table 10: Summary of plant technical capabilities (Maximum operating conditions)

Plant area	Mass flow (kg/s)	Pressure (MPa/kPa)	Temperature (°C)	Power (MW_e)
Boiler				
Feedwater inlet	507	25	247	-
Superheater outlet	507	19.4	540	-
Reheater inlet	448.7 (484.1*[10])	5.08 (4.6*)	332 (351.2*)	-
Reheater outlet	448.7 (495.2*)	5.08 (4.6*)	540	-
Turbines				
HP turbine	491.2*	16.32 (16.0*)	535	175
IP turbine	497.5*	3.62 (4.1*)	535	273.9
LP turbine	445.1*	0.5*	250*	250.2
BFP turbine	-	-	-	22
Main steam condenser				
Cold condenser	168.7 (197.6*)	14 (kPa abs)	-	-
Hot condenser	168.7 (197.6*)	16 (kPa abs)	-	-
Condensate extraction pump (CEP)				
CEP discharge	836	2.1	-	-
Boiler feedwater pump				
BFP suction	529.2 (601.2*)		-	-
BFP discharge	507 (579*)	23.4 (26.9*)	-	-

[10] * Values were sourced from an accepted HBD which has both HPH5 & HPH6 fully bypassed.

3.7 Rankine power cycle model

It is necessary to develop a thermodynamic model of the Rankine cycle of the power station. This model is used to predict the process flow changes that occur in the Rankine cycle of the power station, during the addition of solar heat. This model was developed by General Physics Corporation for Eskom, by using a software programme (VirtualPlant^{TM}), and is referred to as the VirtualPlant^{TM} model, in this study. The description and validation of the VirtualPlant^{TM} model is presented in chapter 4. An illustration of the VirtualPlant^{TM} model at full load[11] is presented in Figure 21.

[11] The generator output in Figure 21 is 612.5 MW_e which is equivalent to 600 MW_e once the fixed generator losses of 4.83 MW_e and a generator efficiency of 98.66 % are taken into account. The fixed losses and the generator efficiency in the VirtualPlant^{TM} model could not be changed.

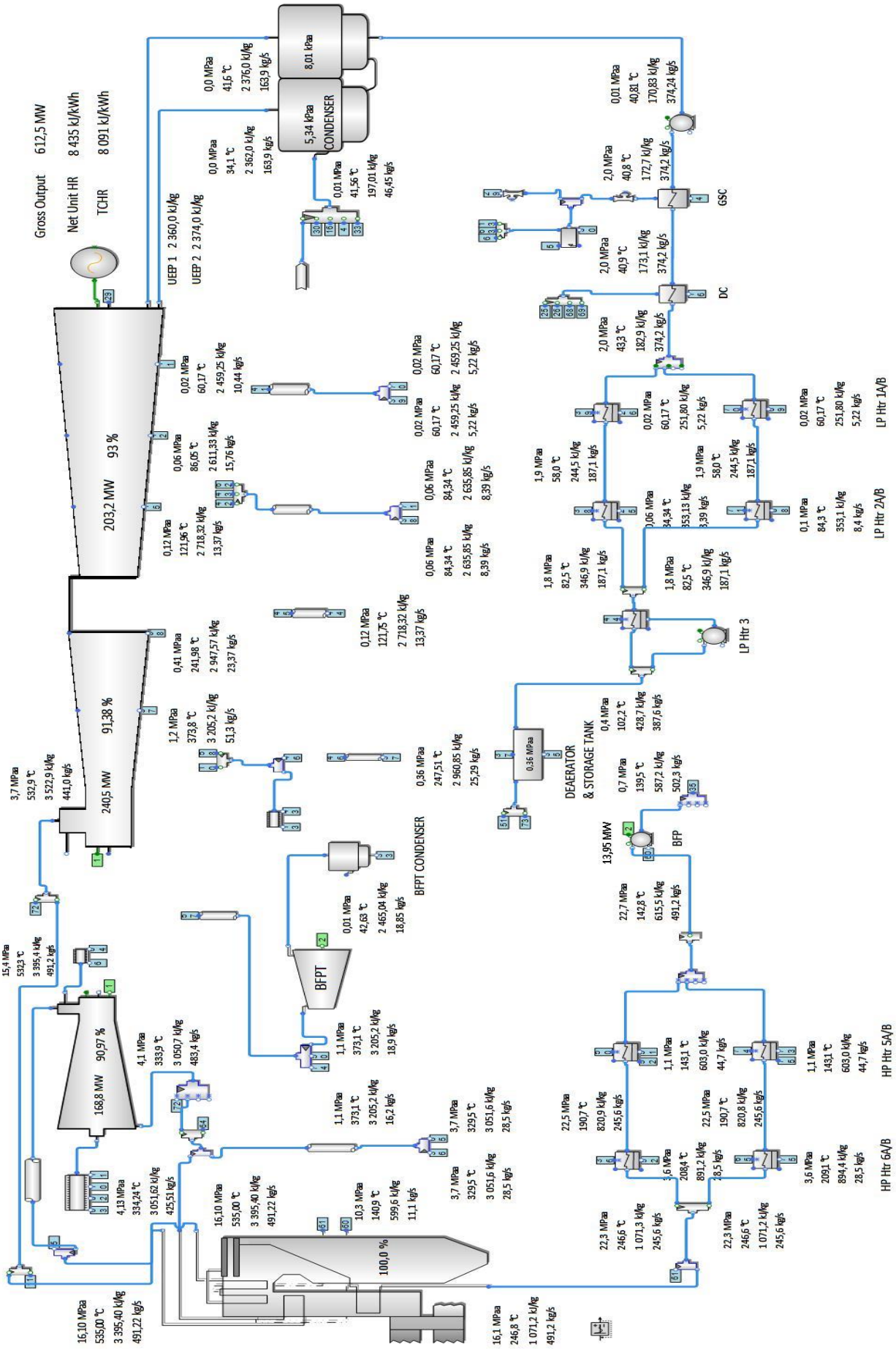

Figure 21: The VirtualPlant™ model at full load conditions

3.8 Solar field sizing

The maximum amount of solar heat that can be supplied by an integration option, to the Rankine power cycle of the power station is calculated as follows. Firstly, an integration option is configured to supply a given amount of solar heat, to the VirtualPlant™ model. The VirtualPlant™ model is then simulated to generate a full load i.e. 600 MW_e. Once the simulation was complete, the process flow conditions of the VirtualPlant™ model were noted. If the process flow conditions were found to exceed the technical capabilities of any plant area of the Rankine cycle of the power station, then the following was done:

1) The amount of solar heat that is supplied by the integration option is reduced.
2) The VirtualPlant™ model is simulated again, and the new process flow conditions are noted.
3) If the new process flow conditions in step 2 still exceeded any of the technical capabilities of the power station, steps 1 & 2 were repeated until all technical capabilities were met.

This process of iteration thus determined the maximum amount of solar heat that can be supplied by an integration option, while not exceeding any of the technical capabilities of every plant area of the Rankine power cycle of the power station. This maximum amount of solar heat is referred to as the 'design point solar heat' of an integration option, and is used as an input to the SAM model to determine the amount of land area and reflective area (aperture area) required for the solar field.

However, economics also does play a role in determining the 'design point solar heat' for each integration option. For example, The South African Revenue Service (SARS) grants a special depreciation allowance for solar energy projects that do not exceed a capacity of 30 MW_e [61]. Thus, to take advantage of this allowance, if the VirtualPlant™ model produced more than 30 MW_e of 'solar' electricity, during the addition of the 'design point solar heat', this amount of solar heat was further reduced until the 30 MW_e was achieved.

3.9 Solar field performance

It is required to predict the annual hourly heat output of the solar field (s) of each integration option. An integration option may have more than one applicable CSP technology, hence it may have more than one type of solar field. For example, the HPH6 (M2) feedwater heating integration option has a PTC and a LFR field, as summarized in Table 8. The annual hourly heat output of each solar field, is used to calculate the annual hourly heat rate reduction of the power station, for each integration option.

The annual hourly heat output from each solar field is predicted by using SAM.SAM calculates the annual hourly heat output from each CSP technology by using performance models. These CSP performance models were validated against performance data from commercial CSP projects. The inputs, that were chosen specifically for this study, to be used in the 3 CSP performance models (PTC, LFR and CR) in SAM, are discussed in detail in Appendix E. A summary of these inputs are provided here for convenience.

3.9.1 Inputs to CSP performance models

The PTC technology is modelled by using the *empirical trough* model in SAM. The EuroTrough ET150 solar collector assembly (SCA), and the Schott PTR70 heat collection element (HCE) was selected for this study.

The CR technology is modelled by using the *molten salt power tower* model in SAM. A heliostat area of 140 m^2, and a cavity tube receiver was selected for this study.

The LFR technology is modelled by using the *linear Fresnel* model in SAM. The Novatec Solar Boiler assembly with a recirculated loop flow configuration, was selected for this study.

3.10 Heat rate reduction of the power station

The hourly heat rate reduction of the power station is required to be calculated for each hour of solar heat input. The heat rate (HR) of the power station is defined as the amount of heat (from coal) that is required to produce a single kilowatt hour of electricity, HR thus has the units of kJ/kWh_e [20]. The HR of the power station is calculated by using equation(1) [20].

$$HR = \frac{3600B}{P} \tag{1}$$

Where,

$$B = \text{Boiler load}, [MW_t]$$
$$P = \text{Gross generator load}, [MW_e]$$
$$HR = \text{Heat rate}, [kJ / kWh_e]$$

The addition of solar heat to the power station, reduces the amount of heat required from coal, and hence reduces the HR of the power station. In the discussion that follows, the power station will be referred to as the coal plant, and when solar heat is added to the power station it will be referred to as the solar-coal plant.

The heat rate reduction of the power station is then the difference between the heat rate of the coal plant @ a given load, and the heat rate of the solar-coal plant @ the same load. This is represented by equation (2).The heat rate of the coal plant and the solar-coal plant were determined by using the VirtualPlant^{TM} model. The heat rate of the coal plant will be referred to as the reference heat rate.

$$\Delta HR = HR_{ref} - HR_{sc} \tag{2}$$

Where,

$$\Delta HR = \text{Heat rate reduction}, [kJ / kWh_e]$$
$$HR_{ref} = \text{Reference heat rate}, [kJ / kWh_e]$$
$$HR_{sc} = \text{Heat rate of the solar - coal plant}, [kJ / kWh_e]$$

But the solar-coal plant produces only two loads during the day i.e. A load = 600 MW_e during the 'Fuel-saving' mode, or a load > 600 MW_e during the 'Power-boosting' mode. Thus, two reference heat rates are to be determined. I.e. The heat rate of the coal plant at a load of 600 MW_e, and the heat rate of the coal plant at a load > 600 MW_e. The precise load during the 'Power-boosting' mode is dependent on the integration option and its 'design point solar heat'. The methods that are used

to calculate the reference heat rates, by use of the VirtualPlant™ model, are explained in sections 3.10.1 & 3.10.2.

Once the reference heat rates were determined, the next step towards calculating the hourly heat rate reduction of the power station was to determine the hourly heat rate of the solar-coal plant. The hourly heat rate of the solar-coal plant can be determined by simulating the VirtualPlant™ model (with an integration option configured) for each hour of solar heat input.

However, this process would be very time consuming. It was thus decided to determine the relationship between the heat rate of the solar-coal plant and solar heat input, for each integration option during the 'Fuel-saving' mode and the 'Power-boosting' mode. This was done by simulating the VirtualPlant™ model (with an integration option configured) at different solar heat input values, and noting the heat rate of the solar-coal plant. The solar heat input was varied from the 'design point solar heat' of each integration option to zero.

It was found that the heat rate of the solar-coal plant reduces approximately linearly as the solar heat input is increased i.e. an approximately linear relationship (of negative gradient) exists between the heat rate of the solar-coal plant and solar heat input. This is illustrated in Figure 22.

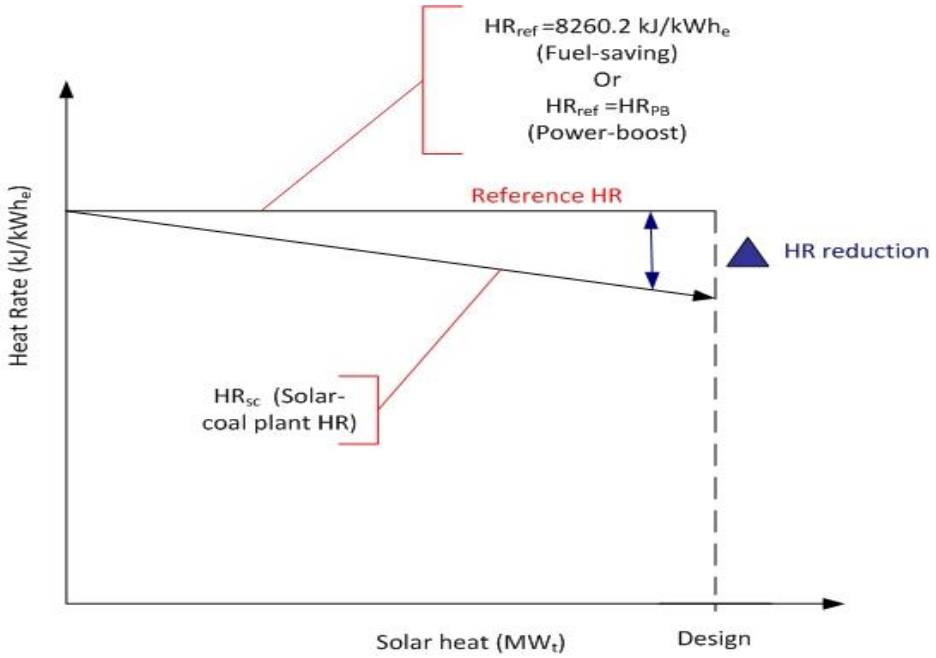

Figure 22: Solar-coal plant heat rate versus solar heat input.

Thus, to determine the annual hourly heat rate reduction of the power station for each integration option, the following was done:

1) The annual hourly heat output of the solar field, was exported from SAM to a Microsoft Office Excel spreadsheet.

2) The two linear relationships (heat rate of the solar-coal plant versus solar heat input, for the 'Fuel-saving' and 'Power-boosting' modes) was then used to determine the annual hourly heat rate of the solar-coal plant.

3) The heat rate reduction of the power station for each hour of the year was then calculated, by subtracting the heat rate of the solar-coal plant for each hour of the year from the applicable reference heat rate.

3.10.1 Fuel-saving mode

During the 'Fuel-saving' mode the VirtualPlant^{TM} model is configured to generate a gross electric output of 600 MW_e, with the addition of solar heat to the Rankine cycle. The boiler superheater outlet flow rate reduces consequentially during the 'Fuel-saving' mode, because of the addition of solar heat to the Rankine cycle. The full load outlet steam flow rate of the superheater is 491.2 kgs.

The reference heat rate during the 'Fuel-saving' mode was calculated by simulating the VirtualPlant^{TM} model to produce 600 MW_e, without the addition of solar heat. The boiler load was then noted from the VirtualPlant^{TM} model, and used in equation (1) to calculate the reference heat rate during the 'Fuel-saving' mode. The reference heat rate for the 'Fuel-saving' mode was calculated to be, excluding a boiler efficiency of 95 %[12]:

$$HR_{ref} = 8260.2 \ kJ / kWh_e$$

a) Heat rate of the solar-coal plant versus solar heat input

The relationship between the heat rate of the solar-coal plant and solar heat input, for each integration option during the 'Fuel-saving' mode, was calculated as follows. The VirtualPlant^{TM} model was simulated to maintain a load of 600 MW_e, whilst reducing the solar heat input to the Rankine cycle from the 'design point solar heat' to zero[13]. The heat rate of the solar-coal plant was noted as the amount of solar heat to the cycle was reduced. As mentioned in section 3.10, the heat rate of the solar-coal plant reduces approximately linearly as the solar heat input increases. The gradient (slope) of this linear relationship does vary across the integration options, because some integration options are more effective at reducing heat rate than others.

An auxiliary power consumption of 25 MW_e is specified for both the 'Fuel-saving' and the 'Power-boosting' modes. The auxiliary power, which is supplied by the generator, is the power consumption of the induced draft & forced draft boiler fans, the coal milling plant, the main cooling water pumps etc. The auxiliary power is subtracted from the generator gross output to calculate the net unit output.

[12] The calculation steps for determining heat rate reduction become simpler if the boiler efficiency is excluded from the reference heat rate. The boiler efficiency is included in the calculation of coal savings, greenhouse gas emission reduction & solar electricity production.

[13] The boiler reheater spray water flow rate is adjusted, according to an OEM trend, as the solar heat is reduced. This adjustment is done to account for the changes in reheater steam flow rate.

3.10.2 Power - boosting mode

During the 'Power-boosting' mode, the boiler in the VirtualPlant^{TM} model is configured to maintain full load superheater outlet flow rate i.e. 491.2 kg/s. The model is then simulated, with the addition of solar heat, and the generator output is observed. The generator output is consequentially > 600 MW_e. The amount of generator power that is produced is dependent on the solar heat integration option and the amount of solar heat supplied. This implies that the reference heat rate differs amongst the solar heat integration options, during the 'Power-boost' mode. Thus, the 'Power-boost' mode reference heat rate should be calculated for each integration option.

a) Reference heat rate

To calculate the 'Power-boost' reference heat rate for an integration option, it is first required to determine the maximum generator output that can be produced by the integration option. This was done by configuring the boiler in the VirtualPlant^{TM} model to maintain full load superheater outlet flow rate, whilst inputting the 'design point solar heat' of the integration option to the Rankine cycle[14]. The model was then simulated, and the generator output was noted. This generator output (> 600 MW_e) is referred to as the Boost Power of the integration option.

The 'Power-boost' reference heat rate of the integration option is thus, the heat rate of the VirtualPlant^{TM} model when it produces the same generator output (= Boost Power) with no addition of solar heat. Thus, it was required to establish a method to generate above 600 MW_e from the generator of the power station, without any solar heat addition to the power station.

It was found that the power station is designed to produce additional power (above 600 MW_e) by bypassing of the HP feedwater heaters, partially or completely. By bypassing the HP heaters, bled steam is saved which increases the generator power output. The complete bypass of the HP heaters can produce a generator output of 665 MW_e, however a review of the generator plant revealed that the generator can be operated safely at approximately 630 MW_e.

Thus, the method of bypassing HP feedwater heaters was used to determine the 'Power-boost' reference heat rate for the integration option. The 'Power-boost' reference heat rate was determined as follows. The boiler in the VirtualPlant^{TM} model is configured to maintain full

[14] The amount of solar heat that is added to the cycle during the 'Power-boosting' mode and during the 'Fuel-saving' mode may not be the same (to operate within the technical capabilities of the plant).

load superheater outlet flow rate, without any solar heat, and a portion of the feedwater flow to the HP heaters is bypassed. The amount of feedwater that is bypassed is such that, when the model is simulated its generator will produce an output that is equal to the Boost Power of the integration option. The boiler load of the model was then noted and used in equation (1) to determine the 'Power-boost' reference heat rate for the integration option. The 'Power-boost' reference heat rate is thus represented as:

$$HR_{ref} = HR_{PB} \tag{3}$$

Where,

$$HR_{PB} = \text{'Power - boost' reference heat rate}, [kJ / kWh_e]$$

b) Heat rate of the solar-coal plant versus solar heat input

The relationship between the heat rate of the solar-coal plant and solar heat input, for each integration option during the 'Power-boosting' mode, was calculated as follows. The VirtualPlant^{TM} model was simulated to maintain a load equal to the Boost Power of the integration option, whilst reducing the solar heat input to the Rankine cycle from the 'design point solar heat' to zero. The heat rate of the solar-coal plant was noted as the amount of solar heat to the cycle was reduced.

3.11 Integration effectiveness

It is unclear as to which integration options are the most effective at reducing plant heat rate, this is because the amount of solar heat supplied by each integration option is not the same. Thus, it was necessary to develop a method to calculate the effectiveness of each integration option. It was decided that the Integration effectiveness (IE) of each integration option, should express the heat rate reduction of the plant relative to the amount of solar heat supplied. The IE of an integration option is thus calculated by using equation(4).

$$IE = \frac{\Delta HR}{SH} \tag{4}$$

Where,

$$IE = \text{Integration effectiveness}, kJ / kWh_e.MW_t$$
$$\Delta HR = \text{Heat rate reduction}, kJ / kWh_e$$
$$SH = \text{Solar heat}, MW_t$$

3.12 Power station operation modes

The power station, as discussed in sections 3.10.1 & 3.10.2, can operate on either a 'Fuel-saving' or a 'Power-boosting' mode, during the addition of solar heat. The selection of an operating mode during the day, is dependent on the time at which the solar resource is available, and the load profile of the national electricity grid. The typical summer and winter daily load profiles, for electricity in South Africa, are shown in Figure 23.

During the winter-autumn months, i.e. April to August, DNI levels are high (> 651 W/m^2), and are available from 9am-3pm. The winter load profile is higher than the summer load profile, and it has two peaks. These peaks occur in the morning (7am-9am) and in the afternoon (5pm- 9pm), as illustrated in Figure 23. Although the time at which the solar resource during the winter-autumn months occurs, does not coincide with the times of two load peaks, it was decided to operate the power station on the 'Power-boosting' mode during 9am-3pm. This will support the electricity grid during the day[15].

During the spring-summer months, i.e. September to March, DNI levels are moderate, due to cloud cover, and are available from 9am-5pm.The summer load profile has no characteristic peaks, unlike the winter load profile. Thus, to take advantage of the solar resource that is available, it was decided to operate the power station on the 'Power-boosting' mode from 9am-5pm, during the spring-summer months.

During the times that the power station does not operate on the 'Power-boosting' mode, it will operate on the 'Fuel-saving' mode. The seasonal operating modes of the power station, as per this discussion, are tabulated in Table 11.

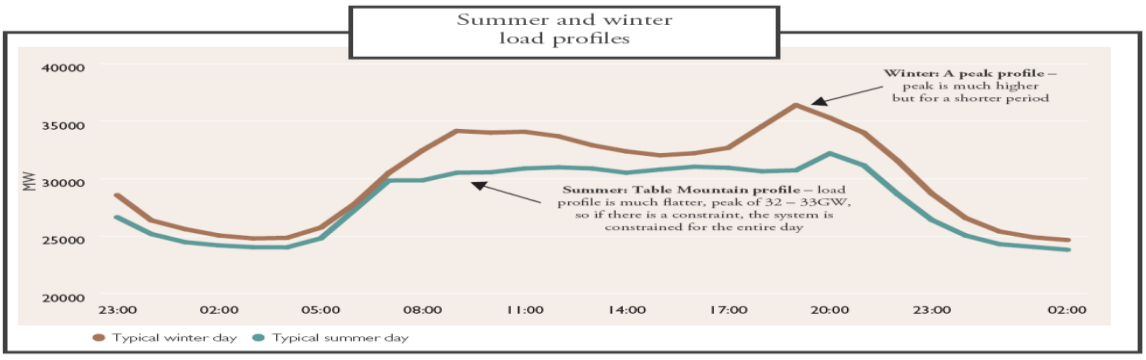

Figure 23: Summer and winter typical daily load profiles. [62]

[15] Thermal energy storage (TES) can be used to supply solar heat to the power station, during the morning and afternoon peaks, however TES was not considered for this use in this study, for the sake of simplicity.

Table 11: Seasonal operating modes of the power station

Seasons	Operating mode	Duration
Winter - Autumn (April - August)	Fuel-saving	3pm to 12pm to 9am
	Power-boosting	9am to 3pm
Summer - Spring (September - March)	Fuel-saving	5pm to 12pm to 9am
	Power-boosting	9am to 5pm

3.13 Project benefits

There are essentially four benefits associated with integrating solar heat to the regenerative Rankine power cycle of the power station. The benefits are coal savings, Greenhouse gas (GHG) emission reduction, 'solar' electricity production and carbon tax savings. The methods that are used to calculate these benefits are described in sections 3.13.1-3.13.4. The first benefit which is calculated is the hourly coal savings of the power station. The hourly coal savings is calculated by using the hourly heat rate reduction of the power station. Once the hourly coal savings were calculated, it was used to calculate the hourly GHG emission reduction and the hourly 'solar' electricity production of the power station. Lastly, the annual carbon tax savings of the power station is calculated.

An annual availability factor and capacity factor of 0.9 & 0.8 respectively, was used for the power station (based on historic data). These factors are applied to the annual coal savings, annual GHG emission reduction and the annual solar electricity production. A solar plant availability factor of 0.96 [61] was specified in the SAM program.

3.13.1 Coal savings

The hourly coal savings that is achieved by each solar heat integration option, is calculated by using equation(5). The derivation of equation(5) is presented in Appendix A. As explained, the hourly heat rate reduction is used in equation(5), to calculate the hourly coal savings.

$$CS = \frac{\dot{E} \times \Delta HR}{1000 \times NCV \times \eta_b} \tag{5}$$

Where,

CS = Hourly coal savings, [tonnes / hour]
$\dot{E}$ = Hourly electricity power output of a single unit, i.e. $\geq$ 600 MW_e
E = Hourly electricity production of a single unit, i.e. $\geq$ 600 MWh_e
ΔHR = Hourly heat rate reduction of the power station, [kJ / kWh]$_e$
NCV = Net calorific value of coal, 22.35, [MJ / kg]
η_b = Coal boiler thermal efficiency, 95 , [%]

The coal NCV has a range of 21.5 - 23.2 MJ/kg, which is based on the agreement between the coal mine and the power station. The average coal NCV of 22.35 MJ/kg is used in this study.

During the 'Fuel-saving' mode, the hourly electricity production of the unit is 600 MWh_e i.e. E= 600 MWh_e. As mentioned in section 3.12, the unit will operate on the 'Fuel-saving' mode during all hours of the day except during, 9am-3pm (in winter) and 9am-5pm (in summer). During the 'Power-boosting' mode, the electricity production of the unit is > 600 MWh_e i.e. E> 600 MWh_e. The precise electricity production of the unit, during the 'Power-boosting' mode, is dependent on the integration option. The unit will operate on the 'Power-boosting' mode during, 9am-3pm (in winter) and 9am-5pm (in summer).

The annual coal savings (expressed in Rands) is calculated by applying the cost of coal (R200/ton) [63, 64] to the annual coal saved (expressed in tons).

3.13.2 Greenhouse gas emission reduction

Greenhouse gases are produced from the combustion of coal. Thus, the hourly greenhouse gas (GHG) emission reduction of the power station, is calculated by using the hourly coal savings of the power station. The hourly GHG emission reduction, in terms of carbon dioxide equivalence (CO_{2eq}), is calculated by using equation(6). The derivation of equation(6) is presented in Appendix A. Carbon dioxide, methane and nitrous oxide are the GHGs that are produced from the combustion of coal, and hence will be examined in this study [65].

$$ER = \frac{(\varepsilon_{CO_2} + \varepsilon_{CH_4} \times GWP_{CH_4} + \varepsilon_{N_2O} \times GWP_{N_2O}) \times NCV \times CS}{1000} \quad (6)$$

Where,

$$\begin{aligned} ER &= \text{Hourly GHG emission reduction, } [tCO_{2eq} \text{ / hour}] \\ \varepsilon_{CO_2} &= \text{Carbon dioxide emission factor, } 96.25, [\text{kg / GJ}] \\ \varepsilon_{CH_4} &= \text{Methane emission factor, } 0.001, [\text{kg / GJ}] \\ GWP_{CH_4} &= \text{Global Warming Potential of } CH_4, 25 \\ \varepsilon_{N_2O} &= \text{Nitrous oxide emission factor, } 0.0014, [\text{kg / GJ}] \\ GWP_{N_2O} &= \text{Global Warming Potential of } N_2O, 298 \\ NCV &= \text{Net calorific value of coal, } 22.35, [\text{MJ / kg}] \\ CS &= \text{Hourly coal savings, } [\text{tonnes / hour}] \end{aligned}$$

The emission factors that are used in this study, are for the existing coal power station fleet of Eskom [66]. The Global Warming Potential factor of methane and nitrous oxide is obtained from the Intergovernmental Panel on Climate Change (IPCC) Fourth Assessment Report [67].

3.13.3 Solar electricity production

The hourly solar electricity production of each solar heat integration option is also calculated by using the hourly coal savings. Equation (7) is used to calculate the hourly solar electricity production. The derivation of equation (7) is presented in Appendix A.

$$E_s = \frac{CS \times NCV \times \eta_b}{HR_{ref}} \quad (7)$$

Where,

E_s = Hourly solar electricity production, [GWh_e]
HR_{ref} = Reference heat rate, [kJ / kWh_e]
CS = Hourly coal savings, [tonnes / hour]
NCV = Net calorific value of coal, 22.35, [MJ / kg]
η_b = Coal boiler thermal efficiency, 95, [%]

The revenue that is generated by selling the solar electricity, is calculated by applying an electricity tariff. Two electricity tariffs are examined in this study i.e. the Homelight 60A tariff and the Renewable Energy Feed-In Tariff.

The Homelight 60A tariff, is the electricity tariff which is charged by Eskom, to residential customers that have medium/high electricity usage. The Homelight 60A tariff, for a residential customer that consumes > 600 kWh_e per a month, is R1.50/ kWh_e. [68]

The Renewable Energy Feed-In Tariff (REFIT), is an electricity tariff that is approved by the National Energy Regulator of South Africa (NERSA) for a renewable energy generator. The REFIT tariff is only applicable to Independent Power Producers (IPPs) and, does not apply to hybrid power plants (such as a solar-coal power plant). However, it would be interesting to investigate what would be the economic outcome, if the REFIT was applicable to this project, as the REFIT tariff structure recognises that the cost of electricity generation from CSP is greater than from coal. The REFIT structure is presented in Table 12. [69]

Table 12: REFIT structure. [69]

Year	Solar technology	Tariff (R/kWh$_e$)
REFIT 2013	CSP Parabolic trough collector	1.967
	CSP Power tower[16]	1.417
	CSP Linear Fresnel reflector[17]	1.967

3.13.4 Carbon tax savings

A carbon tax is proposed for SA, to be effective on the 1st of January 2015.The carbon tax is calculated by applying a carbon tax rate of R120/tCO_{2eq}, to the actual GHG emissions released by the power station. Hence, the carbon taxes that would be payable by the power station are reduced, because the addition of solar heat reduces the annual GHG emissions from the power station. [7]

A tax-free threshold of 60% is granted during the 1st phase of the carbon tax (2015-2019), which implies that 60% of the annual GHG emissions from the power station are exempt from the carbon tax. The carbon tax policy also takes into consideration the carbon intensity of the power station, which is the amount of CO_{2eq} released per a unit of electricity produced. Carbon intensity has the units of tCO_{2eq}/MWh$_e$. For example, if the carbon intensity of the power station is lower than a benchmark intensity (which is stipulated in the carbon tax policy), the tax-free threshold is increased, and vice versa. The average carbon intensity of Eskom's coal-fired power stations, is estimated as 0.96 tCO_{2eq}/MWh$_e$ [70], which is used for the power station. The benchmark carbon intensity for the electricity sector during the first phase of the carbon tax is 0.91 tCO_{2eq}/ MWh$_e$. The benchmark carbon intensities for the electricity sector and the carbon tax rates, during the first two phases of the carbon tax policy are presented in Table 13. The carbon tax savings is calculated by using equation (8). The derivation of equation (8) is presented in Appendix A. [7]

[16] The REFIT tariff specified by NERSA is for the Power Tower technology with 6 hrs thermal energy storage (TES). This tariff is used in this study, although TES is not considered in this study, because a tariff for the Power Tower technology without TES is not available. Also noted is that the tariff for the Power Tower is lower than the tariff for the PTC. One of the reasons for the Power Tower tariff been lower than the PTC tariff is because the Power Tower has 6 hours TES, hence it will have a higher load factor.

[17]There was no REFIT specified for the LFR technology, thus it was assumed for this study that the tariff for the LFR technology is the same as the PTC REFIT, because both are line focusing technologies.

$$CT_{saved} = \left[G_c \times \left(1 - \frac{60}{100} \times \left(\frac{BI}{AI} \right)_c \right) - G_{sc} \times \left(1 - \frac{60}{100} \times \left(\frac{BI}{AI} \right)_{sc} \right) \right] \times \frac{CT_R}{10^6} \quad (8)$$

Where,

CT_{saved} = Annual carbon tax savings, [Rm]

G_c = Annual GHG emissions of the coal power plant, [tCO_{2eq} /year]

G_{sc} = Annual GHG emissions of the solar - coal power plant , [tCO_{2eq} /year]

AI = Power plant actual carbon intensity, [tCO_{2eq} /MWh_e]

BI = Power plant benchmark carbon intensity, [tCO_{2eq} /MWh_e]

CT_R = Carbon tax rate, [R / tCO_{2eq}]

Table 13: Benchmark carbon intensities for the electricity sector and carbon tax rates. [7]

Carbon tax phase	**Benchmark intensity (tCO_{2eq}/MWh_e)**	**Carbon tax rate (R/tCO_{2eq})**
1st phase (2015-2019)	0.91	120, annual 10 % increase.
2nd phase (2020-2025)	0.8	New rate of increase to be announced.

An additional economic benefit which is applicable to this project is depreciation allowance. Depreciation is a means of recovering, through an income tax deduction, the cost of property used in a business [56]. The South African Revenue Service (SARS) grants a special depreciation allowance for solar energy projects which do not exceed 30 MW_e. The allowance is granted during the first 3 years of the life of the project, as stipulated in Table 14. [61]

Table 14: SARS depreciation allowance for solar energy projects. [61]

Tax year	**Depreciation allowance granted (% of CAPEX)**
1	50
2	30
3	20

3.14 Project costs

There are three costs associated with this project i.e. a capital cost, an operating & maintenance cost and an income tax cost. The methods which are used to calculate these project costs are explained in sections 3.14.1-3.14.5.

The capital expenditure (CAPEX) and the operating and maintenance expenditure (OPEX), for each CSP technology, are estimated by using reference cost models. These cost models were developed by the National Renewable Energy Laboratory (NREL) of the United States Department of Energy, with support from organisations such as WorleyParsons Group Inc. and Sandia National Labs. These cost models are available in NREL's System Advisor Model (SAM). [57, 58]

The costing models are tabulated in Table 15 and Table 16. A discussion on the relevant reference values that are used in the cost models, are presented in Appendix D. The income tax for the project is calculated by applying an income tax rate to the taxable income of the project.

3.14.1 Capital expenditure (CAPEX)

The CAPEX for each CSP technology, also referred to as the total installed cost, is the sum of Direct capital costs and Indirect capital costs [71]. These two cost categories are described below:

a) Direct capital costs: Direct capital costs are expenses for specific pieces of equipment or installation services that apply in year zero of the cash flow. E.g. the cost of the field mirrors, the HTF system, etc.

b) Indirect capital costs: Indirect capital costs are expenses that cannot be related with specific pieces of equipment or installation services. E.g. Engineer-procure-construction (EPC) costs, land costs etc.

It should be noted that although the CAPEX cost model does fairly accurately determine the cost of the solar plant, the CAPEX estimate is considered to be at a high level for this project. This is because it does not account for, the cost of plant downtime during implementation, possible inflation in material prices and the cost to 'tie-in' the integration option to the power station. The costs mentioned were not included in this study because it was decided to first evaluate the economic feasibility of the integration options based on the high-level CAPEX estimate. If any integration options were found to be economically feasible based on the high-level CAPEX estimate then the next step would be, to re-evaluate the economic feasibility of those integration option (s) by including the mentioned additional costs.

3.14.2 Annual loan repayment

It was assumed that a financial institution (such as The World Bank) could be approached to finance the CAPEX of this project. This is a fair assumption because the Eskom renewable energy projects i.e. the Upington CSP project and the Sere Wind project, were funded by The World Bank [72]. The annual loan repayment to the financial institution is amortized (divided into equal payments) over the life of the project, and is calculated by using equation (9) [56].

$$L_r = UCRF \times CAPEX \tag{9}$$

The uniform capital recovery factor (UCRF) is defined as:

$$UCRF = \frac{(i \times (1+i)^n)}{((1+i)^n - 1)}$$

Where:

L_r = The annual loan repayment, [Rm]
i = The annual loan interest rate, [%]
n = The loan repayment period, [years]

The loan interest rate applied is 8.8 %, which is the lending interest rate to South Africa by The World Bank [73]. The loan repayment term is 30 years, which is the economic life of each CSP technology [74, 75]. Typically, Eskom's coal-fired power plants have an operating life of 60 years, which is usually extended for a few years beyond the 60 year cycle. The Unit 1 of the power station first came into operation in 1981, thus sufficient remaining power plant life exists to ensure that the solar plant is used to its full expected life.

3.14.4 Operating and maintenance expenditure (OPEX)

The annual OPEX cost for each CSP technology consists of a fixed cost by capacity and a Variable Cost by generation [71]. These two cost categories are described below:

a) Fixed cost by capacity[18]: This is a fixed annual cost that is proportional to the nameplate capacity of the solar plant.

b) Variable cost by generation[18]: This is a variable annual cost that is proportional to the annual solar heat production of the solar field.

[18] Refer to Appendix D.

Table 15: CAPEX cost model (Source: SAM)

Cost category	Unit	CSP Technology		
		Molten Salt Tower	**Parabolic Trough Collector**	**Linear Fresnel Reflector**
Direct capital cost (DC) category				
Site preparation costs (per reflective area)	$/m^2	15	30	20
Solar collector field system (per reflective area)	$/m^2	180	270	210
Heat transfer system (per reflective area)	$/m^2	0	80	35
Steam generation system[18]	$/kW$_t$	144.2	41.15	0
TES system	$/kWh$_t$	27	80	0
Tower	$	$FC \times e^{(h \times 0.0113)}$ [19]		
Receiver	$	$RC \times (RA / RRA)^{0.7}$ [20]		
Contingency allowance	% of DC	10	10	10
Indirect capital cost (IC) category				
EPC & Owner costs	% of DC	11	11	11
Land (per land area)[18]	R/m^2	65	65	65

Table 16: OPEX cost model (Source: SAM)

Cost category	Unit	Molten Salt Tower	Parabolic Trough	Linear Fresnel Reflector
Fixed cost by capacity	$/kW$_t$-yr.	26.8	24.53	20.9
Variable cost by generation	$/MWh$_t$	1.65	1.51	1.52

[19] Reference values from SAM.FC=$3 m, h=tower height (m).

[20] Reference values from SAM.RC=$110 m, RA=receiver area (m^2), RRA=1571 m^2.

3.14.5 Annual income tax

The annual income tax payable to SARS is calculated at a rate of 28 % (which is the income tax rate stipulated for companies) on all taxable income [61]. Taxable income is all revenues, less the depreciation allowance, less the OPEX costs and the loan repayment interest cost [56]. The annual income tax for this project is thus calculated by using equation(10).

$$T_A = T_r \times (R_g + CT_{saved} + CS_A - D_A - L_i - O\&M_F - O\&M_V) \quad (10)$$

Where,

T_A = Annual income tax, [Rm]
T_r = Income tax rate, 28, [%]
R_g = Annual gross revenue, [Rm]
CT_{saved} = Annual carbon tax savings, [Rm]
CS_A = Annual coal savings, [Rm]
D_A = Annual depreciation allowance, [Rm]
L_i = Annual loan interest repayment, [Rm]
$O\&M_F$ = Annual fixed OPEX cost, [Rm]
$O\&M_V$ = Annual variable OPEX cost, [Rm]

3.15 Economic life-cycle assessment

The final stage of the study was to perform an economic life-cycle assessment (LCA) for each integration option. The LCA calculates economic measures by evaluating the projects costs and benefits over each year of the life of the project [56].The economic measures are calculated according to methods explained in [56], these methods are presented in section 3.15.1.The validation of the LCA model is presented in chapter 4 section 4.2.

3.15.1 Economic measures

There are 5 economic measures which are calculated in this study. The 1st two economic measures which are calculated are the Net present value (NPV) and Total life cycle cost (TLCC). The TLCC is then used to calculate the Levelised cost of electricity (LCOE).The final economic measures which are calculated are the Simple payback period (SPB) and the Discounted payback period (DPB). The derivation of the formulas that are used in this study to calculate the economic measures, are presented in Appendix A.

1) Net present value (NPV): The NPV of the project is the difference between the present value of cash inflows and the present value of cash outflows (costs), during the life of the project [76]. The NPV of the project is calculated by using equation(11).

$$NPV = \sum_{n=0}^{n=30} \frac{(R_g + CT_{saved} + CS_A - T_A - L_r - O\&M_F - O\&M_V)_n}{(1+d_r)^n} \quad (11)$$

Where,

R_g = Annual gross revenue, [Rm]
CT_{saved} = Annual carbon tax savings, [Rm]
CS_A = Annual coal savings, [Rm]
T_A = Annual income tax, [Rm]
L_r = Annual loan repayment, [Rm]
$O\&M_F$ = Annual fixed OPEX cost, [Rm]
$O\&M_V$ = Annual variable OPEX cost, [Rm]
d_r = Annual real discount rate, [%]

2) Total life-cycle cost (TLCC): The TLCC of the project is the sum of all costs during the life of the project. These costs are then discounted to the 1st year of the project. The TLCC is calculated by using equation(12). [56]

$$TLCC = \sum_{n=0}^{n=30} \frac{(T_A + L_r + O\&M_F + O\&M_V)_n}{(1 + d_r)^n} \quad (12)$$

Where,

T_A = Annual income tax, [Rm]
L_r = Annual loan repayment, [Rm]
$O\&M_F$ = Annual fixed OPEX cost, [Rm]
$O\&M_V$ = Annual variable OPEX cost, [Rm]
d_r = Annual real discount rate, [%]

3) Levelised cost of electricity (LCOE): The LCOE is the cost of producing each unit of electricity during the life of the project. LCOE is calculated by using equation(13). [56]

$$LCOE = \frac{TLCC}{\sum_{n=1}^{n=30} \frac{Q_n}{(1+d_r)^n}} \quad (13)$$

Where,

LCOE = The levelised cost of electricity, [R / kWh_e]
TLCC = The total life - cycle cost, [Rm]
Q_n = Solar electricity produced in year n, [GWh_e]
d_r = Annual real discount rate, [%]

4) Simple payback period (SPB): The SPB is the number of years required to recover the project's capital investment cost (CAPEX) [56]. SPB is the first point in time when [56]:

$$\sum_{n} \Delta I_n \leq \sum_{n} \Delta S_n \quad (14)$$

Where,

SPB = The minimum number of years required for the nondiscounted sum of annual cash inflows net annual costs to equal the nondiscounted investment costs, [years]
ΔI = The nondiscounted incremental investment costs, [Rm]
ΔS = The nondiscounted sum of annual cash inflows net annual costs, [Rm]

5) Discounted payback period (DPB): The DPB is the number of years required to recover the project's capital investment cost (CAPEX), taking into consideration the time value of money [56]. DPB is the point in time when [56]:

$$\sum_n \frac{\Delta I_n}{(1 + d_r)^n} \leq \sum_n \frac{\Delta S_n}{(1 + d_r)^n} \quad (15)$$

Where,

DPB = The minimum number of years required for the discounted sum of annual net savings to equal the discounted incremental investment costs, [years]

ΔI = The incremental investment costs, [Rm]

ΔS = The annual net savings, [Rm]

d_r = The real discount rate, [%]

The value of the real discount rate that is used in this study is 8 %.This rate was approved by NERSA, for state owned companies, such as Eskom. [77]

4. Model validation

The following chapter provides the validation of the models which are described in sections 3.7 and 3.15 of chapter 3. The models are:

1. The power plant model
2. The economic life-cycle assessment model

4.1 The power plant model

The power plant model is used to predict the thermodynamic performance of a unit of the power station i.e. Heat rate reduction and process flow changes. The power plant model was developed by using the VirtualPlant™ software programme, thus it is referred to as the VirtualPlant™ model in this study. In the discussion that follows a description of the plant components that constitute the VirtualPlant™ model & their respective inputs is provided. A summary and discussion of the validation results of the VirtualPlant™ model is provided at the end of this section.

4.1.1 Software tool

VirtualPlant™ is a software programme that is designed to model the steady state performance of power cycles such as conventional fossil power plants, combined cycle power plants and nuclear power plants [78]. VirtualPlant™ is obtained by Eskom through a license agreement with General Physics Corporation.

The VirtualPlant™ model, originally built by General Physics Corporation for Eskom, was 'fine-tuned' to achieve the accuracy required to validate the model for this study. The model consists of connected power plant components such as, a boiler, a feedwater pump etc. During a simulation of the VirtualPlant™ model, the results of the model will converge once the conservation of mass and energy for each plant component is satisfied according to the 1st law of thermodynamics [78].

4.1.2 Power plant components

The VirtualPlant^{TM} model consists of a coal-fired boiler, a HP turbine, an IP/LP turbine, a condenser, a feedwater heating plant, a boiler feedwater pump, a solar heat source and a generator. The following section provides a description of the functionality of each plant component and the input value (s) required for each plant component. The input value (s) for each power plant component is referenced from the relevant plant OEM.

a) Coal-fired boiler

The coal-fired boiler component from VirtualPlant^{TM} is presented in Figure 24. The coal-fired boiler is responsible for the superheating of the feedwater flow and the reheating of the exhaust steam from the HP turbine. The required heat for the boiler is calculated by applying an energy and mass balance across the boiler. An outlet steam temperature of 535 ^{o}C is specified for both the superheater & reheater. The pressure drop in the reheater is set at 13,4 % of the absolute pressure at the reheater inlet. The combustion efficiency of the boiler is set at 95 %.The reheater attemperating spray water flow, which is supplied from an intermediate stage of the boiler feedwater pump, is determined by using the OEM trend illustrated in Figure 25.

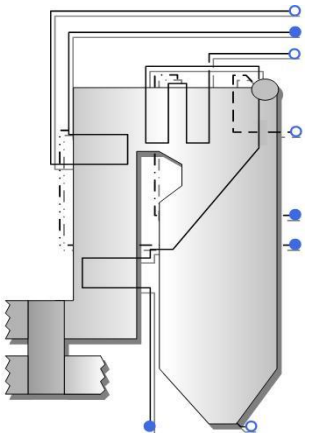

Figure 24: Coal-fired boiler. [78]

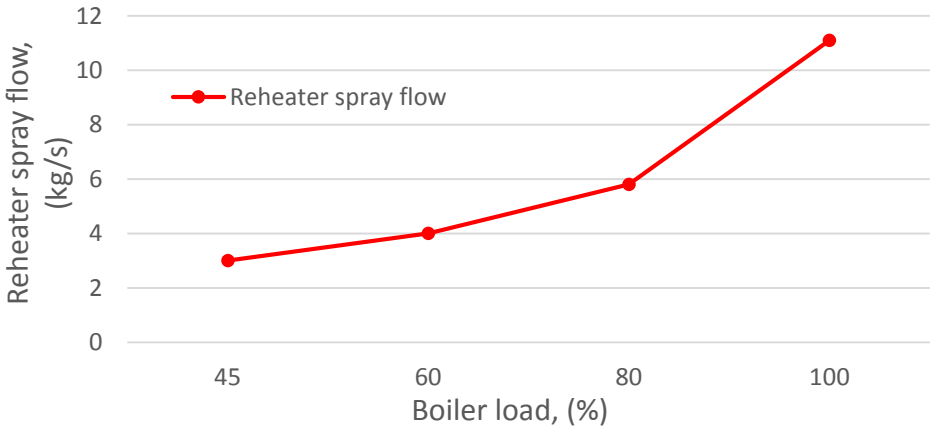

Figure 25: Reheater spray water flow versus boiler load. [79]

As illustrated in Figure 25, the reheater spray water flow increases with boiler load, the explanation for this trend is as follows. The reheater is heated by flue gases in the boiler. Thus, as the boiler load increases (hence the flue gas flow increases) more spraywater is required to control the reheater outlet temperature. The trend illustrated in Figure 25 is applicable during normal plant operation.

Thus, the use of this trend may not be entirely correct because the integration options produce process flow changes in the plant. However, the impact of reheater spray flow does not significantly affect the results. For example, the VirtualPlant™ model was simulated to produce 600 MW_e, but with the reheater spray flow reduced from 11,1 kg/s to 0 kg/s. The results revealed that the heat rate of the plant changed by just 0,5 %.

The input values and figure mentioned are sourced from STEINMÜLLER documentation, as these values accurately represent the boiler performance at design.

b) High-pressure turbine

The HP turbine component from VirtualPlant™ is presented in Figure 26.The high-pressure turbine extracts power from and expands the outlet superheater steam flow. The power extracted by the HP turbine and the efficiency of the HP turbine is calculated by using a publication by The American Society of Mechanical Engineers (ASME) [80, 78]. The pressure before the HP turbine governor valves is fixed at 16.1 MPa. The pressure loss across the HP turbine governor valves is specified as 6 % during full load plant operation. The valves-wide-open (full load) steam flow to the HP turbine is set at 491.2 kg/s.

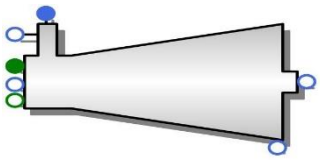

Figure 26: HP turbine. [78]

The input values mentioned are sourced from GEC Turbine-Generators Ltd. documentation, as these values accurately represent the turbine performance at design.

c) Intermediate-pressure and low-pressure turbine

The IP/LP turbine component from VirtualPlant™ is presented in Figure 27. The double-flow intermediate-pressure (IP) turbine and the two double-flow low-pressure (LP) turbines of the power station are modelled in *VirtualPlant™ by* an IP/LP turbine component.

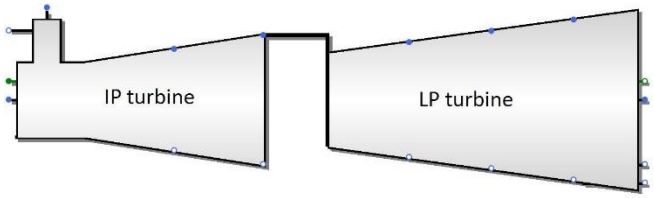

Figure 27: IP and LP turbine. [78]

The IP turbine extracts power from and expands the reheated steam flow. The exhaust steam flow from the IP turbine expands through the LP turbines to the condenser. Steam is extracted from two points on the IP turbine cylinder and from three points on the LP turbine cylinder to supply the HP and LP feedwater heating plant.

The power extracted by the IP/LP turbine, the efficiency of the IP/LP turbine, the exhaust losses and the extracted steam mass flow rates are predicted by using a publication by The American Society of Mechanical Engineers (ASME) [80, 78]. The two extraction pressures on the IP turbine cylinder

are specified as 1.21 MPa and 0.41 MPa. The three extraction pressures on the LP turbine cylinder are specified as 0.12 MPa, 0.06 MPa and 0.02 MPa. The pressure loss across the IP turbine governor valves is specified as 3.7 %.

The input values mentioned are sourced from GEC Turbine-Generators Ltd documentation, as these values accurately represent the turbine performance at design.

d) Condenser

The condenser component from VirtualPlant™ is presented in Figure 28. The condenser at the power station is of a double vacuum design i.e. two condensing sections with different operating pressures. The condenser is responsible for condensing the exhaust steam from the LP turbine. The two operating pressures of the condenser are calculated by using *Heat Exchanger Institute (HEI) 9th Edition* calculations [78].

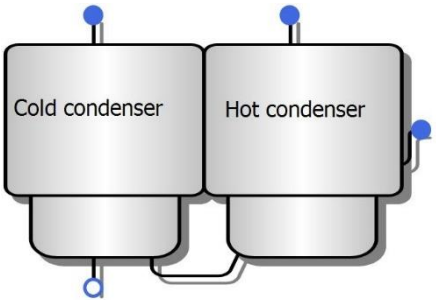

Figure 28: Cold and Hot condenser. [78]

The condenser is cooled by water (cooling water) which has a fixed temperature of 22 °C and a flow rate of 10.23 m^3/s, at the condenser cooling water inlet. The cooling water temperature of 22 °C is noted from the acceptance test documents of the power station. The inlet cooling water temperature of 22 °C is specified because the VirtualPlant™ model is validated against the acceptance test results of the power station. The design data for the condenser such as tube material, tube diameters, condenser surface etc. are also specified. The input values mentioned are sourced from Hamon Sobelco, as these values accurately represent the condenser performance at design.

The condenser cooling water inlet temperature is however not constant during the year, as it is dependent on the ambient weather conditions, such as dry-bulb air temperature etc. This shortcoming of this study is discussed in section 5.11, and a recommendation is provided in section 7.2 of chapter 7.

e) Low-pressure feedwater heating plant

The LP feedwater heating components from VirtualPlant™ are presented in Figure 29. The LP feedwater heating plant is responsible for raising the temperature of the LP feedwater flow. The LP feedwater heating plant consists of a gland steam condenser (GSC), three LP heaters and a deaerator. The GSC and the LP heaters are of a shell and tube heat exchanger design, and are heated by gland steam and bled steam (which is extracted from the LP turbine cylinders), respectively. The deaerator is of an open contact heat exchanger design which is heated by IP turbine bled steam.

The temperature of the outlet feedwater flow and drain flow from each feedwater heater, and the extracted steam mass flow rate to each LP heater, are calculated by using heat transfer analysis [78]. The extracted steam mass flow rate to the deaerator is calculated by heat and mass balance equations [78]. A pressure loss of 93 kPa, 99.5 kPa and 76.7 kPa is specified for the feedwater flow through the LPH1, LPH2 and LPH3, respectively. Also specified for each feedwater heater is process data, tube data and heat transfer data, such as design feedwater conditions, tube diameters and thermal conductivity and heat transfer coefficients etc., respectively. The deaerator is located at a height of 36.4 m above the centreline of the boiler feedwater pump suction. The input values mentioned are sourced from documents by James Brown and Hammer Ltd. South Africa.

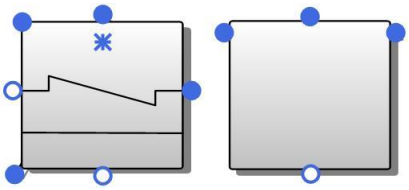

Figure 29: Closed and open feedwater heater (right). [78]

f) Boiler feedwater pump

The boiler feedwater pump component from VirtualPlant™ is presented in Figure 30.The boiler feedwater pump (BFP) pressurizes the feedwater flow to the boiler. The feedwater flow requires a high-pressure to overcome the pressure drop in the boiler, and to raise the upper pressure of the Rankine cycle. The BFP is driven by the boiler feedwater pump turbine (BFPT). The discharge pressure and the required power of the BFP are calculated by using pump performance curves. The performance curves of the BFP are presented in Figure 50 and Figure 51 of Appendix B. The reheater attemperating spray water flow is bled from an intermediate stage of the BFP, at a pressure of 10.3 MPa. The performance curves and process data are sourced from SULZER, which is the OEM of the boiler feedwater pump.

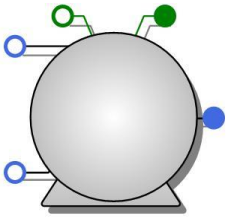

Figure 30: Boiler feedwater pump. [78]

g) High-pressure feedwater heating plant

The HP feedwater heating plant is responsible for raising the temperature of the high-pressure feedwater flow. The HP feedwater heating plant consists of two high-pressure heaters which are of a shell and tube heat exchanger design. The second HP heater (before the boiler inlet) is heated by steam from the HP turbine exhaust, and the first HP heater is heated by bled steam which is extracted from the IP turbine cylinder.

The temperature of the outlet feedwater flow and drain flow from each feedwater heater, and the steam mass flow rate to each HP heater, are calculated by using heat transfer analysis [78]. A pressure loss of 164.5 kPa and 172.7 kPa is specified for the feedwater flow through the first and second HP feedwater heaters, respectively. Also specified for each HP heater is process data, tube

data and heat transfer data. The input values mentioned are sourced from Hamon Sobelco, which is the OEM of the HP heaters.

h) Heat source

The heat source component from VirtualPlant™ is presented in Figure 31. The power plant component library in VirtualPlant™ does not have any CSP technology components. The heat source component is thus used to represent the solar field heat output. The amount of heat supplied by the heat source is calculated by using the outlet steam/water enthalpy (which is specified as an input) of the heat source, and the inlet water enthalpy & mass flow rate to the heat source. For each integration option the outlet steam/water enthalpy of the heat source, is specified as per Table 6 & Table 7.

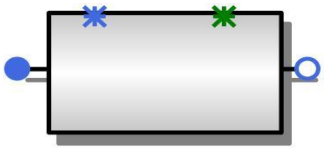

Figure 31: Heat source. [78]

i) Generator

The generator component from VirtualPlant™ is presented in Figure 32.The generator converts the mechanical power that is produced by the turbine plant into electrical power. A fixed mechanical loss of 4.83 MW_e is specified for the turbine plant, to account for bearing friction losses etc. The efficiency of the generator is specified as 98.66 %. The input values mentioned are sourced from GEC Turbine-Generators Ltd. documentation.

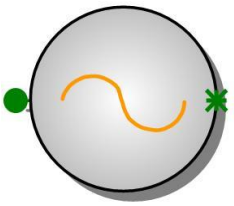

Figure 32: Generator. [78]

4.1.3 Validation results

The results from the VirtualPlant™ model was compared to the HBDs of the power station. The HBDs of the power station were verified against the actual plant performance during the acceptance tests of the station.

a) Model configuration

The VirtualPlant™ model was simulated between the 80 % - 110 % load range, by using four different operating modes, which are listed below.

1. Full load boiler operation with both HP feedwater heaters out-of-service: 110 % load.
2. Full load boiler operation with 50 % of the HP heater feedwater flow bypassed: 105 % load.
3. Normal full load plant operation: 100 % load.
4. Boiler operation at 80 % of full load.

During each simulation a boiler superheater outlet steam mass flow rate was specified, thereafter the total turbine power produced and the gross unit heat rate was noted. A boiler superheater outlet steam mass flow rate of 491.2 kg/s and 392.6 kg/s is specified for full load & 80 % full load boiler operation, respectively.

b) Model results

The total turbine power and the gross unit heat rate, from the VirtualPlant™ model and from the HBDs, during each of the operating modes defined in section a), are presented in Figure 33 and Figure 34 respectively. The complete set of results for the validation of the VirtualPlant™ model are presented in Appendix C.

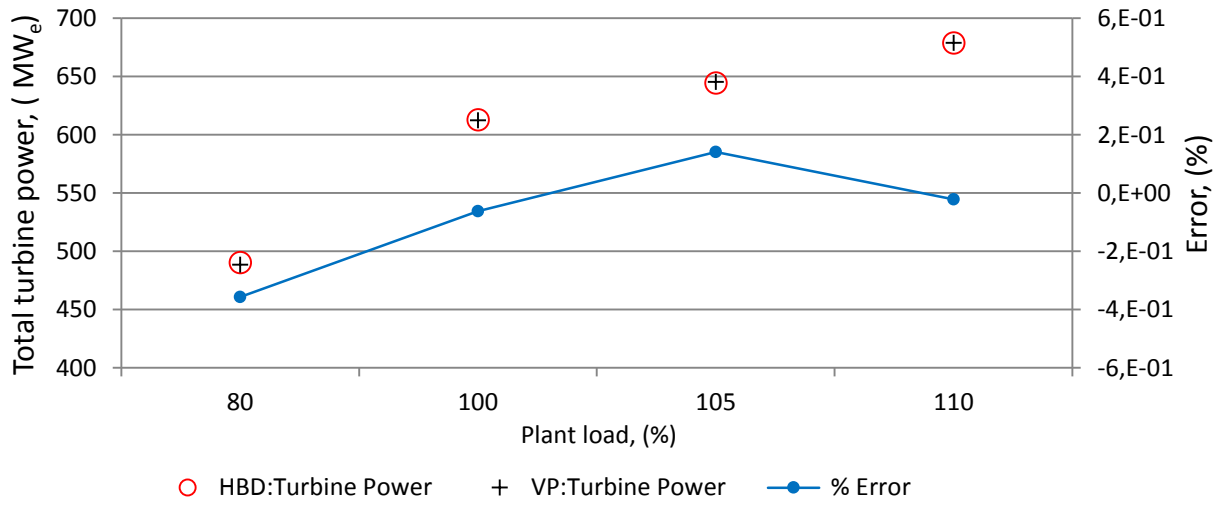

Figure 33 : Total turbine power versus Plant load

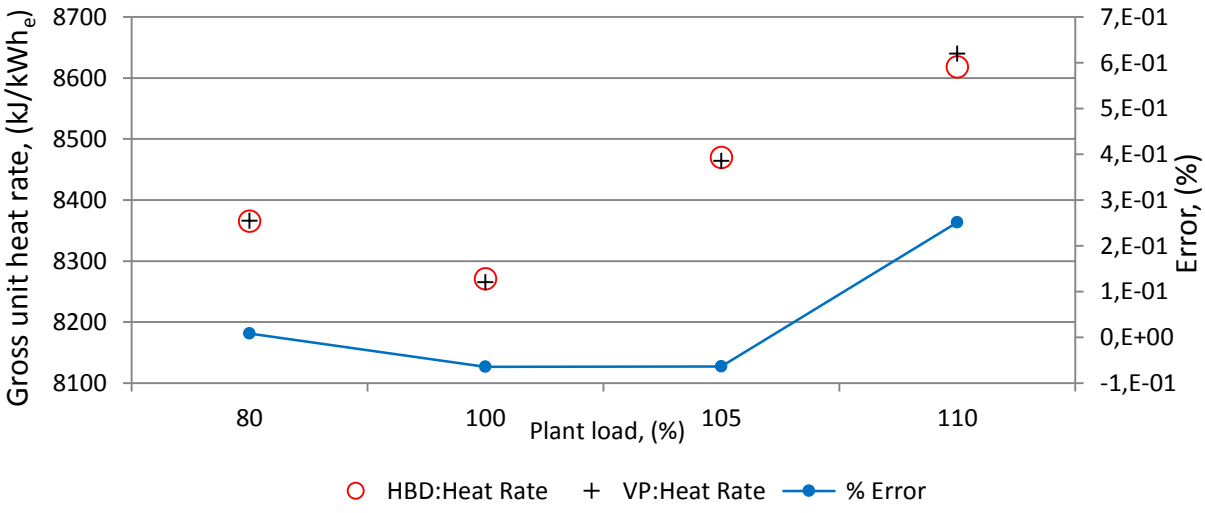

Figure 34: Gross unit heat rate versus Plant load

It is observed in Figure 34 that the gross unit heat rate is at a minimum during 100 % load, this is because the plant is designed ('optimised') to operate at 100 %.

c) Discussion of results

The average error difference between the total turbine power noted on the HBDs, and from the VirtualPlant^{TM} model is 0.08 %. The average error difference between the gross unit heat rate noted on the HBDs and from the VirtualPlant^{TM} model is 0.03 %.

A possible reason for the error difference between the HBDs and the VirtualPlant^{TM} model is that the turbine power produced by the VirtualPlant^{TM} model is predicted by using *'A Method for Predicting the Performance of Steam Turbine-Generators….16,500 kW and Larger '* [80, 78]. This method is based on the results of testing turbines [80] which are similar to the power plant's turbines, but are not exactly the same.

d) Conclusion

Typically, power plant models are accepted if they predict the plant output within 1 MW_e. At 100 % load the difference between the total turbine power noted on the HBD and from the VirtualPlant^{TM} model is 0.4 MW_e. Thus, the VirtualPlant^{TM} model is accepted for use in this study.

4.2 Economic life-cycle assessment model

The economic life-cycle assessment (LCA) model is used to determine the economic measures for each integration option. The economic measures calculated are Net present value (NPV), Total life-cycle cost, levelised cost of electricity (LCOE) etc. The LCA model, which is presented in section 3.15, is based on methods from NREL [56]. In the discussion that follows it is explained how Microsoft Excel is used to implement the LCA model. A summary and discussion of the validation results are provided at the end of this section.

4.2.1 Software tool

Initially, all the incomes and costs of the project are calculated for each year of the life of the project, in a Microsoft Excel spreadsheet. For example, the revenue from the sale of solar electricity, operating and maintenance costs etc. Thereafter the economic measures are calculated based on the relevant incomes and costs, the equations that are used to calculate the economic measures are presented in section 3.15.1.

4.2.2 Validation results

The results from the LCA model were compared to the results from the financial model in SAM, the financial model in SAM is also based on methods from NREL [71].

a) Model configuration

A hypothetical scenario of a stand-alone PTC power plant of 100 MW_e was used to validate the LCA model. The inputs for the LCA model and the SAM financial model, are presented in Table 17 . The models calculated the NPV, TLCC & LCOE through an electricity tariff range of 0.1-0.3 $/kWh$_e$.

Table 17: Economic model reference values

Parameter	Unit	Value
Real discount rate	%	8
Economic life of plant / Loan repayment term	Years	30
Loan interest rate	%	8.8
Income tax rate	%	28
CAPEX	$m	90
Annual electricity production	MWh_e	220000
Plant capacity	MW_e	100
OPEX variable	$/$MWh_e$	4
OPEX fixed	$/$kW_e$	65

Table 18: Microsoft Excel snap shot of the LCA model

Economic parameter / Cash flow	Unit	Year 1 1	Year 2 2	Year 3 3	Year 4 4	Year 5 5	Year 6 6	Year 7 7	Year 8 8
Electricity tarriff	$/kWhe	0,30	0,30	0,30	0,30	0,30	0,30	0,30	0,30
Discount factor		0,93	0,86	0,79	0,74	0,68	0,63	0,58	0,54
Annual electricity production	MWhe	220000,00	220000,00	220000,00	220000,00	220000,00	220000,00	220000,00	220000,00
O&M Fixed costs	$m	6,50	6,50	6,50	6,50	6,50	6,50	6,50	6,50
O&M variable costs	$m	0,88	0,88	0,88	0,88	0,88	0,88	0,88	0,88
Operating costs	$m	7,38	7,38	7,38	7,38	7,38	7,38	7,38	7,38
Annual loan repayment	$m	8,61	8,61	8,61	8,61	8,61	8,61	8,61	8,61
Outstanding principal amount	$m	90,00	89,31	88,57	87,76	86,88	85,91	84,87	83,73
Annual loan interest payment	$m	7,92	7,86	7,79	7,72	7,65	7,56	7,47	7,37
Debt payment	$m	0,69	0,75	0,81	0,88	0,96	1,04	1,14	1,24
Annual costs	$m	17,58	22,64	25,18	30,24	30,26	30,28	30,31	30,34
Gross Revenue	$m	66,00	66,00	66,00	66,00	66,00	66,00	66,00	66,00
Tax rate	%	28,00	28,00	28,00	28,00	28,00	28,00	28,00	28,00
Depreciation	$m	45,00	27,00	18,00	0,00	0,00	0,00	0,00	0,00
Taxable income	$m	5,70	23,76	32,83	50,90	50,97	51,06	51,15	51,25
Tax	$m	1,60	6,65	9,19	14,25	14,27	14,30	14,32	14,35
After tax cash flow	$m	48,42	43,36	40,82	35,76	35,74	35,72	35,69	35,66
Discounted costs	$m	16,28	19,41	19,99	22,22	20,59	19,08	17,68	16,39
Energy	MWhe	220000,00	220000,00	220000,00	220000,00	220000,00	220000,00	220000,00	220000,00
Discounted energy	MWhe	203703,70	188614,54	174643,09	161706,57	149728,30	138637,32	128367,89	118859,15
After tax cash flow discounted	$m	44,83	37,18	32,41	26,29	24,33	22,51	20,83	19,27

NPV	$m	421,60
TLCC	$m	321,41
LCOE	c/kWhe	12,98

b) Model results

The results from the LCA model and from the SAM financial model are presented in Table 19.The results of both models are expressed in United States dollars, as that is the default currency that is used in the SAM financial model.

Table 19: Results: The LCA model and the SAM financial model

Model	**Tariff ($/kWh$_e$)**	**TLCC ($m)**	**LCOE (c/kWh$_e$)**	**NPV ($m)**	**Error (%)**
LCA		182.7	7.38	65.0	
SAM	0.1	182.7	7.31	65.0	0.92
LCA		252.1	10.17	243.3	
SAM	0.2	252.1	10.11	243.3	0.59
LCA		321.4	12.98	421.6	
SAM	0.3	321.4	12.91	421.6	0.52
Average error					0.67

c) Discussion and conclusion of results

The LCA model accurately predicts the economic measures evaluated. The average error between the two models is 0.67 %. The error difference is due to the rounding off of values within the SAM model i.e. the after tax annual cash flows in both models were observed to be the same. The LCA model of this study is thus acceptable as it produces results with a small positive error (a positive error provides a conservative margin on the results).

5. Research results

The following chapter presents the results, based on the methodology established in chapter 3. The results presented are, the available land and solar resource at the power station, the solar field size of each integration option, solar-coal plant performance during the 'Fuel-saving' and the 'Power-boosting' modes, the relationship between the heat rate of the solar-coal plant and solar heat input. Lastly, the results from the economic life-cycle assessment of each integration option are presented.

5.1 Land assessment

The surrounding land areas of the power station were assessed to find the most suitable land area to locate the solar field. Based on an evaluation of all the Sites (1-3), as illustrated in Figure 35, Site 1 was found to be the most suitable location for the solar field. The evaluation of all the sites in Figure 35, is presented in Appendix F. The area of Site 1 is estimated to be 2.85 km^2.

Figure 35: Aerial view of the power station and surrounding land areas [81] .

5.2 Solar resource assessment

The annual hourly solar resource of the site of the power station is required by SAM, in order to predict the annual hourly heat output from the solar field. The annual hourly solar resource is contained in a weather file (amongst other annual hourly weather conditions) which is predicted by the Meteonorm software. The Meteonorm software was chosen for this study because it produces high resolution data [82]. The solar resource predicted by the Meteonorm weather file does compare well with data from other sources such as NASA and NREL, this is illustrated in Figure 36 and Table 20. The solar resource estimated by NASA is of low resolution and the solar resource estimated by NREL is of moderate resolution [83]. The daily average DNI in Figure 36 represents the total DNI available during the day, and the annual solar resource in Table 20 represents the total DNI resource available during the year.

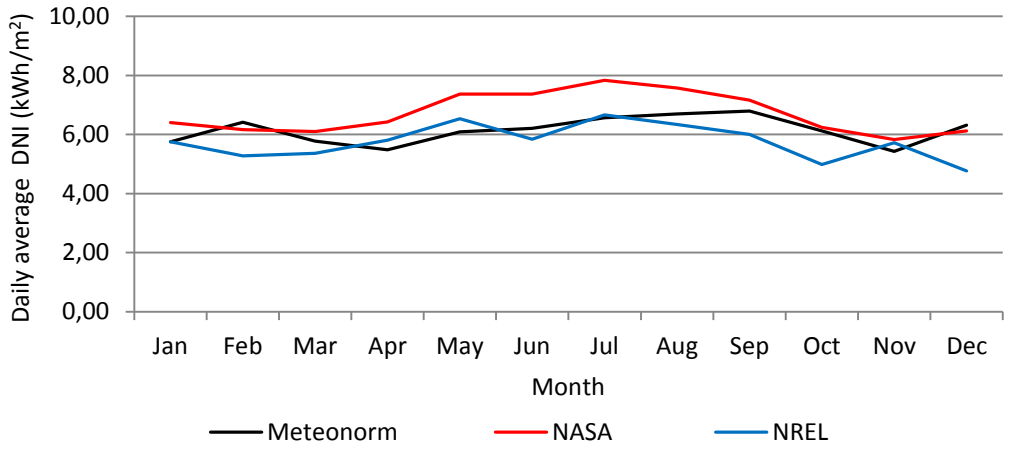

Figure 36: Average daily DNI for the site of the power station. [83]

Table 20: Annual solar resource (DNI) estimates for the site of the power station [83] .

Source	**Unit**	**NASA**	**Meteonorm**	**NREL**
Annual solar resource (DNI)	kWh/m^2	2452.7	2240.1	2101

5.3 Solar field sizes

The maximum amount of solar heat that can be supplied to the Rankine cycle of the power station, by each integration option during the 'Fuel-saving' mode is tabulated in Table 21 and Table 22. The maximum amount of solar heat is determined according to an iterative method as described in section 3.8.The maximum amount of solar heat for each integration option, is used by SAM to calculate the required reflective area and land area for the solar field of each integration option. The reflective area and land area of each solar field is also tabulated in Table 21 and Table 22. The land area required by the solar field is used to determine if the solar field would be accommodated by Site 1. It was found that the required land area of each solar field was less than 2.85 km^2, and could thus be accommodated by site 1. The reflective area and land area are used to estimate the CAPEX of the solar plant.

Table 21: Solar field specifications: Feedwater heating options

Feedwater heater(s) (Method, Technology)	**Solar heat (MW_t)**	**Reflective area (km^2)**	**Land area (km^2)**
HPH6 (M1, PTC)	95	0.210	0.764
HPH6 (M2, LFR)	101	0.248	0.368
HPH6 (M2, PTC)	101	0.223	0.813
HPH5 (M1, PTC)	100	0.221	0.805
HPH5 (M2, LFR)	86	0.212	0.314
HPH5 (M2, PTC)	86	0.190	0.692
DA (M2, LFR)	65	0.158	0.240
DA (M2*[21], PTC)	66	0.146	0.530
LPH3 (M1, LFR)	32	0.076	0.118
LPH3 (M1, PTC)	32	0.0708	0.258
LPH3 (M2, LFR)	30	0.0724	0.107
LPH3 (M2*, PTC)	32	0.0708	0.258
LPH1&2 (M1, LFR)	63	0.150	0.220
LPH1&2 (M1, PTC)	63	0.139	0.505

Table 22: Solar field specifications: Superheated steam supply options

Turbine plant area (Solar technology)	**Solar heat (MW_t)**	**Reflective area (km^2)**	**Land area (km^2)**
HP turbine (ST)	74	0.125	2.04
IP turbine (ST)	93	0.153	2.5
BFP turbine (LFR)	51	0.126	0.191
BFP turbine (PTC)	51	0.113	0.408
LP turbine (LFR)	196	0.478	0.719
LP turbine (PTC)	184	0.407	1.48

[21] The M2* method uses low-pressure feedwater flow (~ 2MPa) for steam production which is supplied to the feedwater heater.

Table 23: Reflective area and land area usage of the three CSP technologies

Solar technology	Reflective area usage (m^2/MW_t)	Land area usage (m^2/MW_t)
PTC	2210	8035
LFR	2430	3662
ST	1667	27224

It is observed in Table 23 that the PTC and LFR have similar reflective area usages, however the land area usage of the PTC is more than twice the land area usage of the LFR. It is also noted in Table 23 that the ST has the lowest reflective area usage and the highest land area usage.

5.4 Solar-coal plant performance

The performance of the solar-coal plant, in terms of heat rate, was predicted for each integration option during the 'Fuel-saving' and 'Power-boosting' mode. The solar-coal plant performance was predicted by using the VirtualPlant^{TM} model.

5.4.1 Fuel-saving mode

During the 'Fuel-saving' mode, the VirtualPlant^{TM} model was configured with an integration option, and then simulated to produce a gross unit output of 600 MW_e. The heat rate of the solar-coal plant was then calculated by using equation(1). The heat rate reduction of the solar-coal plant was then calculated by subtracting the heat rate of the solar-coal plant from the reference heat rate, as per equation(2). The reference heat rate during the 'Fuel-saving' mode is 8260.2 kJ/kWh_e, as explained in section 3.10.1. The heat rate reduction that is produced by each integration option during the 'Fuel-saving' mode is presented in Table 24 and Table 25.

N.B The amount of solar heat that is supplied by each integration option, as per Table 24 and Table 25, is the maximum amount of solar heat that can be supplied by each integration option during the 'Fuel-saving' mode. The maximum amount of solar heat that can be supplied by an integration option during the 'Power-boosting' mode, can be less than the maximum amount of solar heat that can be supplied by the integration option during the 'Fuel-saving' mode. The maximum amount of solar heat added during the 'Power-boosting' mode is sometimes less than the maximum amount of solar heat added during the 'Fuel-saving', to prevent the plant from exceeding any technical capabilities.

Table 24: Heat rate reduction: Feedwater heating options (Fuel-saving mode)

Feedwater heater(s) (Method, Technology)	Solar-coal plant gross heat rate (kJ/kWh$_e$)	Heat rate reduction (kJ/kWh$_e$)	Solar heat (MW$_t$)	Solar electricity (MW$_e$)
HPH6 (M1,PTC)	7847.9	412.3	94.8	30
HPH6 (M2,LFR or PTC)	7850.3	409.9	100.9	30
HPH5 (M1,PTC)	7944.0	316.2	99.8	23.0
HPH5 (M2,LFR or PTC)	7988.0	272.2	85.5	19.8
DA (M2,LFR)	8126.3	133.9	64.2	9.7
DA (M2*,PTC)	8116.0	144.2	65.2	10.5
LPH3 (M1,LFR or PTC)	8227.3	32.9	31.6	2.4
LPH3 (M2, LFR)	8237.3	22.9	29.2	1.6
LPH3 (M2*,PTC)	8226.5	33.7	31.8	2.5
LPH1&2 (M1,LFR or PTC)	8246.2	14.0	62.5	1.0

From all the feedwater heaters, as noted in Table 24, the high-pressure feedwater heaters (HPH) could be supplied with the most amount of solar heat. It is also noted in Table 24 that the HPH6 feedwater heating option is the only feedwater heating option that can achieve the 30 MW$_e$.

Table 25: Heat rate reduction: Superheated steam supply options (Fuel-saving mode)

Turbine plant area (Technology)	Solar-coal plant gross heat rate (kJ/kWh$_e$)	Heat rate reduction (kJ/kWh$_e$)	Solar heat (MW$_t$)	Solar electricity (MW$_e$)
HP turbine (ST)	7847.8	412.4	73.4	30.0
IP turbine (ST)	7848.2	412.0	92.9	30.0
BFP turbine (LFR or PTC)	8105.6	154.6	49.2	11.2
LP turbine (LFR)	7847.7	412.5	195.6	30.0
LP turbine (PTC)	7847.9	412.3	183.3	30.0

From all the steam supply integration options, as noted in Table 25, the LP turbine steam supply integration option, could accept the most amount of solar heat. However, all of the superheated steam supply options, except for the steam supply to the BFPT, could achieve the 30 MW$_e$.

5.4.2 Power-boosting mode

During the 'Power-boosting' mode, the VirtualPlant^{TM} model was configured with an integration option. The model was then simulated whilst the boiler produced a superheater outlet flow rate of 491.2 kg/s. Hence, the gross power output of the unit was > 600 MW$_e$. The heat rate reduction of the solar-coal plant is calculated by using the same process as discussed in section 5.4.1, except that the reference heat rate is different for each integration option. The reference heat rate for each integration option during the 'Power-boost' mode is calculated by using the method explained in 3.10.2. The heat rate reduction that is produced by each integration option during the 'Power-boosting' mode is presented in Table 26 and Table 27.

N.B The amount of solar heat that is supplied by each integration option, as per Table 26 and Table 27, is the maximum amount of solar heat that can be supplied by each integration option during the

'Power-boosting' mode. It can be noted by comparing, Table 24-Table 27, that the maximum amount of solar heat supplied during the 'Power-boosting' mode can be less than the maximum amount of solar heat that can be supplied during the 'Fuel-saving' mode.

Table 26: Heat rate reduction: Feedwater heating options (Power-boosting mode)

Feedwater heater(s) (Method, Solar technology)	Gross heat rate (kJ/kWh_e)			Solar heat (MW_t)	Gross Unit power (MW_e)	Solar electricity (MW_e)
	Reference	Solar-coal plant	Heat rate reduction			
HPH6 (M1,PTC)	8469.0	7855.0	614.0	94.8	632.6	45.9
HPH6 (M2,LFR or PTC)	8468.3	7853.6	614.8	100.9	631.9	45.9
HPH5 (M1,PTC)	8421.0	7943.5	477.4	99.8	623.8	35.4
HPH5 (M2,LFR or PTC)	8402.4	7983.5	419.0	85.5	620.6	30.9
DA (M2,LFR)	8340.0	8122.7	217.3	64.2	610.1	15.9
DA (M2*,PTC)	8341.2	8112.5	228.7	65.2	610.9	16.8
LPH3 (M1,LFR or PTC)	8287.4	8226.3	61.1	31.6	602.4	4.4
LPH3 (M2,LFR)	8278.4	8235.6	42.8	29.2	601.7	3.1
LPH3 (M2*,PTC)	8285.9	8225.8	60.1	31.8	602.5	4.4
LPH1&2 (M1,LFR or PTC)	8279.0	8246.2	32.8	62.5	601.0	2.4

It was found that the maximum amount of solar heat that can be supplied by each feedwater heating option, during the 'Fuel-saving' mode could also be supplied during the 'Power-boosting' mode, without exceeding any plant capabilities. Also, it was noted that during the 'Power-boosting' mode, the HPH6 and the HPH5 feedwater options produced > $30MW_e$.

Table 27: Heat rate reduction: Superheated steam supply (Power-boosting mode)

Turbine plant area (Solar technology)	Gross heat rate (kJ/kWh_e)			Solar heat (MW_t)	Gross Unit power (MW_e)	Solar electricity (MW_e)
	Reference	Solar-coal plant	Heat rate reduction			
HP turbine (ST)	8440.2	7943.0	497.1	56.0	626.2	36.9
IP turbine (ST)	8414.5	7849.8	564.6	92.8	622.9	41.8
BFP turbine (LFR or PTC)	8349.0	8097.1	252.0	50.3	612.0	18.5
LP turbine (LFR)	8465.8	7846.1	619.7	182.9	631.4	46.2
LP turbine (PTC)	8468.5	7837.5	631.0	176.6	632.2	47.1

For some steam supply integration options it was found that the maximum amount of solar heat that can be supplied during the 'Power-boosting' mode, was less than the maximum amount of solar heat that can be supplied during the 'Fuel-saving' mode. This is applicable to the HP and LP turbine steam supply options. However, all of the steam supply options, except for the BFPT steam supply option, could still achieve >$30MW_e$.

5.5 Integration effectiveness

The IE of all the integration options during the 'Fuel-saving' mode are displayed in Figure 37 and Figure 39.

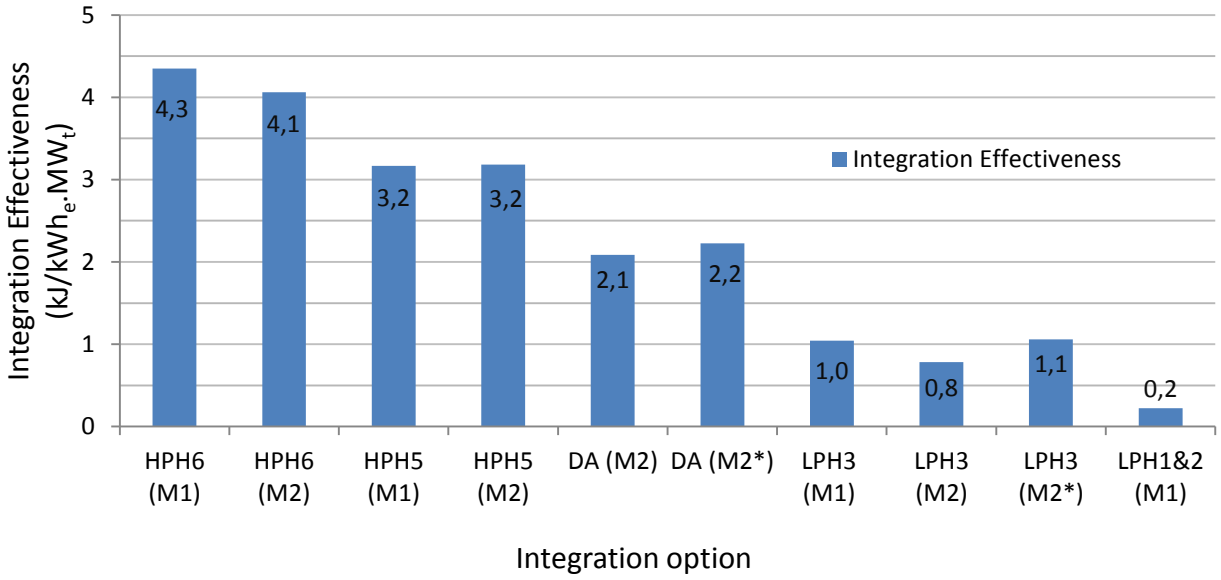

Figure 37: Integration effectiveness (Feedwater heating options, 'Fuel-saving' mode)

It is observed in Figure 37, that the IE of the feedwater heating options is the highest amongst the HPHs and reduces towards the LPHs. The results of this study display a similar trend to the results of a study performed by [24], which are presented in Figure 38. The study by [24] investigated the benefit of solar aided feedwater heating in a coal-fired subcritical power plant, and expresses the benefit of solar aided feedwater heating in each feedwater heater as the Energy Performance Index (EnPI)[22]. The Exergy Performance Index (ExPI) illustrated in Figure 38, is similar to the EnPI but uses exergy rather than energy [24].

[22] EnPI is defined as the excess power generated over the design rated capacity divided by the energy input to the solar collector field [24].

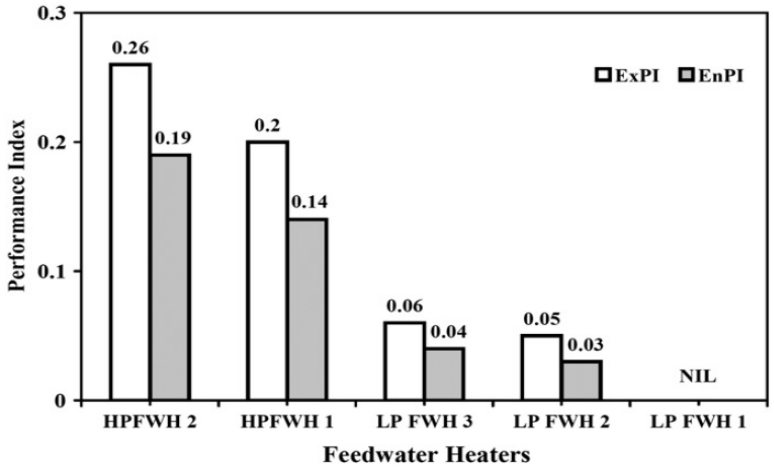

Figure 38: The EnPI of the feedwater heaters of a 500MW$_e$ subcritical power plant during solar aided feedwater heating. [24]

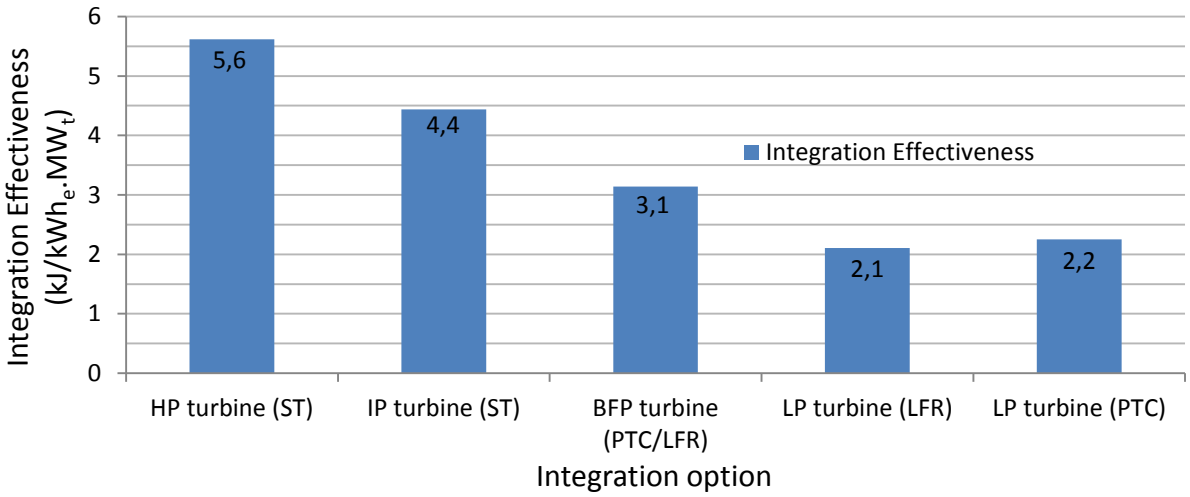

Figure 39: Integration effectiveness (Superheated steam supply options, fuel-saving mode)

Amongst all of the steam supply options, the steam supply to the HP and the IP turbine has the highest IE, and the IE reduces towards the LP turbine steam supply options, as noted from Figure 39. The IE of the steam supply to the HP and the IP turbine is 5.6 kJ/kWh$_e$.MW$_t$ and 4.4 kJ/kWh$_e$.MW$_t$ respectively.

5.6 Solar field daily performance

It was mentioned in section 3.1, that the heat output from the solar field is not constant, as it varies for each hour of the year. This is because the DNI and the angle of incidence varies during the year. As the incidence angle increases, less heat is collected by the solar field and hence the solar field optical efficiency[23] reduces. Thus, the heat rate reduction of the solar-coal plant also varies during the year. The angle(s) of incidence that are applicable to each CSP technology are briefly explained below.

The angle of incidence for the PTC is the angle between the DNI (Beam) radiation and the normal to the aperture plane [84], as illustrated in Figure 40. The angle of incidence has a significant impact on the performance of the PTC field [85].

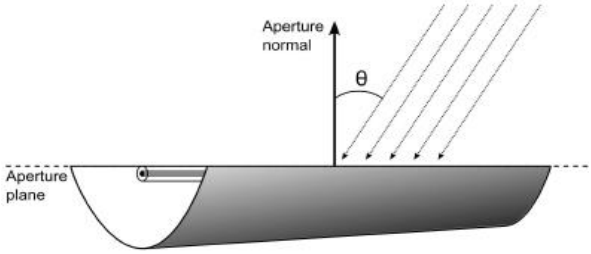

Figure 40: The angle of incidence in a PTC. [84]

The performance of the LFR field is dependent on two incidence angles of the DNI, i.e. a transversal incidence angle (Φ_T) and a longitudinal incidence angle (Φ_L) [86]. These two incidence angles are illustrated in Figure 41.

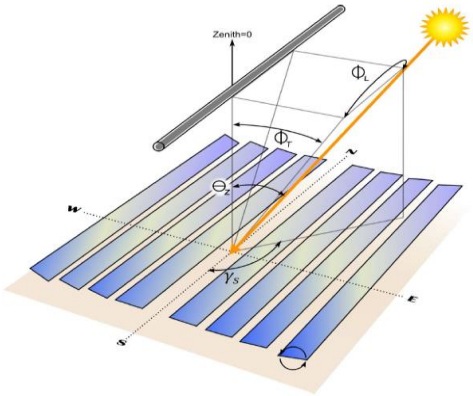

Figure 41: The transversal incidence angle (Φ_T) and the longitudinal incidence angle (Φ_L) of the LFR. [86]

[23] Solar field optical efficiency is the amount of heat collected by the solar field relative to the amount of solar heat incident on the solar field.

The heliostat field performance of the CR is also affected by the angle between the DNI and the normal to the heliostat. Other losses which affect the heliostat field performance, are the receiver reflective losses, shadowing and blocking losses, atmospheric attenuation (the scattering of the reflected DNI which occurs as it passes through the air) etc. Some of the losses mentioned are illustrated in Figure 42. [87]

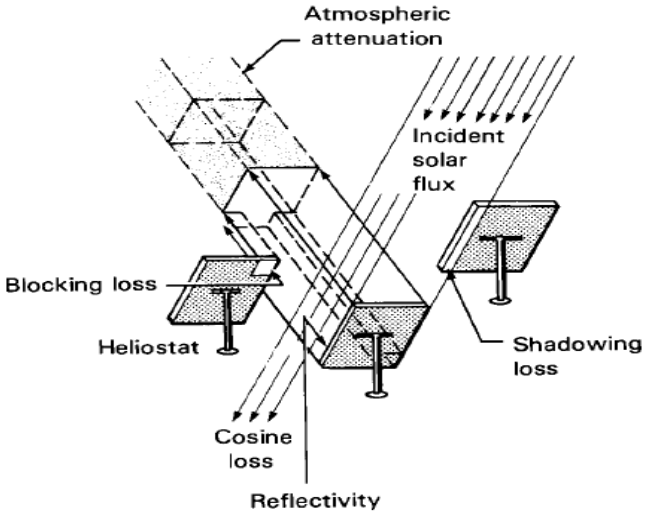

Figure 42: Losses effecting heliostat field performance. [88]

To illustrate the hourly performance of each CSP technology, it was decided to simulate the performance of a solar field (of 100 MW_t size) of each CSP technology, during a typical winter and summer day, using SAM. The technology performance during a winter and summer day illustrates the two extremes in technology performance during the year.

The hourly DNI resource and solar incidence angle during a typical winter and summer day is shown in Figure 43. The hourly solar field performance of the PTC, LFR and ST during a typical winter and summer day are presented in Figure 44 and Figure 45, respectively.

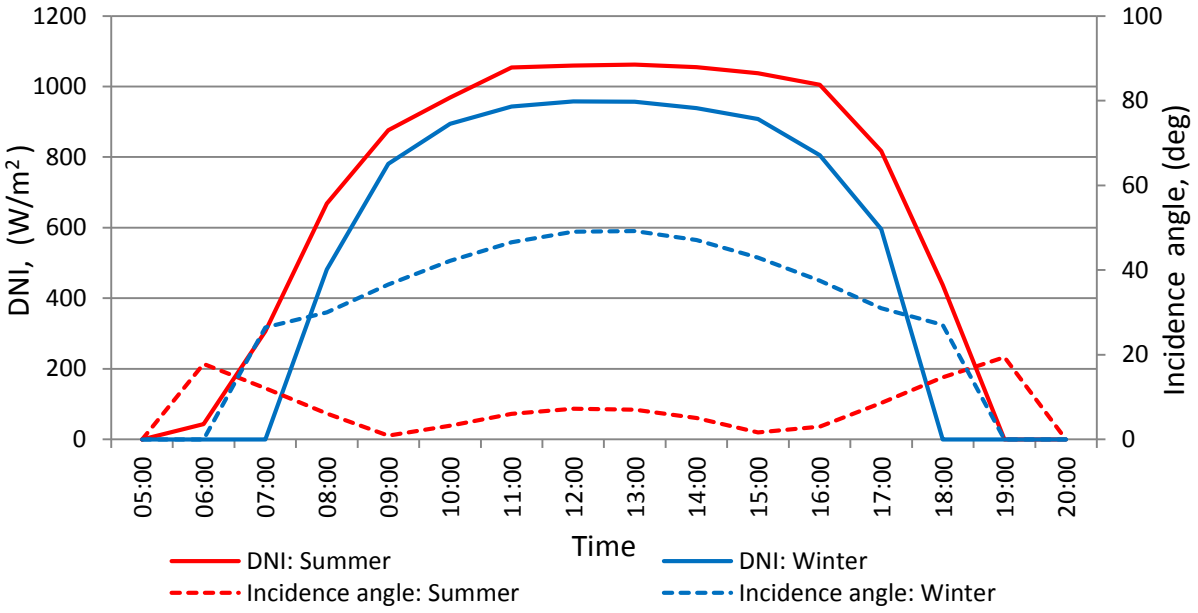

Figure 43: Typical DNI resource and incidence angle in winter and summer

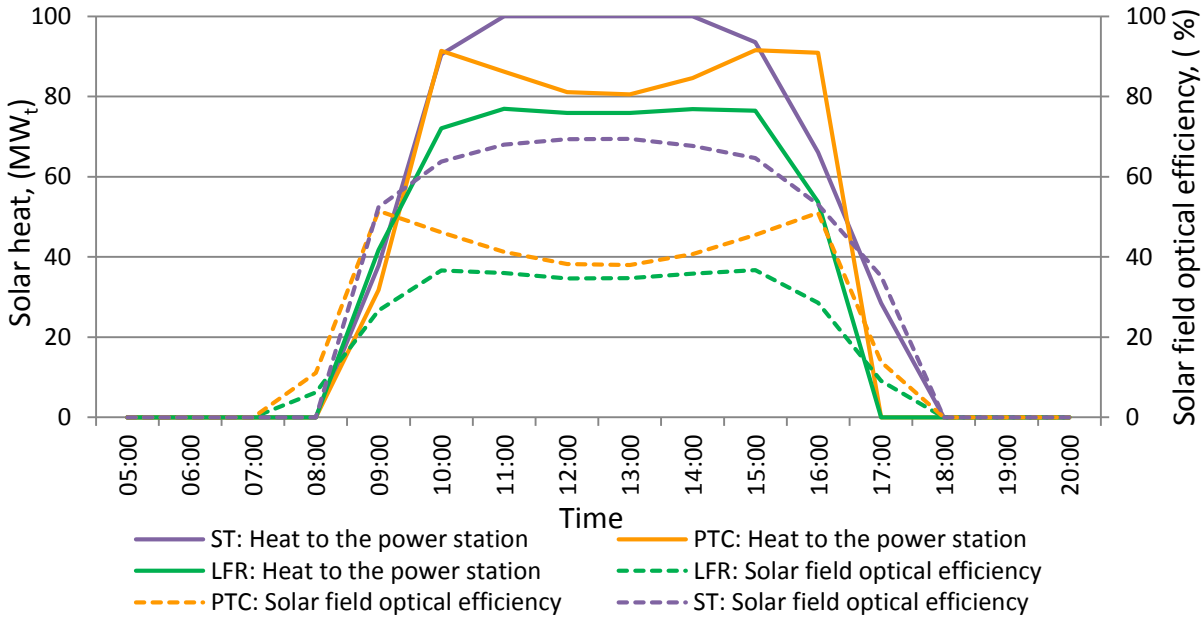

Figure 44: PTC, LFR and ST solar field daily performance: Winter day (6th June)

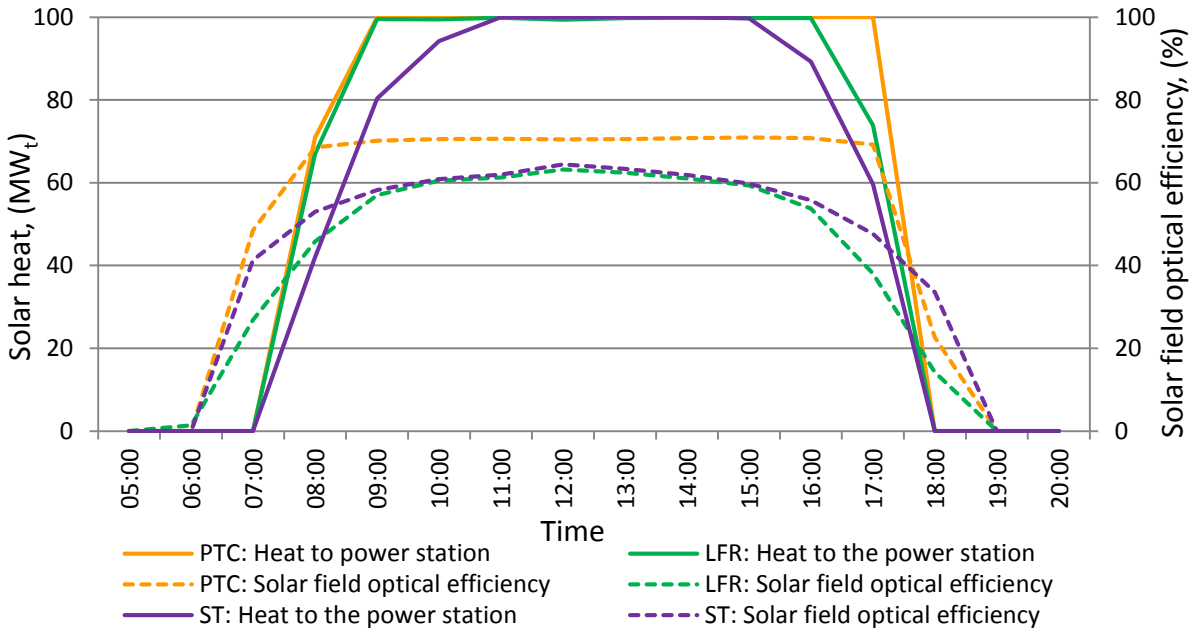

Figure 45: PTC, LFR and ST solar field daily performance: Summer day (11th November)

It was found that the PTC and the LFR solar fields have the greatest optical efficiency during the summer months i.e. 71 % and 62 % respectively, and the lowest optical efficiency during the winter months i.e. 38 % and 34 % respectively. The solar field optical efficiencies of both the PTC and LFR technologies are reduced in winter because of the high solar incidence angle during the winter months as illustrated in Figure 43. The solar incidence angle can reach up to 50^{o} during a winter day. Also noted from Figure 44, is that because of the reduction in solar field optical efficiency during the winter months, the PTC and LFR solar fields often do not produce the required 100 MW_t.

The heliostat field of the ST has an optical efficiency of 64 % and 70 % during the summer and winter months respectively. The optical efficiency of the heliostat field does not change as drastically as the optical efficiency of the PTC and LFR fields, because the distribution of the heliostats are optimised by SAM.

5.7 Solar-coal plant heat rate versus solar heat input

As illustrated in section 5.6, the heat output from the solar field varies during each hour of the day, and during the year. This would imply that the heat rate reduction of the solar-coal plant also varies for each hour of the year (during night hours the heat rate reduction of the solar-coal plant is constant (=0) due to no solar heat). Thus, to assist in calculating the annual hourly heat rate reduction of the solar-coal plant, it was necessary to determine the relationship between the solar-coal plant heat rate and solar heat input. The VirtualPlant™ model was used to simulate the solar-coal plant heat rate reduction, at solar heat inputs less than the design point solar heat, for each integration option. It was found that the heat rate of the solar-coal plant reduces approximately linearly as the solar heat input is increased.

The linear relationship between the heat rate reduction (HRR) of the solar-coal plant and solar heat input, for some integration options, during the 'fuel-saving' mode is illustrated in Figure 46.

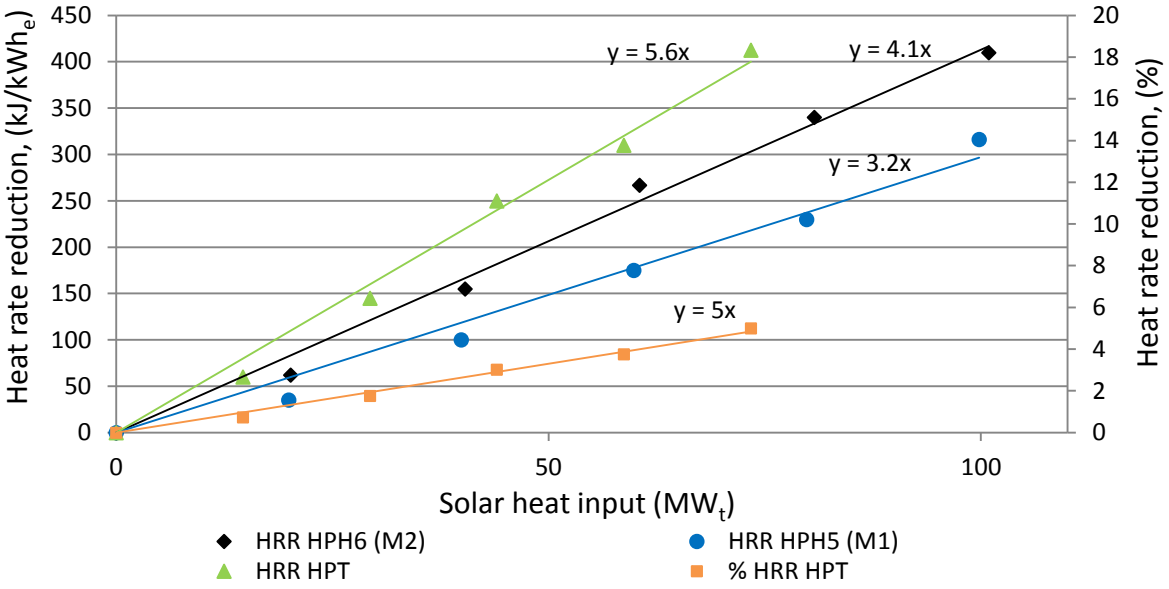

Figure 46: Solar-coal plant heat rate reduction versus solar heat input, during the 'Fuel-saving' mode: HPH6 (M2), HPH5 (M1) & HPT

5.8 Annual project benefits

The annual project benefits, such as the coal savings, GHG emission reduction, solar electricity etc., were calculated for each integration option. The methods that are used to calculate the project benefits are described in section 3.13. The project benefits for each integration option are presented in Table 28 and Table 29, and are used in the economic life-cycle assessment of each integration option.

It is noted from Table 28 and Table 29 that the high-pressure feedwater heating options and the high-temperature/pressure steam supply options (such as the steam supply to the HP, IP and BFPT turbine), are the most effective at reducing coal consumption, GHGs etc. For example, the steam supply option to the HP turbine reduces coal consumption by 0.24t/MWh_t of solar heat, in comparison to the LPH3 (M1, PTC) feedwater heating option which reduces coal consumption by 0.05t/MWh_t of solar heat. Hence, it is established that the integration options which have a high IE return the best economic benefits.

Table 28: Annual project benefits: Feedwater heating options

Feedwater heater(s) (Method, technology)	**Solar heat (GWh_t)**	**Solar elec (GWh_e)**	**Coal saved (ktons)**	**GHGs avoided ($ktCO_{2eq}$)**	**Carbon intensity (tCO_{2eq}/MWh_e)**	**Parasitic power[24] (GWh_e)**	**Carbon tax savings (Rm)**
HPH6 (M1, PTC)	144.2	64.2	25.6	55.2	0.945	4.4	6.6
HPH6 (M2, LFR)	142.3	60.3	24.0	51.9	0.946	-	6.2
HPH6 (M2, PTC)	153.2	64.1	25.5	55.1	0.945	4.6	6.6
HPH5 (M1, PTC)	151.6	49.4	19.6	42.2	0.949	4.6	5.0
HPH5 (M2, LFR)	124.3	41.6	16.5	35.5	0.950	-	4.2
HPH5 (M2, PTC)	130.3	43.1	17.1	36.8	0.950	3.9	4.4
DA (M2, LFR)	81.5	18.6	7.3	15.8	0.956	-	1.9
DA (M2*, PTC)	100.1	23.3	9.2	19.8	0.955	3.0	2.4
LPH3 (M1, LFR)	48.3	6.1	2.4	5.2	0.959	0.2	0.6
LPH3 (M1, PTC)	48.6	6.1	2.4	5.2	0.959	1.5	0.6
LPH3 (M2, LFR)	42.6	4.0	1.6	3.3	0.959	-	0.4
LPH3 (M2*, PTC)	48.6	6.0	2.3	5.0	0.959	1.5	0.6
LPH1&2 (M1, LFR)	92.8	3.1	1.3	2.7	0.959	0.2	0.3
LPH1&2 (M1, PTC)	95.6	3.1	1.3	2.7	0.959	2.9	0.3

[24] Parasitic power consumption is the annual electricity requirement of the HTF pumps. All of the PTC and ST options have a parasitic power requirement, for pumping thermal oil and solar salt respectively between the solar field and the power station. Most of the LFR options do not have a parasitic power consumption because the high-pressure feedwater flow that is used in the M2 options is supplied by the BFP discharge. The LPH options which use the LFR technology for M1 feedwater heating have a parasitic power consumption for a booster pump, as explained in Chapter 6.

Table 29: Annual project benefits: Superheated steam supply options

Steam supply option (Solar technology)	Solar heat (GWh_t)	Solar elec (GWh_e)	Coal saved (ktons)	GHGs avoided ($ktCO_{2eq}$)	Carbon intensity (tCO_{2eq}/MWh_e)	Parasitic power (GWh_e)	Carbon tax savings (Rm)
HP turbine (ST)	84.0	51.2	20.3	43.9	0.948	0.4	5.2
IP turbine (ST)	119.3	50.9	20.2	43.5	0.948	0.5	5.2
BFP turbine (LFR)	75.1	25.1	9.9	21.4	0.954	-	2.5
BFP turbine (PTC)	77.6	25.6	10.1	21.8	0.954	2.4	2.6
LP turbine (LFR)	233.9	51.8	20.7	44.6	0.948	-	5.3
LP turbine (PTC)	278.7	65.5	26.1	56.4	0.945	8.4	6.7

5.9 Project costs

As mentioned in section 3.14, there are 3 costs associated with this project, i.e. a capital cost, an operating & maintenance cost and an income tax cost. Only the capital cost of each integration option is presented in this section, as the operating & maintenance cost and income tax cost do not require much explanation. The methods that are used to calculate the project costs are presented in section 3.14. The project costs of each integration option is used in the life cycle assessment of each integration option.

The capital expenditure (CAPEX) of the integration options are calculated by using the reference cost models from SAM, these cost models are presented in section 3.14.1. Once the CAPEX of each integration option was determined, the installed capacity cost of each integration option was determined. The installed capacity cost (ICC) of each integration option is calculated by dividing its CAPEX by its solar electricity capacity (as listed in Table 24 and Table 25). The ICC thus has the units of R/kW_e, and is used to compare the relative costs of each integration option. The CAPEX and the ICC of each integration option is presented in Table 31 and Table 32.

One of the benefits of adding solar heat to a coal-fired power plant, as mentioned in section 1.2, is that cost reduction opportunities are created for electricity generation from solar heat. This is because the existing infrastructure of the coal-fired power plant is utilised to generate electricity from solar heat. Thus, to establish the cost reduction created by each integration option, the installed capacity cost of each integration option was compared to the installed capacity cost of the relevant hypothetical stand-alone CSP power plant located at the power station. The installed capacity cost of each stand-alone 30 MW_e CSP power plant, as per Table 30, was derived from SAM[25].

Table 30: Installed capacity cost (Stand-alone CSP plants at the power station, 30 MW_e) (Exchange rate, 1 USD= 10.6 ZAR)

CSP technology	**Installed capacity cost (R/kW_e)**
Parabolic trough collector	43507
Linear Fresnel reflector	33826
Molten salt power tower	53937

[25] These results are based on a power cycle maximum operating steam temperature of 375 ^oC (PTC), 500 ^oC (LFR), and 535 ^oC (ST).

Table 31: CAPEX estimate: Feedwater heating options (Exchange rate, 1 USD= 10.6 ZAR)

Feedwater heater(s) (Solar technology)	Solar field size (MW_t)	CAPEX (Rm)	Installed cost (R/kW_e)	% of Stand-alone CSP plant
HPH6 (M1, PTC)	95	1122.3	37410.1	86.0
HPH6 (M2, LFR)	101	845.2	28172.3	83.3
HPH6 (M2, PTC)	101	1192.0	39731.7	91.3
HPH5 (M1, PTC)	100	1181.2	51355.0	118.0
HPH5 (M2, LFR)	86	722.4	36487.2	107.9
HPH5 (M2, PTC)	86	1015.5	51287.4	117.9
DA (M2, LFR)	65	538.8	55548.0	164.2
DA (M2*, PTC)	66	780.2	74301.6	170.8
LPH3 (M1, LFR)	32	259.3	108059.8	319.5
LPH3 (M1, PTC)	32	378.4	157661.9	362.4
LPH3 (M2, LFR)	30	246.7	154191.9	455.8
LPH3 (M2*, PTC)	32	378.4	151355.4	347.9
LPH1&2 (M1, LFR)	63	511.0	511024.0	1510.7
LPH1&2 (M1, PTC)	63	742.9	742874.6	1707.5

Amongst all of the feedwater heating options, it was found that the high-pressure feedwater heating options (HPH6 and HPH5) have the lowest installed capacity costs. Amongst the HPH6 and HPH5 feedwater heating options, the use of the LFR technology to supply steam to the HPH6 and HPH5 (i.e. the HPH6 (M2, LFR) and HPH5 (M2, LFR) options) has the lowest installed capacity costs, i.e. 28.1-36.5 kR/kW_e. However, from these two options, only the HPH6 (M2, LFR) option creates a cost reduction opportunity i.e. 16.7 %.

The remaining HPH6 and HPH5 options use the PTC technology, either for M1 or M2 feedwater heating. These feedwater heating options have an installed capacity cost of 37.4-51.3 kR/kW_e. However, from these options, only the HPH6 (M1, PTC) and the HPH6 (M2, PTC) options create cost reduction opportunities i.e. 14 % and 8.7 % respectively.

Table 32: CAPEX estimate: Superheated steam supply options (Exchange rate, 1 USD= 10.6 ZAR)

Steam supply option (Solar technology)	Solar field size (MW_t)	CAPEX (Rm)	Installed cost (R/kW_e)	% of Stand-alone CSP plant
HP turbine (ST)	74	1138.6	37954.7	70.4
IP turbine (ST)	93	1299.2	43306.1	80.3
BFP turbine (LFR)	51	429.7	38362.8	113.4
BFP turbine (PTC)	51	603.6	53896.5	123.9
LP turbine (LFR)	196	1629.6	54321.0	160.6
LP turbine (PTC)	184	2175.0	72500.6	166.6

Amongst all of the steam supply options, the steam supply to the HP and IP turbine (using the ST) and the steam supply to the BFPT (using the LFR), have the lowest installed capacity cost i.e. 37.9-43.3 kR/kW_e. However, from these 3 options, only the HP and the IP turbine steam supply options create cost reduction opportunities i.e. 29.6 % and 19.7 % respectively.

It is also important to establish the heat-cost of each CSP technology, which is calculated by dividing the CAPEX of each integration option by its solar field size. The heat-cost of each CSP technology is tabulated in Table 33.It is observed that the LFR has the lowest heat-cost and the ST has the highest heat-cost.

Table 33: Heat-cost of the 3 CSP technologies.

Solar technology	**Heat cost (Rm/MW_t)**
LFR	8.3
PTC	11.8
ST	14.7

5.9.1 CAPEX breakdown

The CAPEX breakdown of each hypothetical 30 MW_e stand-alone CSP power plant located at the power station as mentioned in section 5.9, is presented in Table 34. Also included in Table 34 is the CAPEX breakdown of the integration options[26] which could achieve the 30 MW_e during the 'Fuel-saving' mode. The CAPEX breakdown is presented as it illustrates the % that each plant area contributes to the total plant CAPEX. Also by comparing the CAPEX breakdown of the solar-coal power plant and the respective the stand-alone CSP power plant, cost reduction opportunities (for specific plant areas) are highlighted.

As mentioned in section 1.2.2, the solar-coal power plant utilises the power block, steam condenser etc. which is available in the existing coal-fired power plant. Thus the cost of a power block, steam condenser etc. is not included in the CAPEX of the solar-coal power plant. The elimination of the power block, steam condenser costs etc. creates a cost reduction opportunity for electricity generation from solar heat.

It is observed from Table 34 that the CAPEX of the stand-alone ST power plant is dominated by the cost of the receiver and the tower i.e. the tower and the receiver contributes to 29 % of the CAPEX of the stand-alone ST power plant. The CAPEX of the LFR and the PTC stand-alone power plants are dominated by the cost of the solar field i.e. 42.9 % and 40 % respectively. Thus, because of the elimination of the power plant[27] cost from the CAPEX of the ST solar-coal power plant, the tower and the receiver now contributes to 40.4 % of the CAPEX of the ST solar-coal power plant. The %

[26] For each CSP technology, the integration option with the highest IE which could achieve the 30 MW_e is included in Table 34.

[27] The power plant cost in SAM represents the cost of the power block, steam condenser etc.

contribution of the solar field cost to the CAPEX of the LFR and PTC solar-coal power plants also increases to 65.2 % and 53.5 % respectively.

By observing the CAPEX breakdown of the LFR and PTC solar-coal power plants in more detail revealed that the reflective area of the LFR and PTC influences the CAPEX cost by 82 % and 75 % respectively[28].

Table 34: CAPEX breakdown comparison of each stand-alone CSP plant and their respective solar-coal plant options

	% of CAPEX					
Cost category	**ST Stand-alone**	**(ST) HPT**	**LFR Stand-alone**	**LFR HPH6 (M2)**	**PTC Stand-alone**	**PTC HPH6 (M1)**
Site improvements	1.24	1.74	4.08	6.21	4.45	5.94
Solar field	14.89	20.93	42.87	65.26	40.03	53.50
Balance of plant	7.00	9.92	-	-	2.77	3.69
Power plant	24.01	-	29.10	-	20.91	-
EPC & Owner costs	8.37	8.03	9.15	9.06	8.80	8.69
Land	7.88	11.65	1.83	2.83	3.18	4.42
HTF system	-	-	7.15	10.88	11.86	15.85
Contingencies	7.61	7.30	5.82	5.76	8.00	7.90
Tower	8.21	11.44	-	-	-	-
Receiver	20.78	28.98	-	-	-	-

[28] 3 CAPEX cost categories, of both the LFR and the PTC, are calculated by using the reflective area. The cost categories are site preparations, solar collector field system and the heat transfer system, as per the CAPEX cost model in Table 15.

5.10 Economic life-cycle assessment

The economic life-cycle assessment (LCA) of each integration option, calculates the 5 economic measures for each integration option, as mentioned in section 3.15.1. The economic measures that are calculated are the Net present value (NPV), the Total life-cycle cost (TLCC), the Simple payback period (SPB), the Discounted payback period (DPB) and the Levelised cost of electricity (LCOE).The methods that are used to calculate the economic measures are described in section 3.15.1.Once the economic measures for all the integration options were calculated, they were then compared to determine the most economically feasible integration options.

5.10.1 Sensitivity analysis

Prior to carrying out the LCA of each integration option, it was decided to conduct a sensitivity analysis on the real LCOE[29].The real LCOE was chosen to be analysed, amongst the other economic measures, because it is an important economic measure which is used to compare integration options.

A sensitivity analysis is performed by varying each input that is used to calculate the real LCOE, and then noting the variation in the real LCOE. Once completed, this analysis would reveal the most sensitive inputs that are used to calculate the real LCOE. After identifying the most sensitive inputs, steps should be taken to improve the accuracy of these inputs, if necessary. The results of the sensitivity analysis on real LCOE are presented in Figure 47. [56]

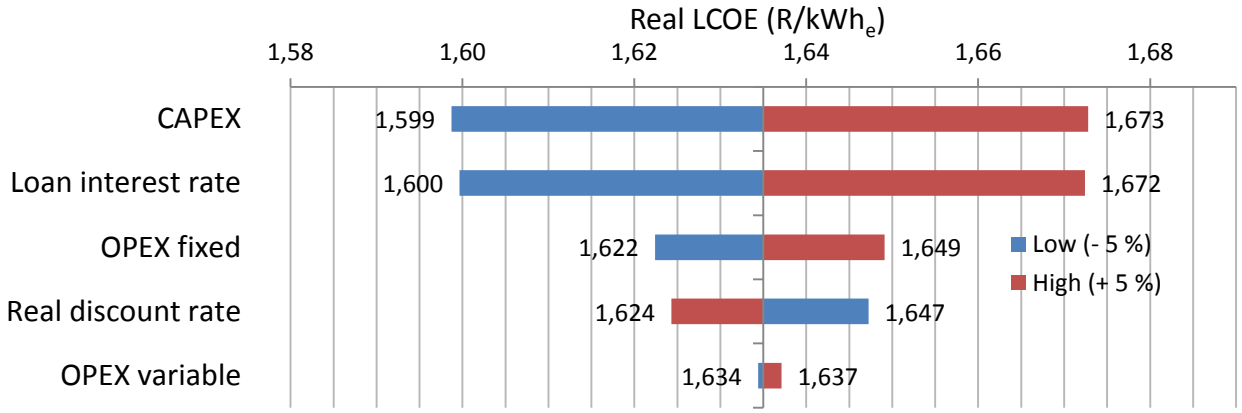

Figure 47: Sensitivity analysis on real LCOE

[29] There are two types of LCOE, i.e. a real LCOE and a nominal LCOE. The nominal LCOE is calculated by using a nominal discount rate (which includes inflation). The real LCOE was selected for this study because it is normally used for long-term studies. [56]

The sensitivity analysis revealed that the real LCOE is most sensitive to changes in CAPEX, loan interest rate and fixed OPEX. The CAPEX and OPEX estimates for each integration option are justifiable, because the CAPEX and OPEX cost models that were used in this study, were developed by NREL and are also relied upon by project developers, policy makers etc. [59]. Thus, the accuracy of these costs were not required to be improved.

An important point of note is that the cost of staff is one of the major costs contributors for operating & maintenance costs, and it is included in the fixed OPEX cost [89]. In South Africa the labour rates [90] are typically lower than the US market [91], thus the fixed OPEX cost used in this study, should be reduced accordingly. However, it was not reduced as this allows for a conservative estimate of real LCOE.

The loan interest rate of 8.8 % that is used in this study is also a justifiable estimate, as it is the lending rate to South Africa by The World Bank, as discussed in section 3.14.1. Thus, it was also not necessary to improve the accuracy of the loan interest rate.

5.10.2 LCA Results

The results of the LCA of each integration option are presented in Table 35 and Table 36.These results are based on the REFIT tariff as explained in section 3.13.3.It was found that none of the integration options were feasible when the Homelight 60A tariff was applied, hence these results were not presented.

Table 35: Economic life cycle assessment (REFIT): Feedwater heating options

Feedwater heater(s) (Method, technology)	**NPV (Rm)**	**TLCC (Rm)**	**SPB (years)**	**DPB (years)**	**Real LCOE (R/kWh$_e$)**
HPH6 (M1, PTC)	163.1	1294.6	11	25.6	1.92
HPH6 (M2, LFR)	346.0	1110.4	8.1	14.6	1.64
HPH6 (M2, PTC)	-26.7	1346.7	12.3	>30	2.01
HPH5 (M1, PTC)	-148.6	1238.9	19.7	>30	2.46
HPH5 (M2, LFR)	122.3	881.3	10.5	23.8	1.88
HPH5 (M2, PTC)	-115.2	1069.3	18.9	>30	2.42
DA (M2, LFR)	-124.6	573.5	26.9	>30	2.74
DA (M2*, PTC)	-259.0	755.0	>30	>30	3.3
LPH3 (M1, LFR)	-115.4	257.9	>30	>30	3.88
LPH3 (M1, PTC)	-216.9	330.7	>30	>30	6.39
LPH3 (M2, LFR)	-136.7	233.2	>30	>30	5.18
LPH3 (M2*, PTC)	-218.7	330.0	>30	>30	6.51
LPH1&2 (M1, LFR)	-378.5	448.9	>30	>30	13.75
LPH1&2 (M1, PTC)	-579.4	590.0	>30	>30	262.04

Amongst all of the feedwater heating options, it was found that the use of the LFR technology to supply steam to the HPH6 and HPH5 were the most economically feasible options. i.e. HPH6 (M2, LFR) and the HPH5 (M2, LFR) options. These options have a LCOE of 1.64 -1.88 R/kWh$_e$ and a DPB of 14.6-23.8 years. The HPH6 (M1, PTC) option is the 3rd most feasible feedwater heating option, and has a LCOE of 1.92 R/kWh$_e$ and a DPB of 25.6 years.

Table 36: Economic life cycle assessment (REFIT): Superheated steam supply options

Steam supply option (Solar technology)	**NPV (Rm)**	**TLCC (Rm)**	**SPB (years)**	**DPB (years)**	**Real LCOE (R/kWh$_e$)**
HP turbine (ST)	-203.4	1114.7	25.3	>30	1.95
IP turbine (ST)	-352.0	1257.3	>30	>30	2.22
BFP turbine (LFR)	78.6	526.3	10.3	22.9	1.86
BFP turbine (PTC)	-70.3	634.5	19.1	>30	2.43
LP turbine (LFR)	-451.1	1701.9	>30	>30	2.92
LP turbine (PTC)	-712.9	2108.3	>30	>30	3.28

Amongst all of the steam supply options, only the steam supply to the BFPT by using the LFR technology is feasible. This steam supply option, has an LCOE of 1.86 R/kWh$_e$ and a DPB of 22.9 years.

5.11 Reference heat rate versus cooling water temperature

As mentioned in section 4.1.2d, the cooling water (CW) inlet temperature to the condenser is specified as 22 °C in this study, however the CW inlet temperature does vary during each hour of the year. Thus, to illustrate the effect of CW inlet temperature on the results of this study, the VirtualPlant™ model was configured to maintain a gross power output of 600 MW_e, whilst varying the CW inlet temperature. The effect of CW inlet temperature on the heat rate of the coal- power plant is illustrated in Figure 48.

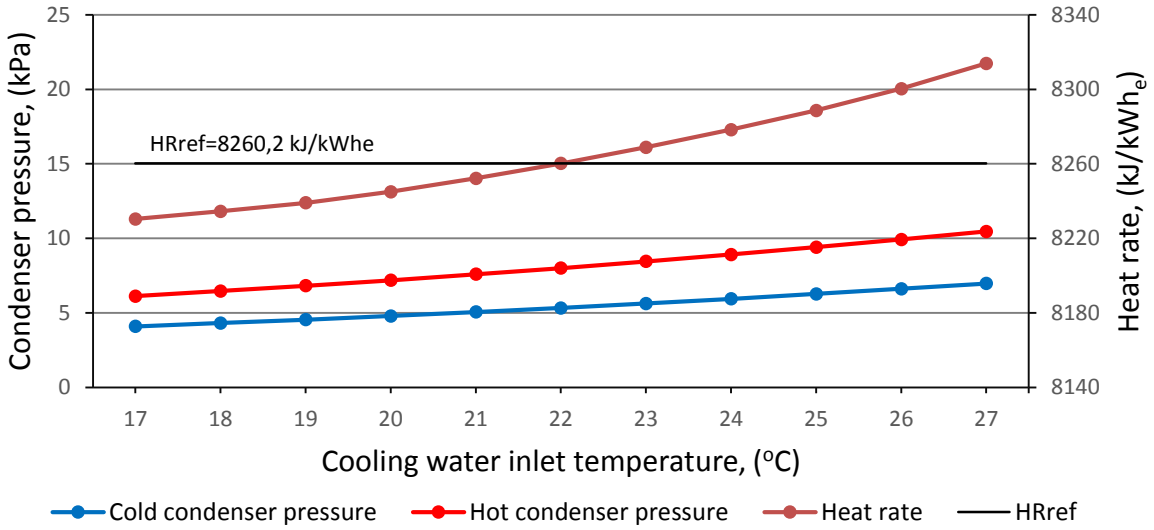

Figure 48: The effect of cooling water inlet temperature on heat rate of the coal power plant.

The results in Figure 48 indicate that the change in cooling water inlet temperature effects the condenser pressures. The change in condenser pressures thus effects the heat rate of the coal-power plant. This illustrates that the reference heat rates used in the study are not constant, and do change with CW inlet temperature. However, the variation in the reference heat rate due to changes in CW inlet temperature is minor, thus the reference heat rate can be used as a constant in this study. For example, at a CW inlet temperature of 27 °C the heat rate of the coal plant is just 0.7 % greater than 8260.2 kJ/kWh_e.

The reason for the increase in the heat rate of the plant is as follows. The higher condenser pressures (due to an increase in CW temperature), effectively reduces the pressure difference across the LP turbines. Hence, the available energy[30] to the LP turbines are reduced, and thus the power output from the LP turbines reduces. [92]

[30] Available energy is the isentropic enthalpy difference between two steam pressures. [80]

Thus, to maintain the 600 MW_e power output from the unit, the boiler will be required to produce more steam, thus the boiler load increases. An increase in the boiler load implies that the plant heat rate will increase.

6. Discussion

The following chapter discusses firstly the process flow changes that occur within the Rankine cycle of the power station, during the 'Fuel-saving' and 'Power-boosting' mode, as predicted by the VirtualPlant^{TM} model. This discussion is limited to the process flow changes that occur due to the HPH6 feedwater heating options, because the HPH6 options have the best economic feasibility, as illustrated in section 5.10.2.The process flow changes that occur due to some of the other integration options, is presented in Appendix G. The second section of this chapter discusses the observations and findings based on the results from chapter 5. The last section of this chapter discusses the expected plant response to cloud cover.

6.1 Process flow changes

The following section discusses the process flow changes that occur within the boiler plant, the turbine plant, the main steam condenser and the boiler feedwater pump, for the HPH6 feedwater heating integration option. The terms 'reduced', 'lower', 'increased' etc., are used to describe the process flow conditions of the solar-coal plant, in relation to the process flow conditions of the reference plant, which is illustrated in Figure 21. As mentioned in section 3.8, the amount of solar heat added to the Rankine cycle of the power station was such that none of the technical capabilities of the power station were exceeded.

6.1.1 HP feedwater heater 6: Fuel-saving mode

During the 'Fuel-saving' mode the superheater outlet flow rate of the boiler is reduced because some bled steam to HPH6 is saved. The saved bled steam mass flow rate adds to and increases the boiler reheater mass flow rate. A higher reheater pressure is now required for the increased reheater mass flow rate.

The reheater spraywater flow reduces by 1.3 kg/s, because of the reduction in boiler load. The HP turbine power output reduces because of the lower superheater outlet flow rate and high back pressure of the reheater inlet. The increased outlet reheater flow rate and pressure increases the IP turbine's and LP turbine's power output. The main steam condenser pressures increase due to the increased LP turbine exhaust mass flow rate. The condenser pressures increase because the cooling water flow to the condenser is constant whilst the heat load of the condenser increases. The efficiencies of the HP, IP & LP turbines and steam extraction mass flow rates remain relatively unchanged.

The HPH6 feedwater heating solar heat integration option utilises either the PTC, for methods 1 & 2, or the LFR, for method 2. Method 1 and method 2 require 94.8 MW_t and 100.9 MW_t of solar heat to be delivered to the power plant respectively. It was noted from the VirtualPlant™ model simulation that method 1 has an integration effectiveness of 0.29 $kJ/kWh_e.MW_t$ more than method 2.The difference in integration effectiveness between method 1 and method 2 is explained as follows:

1. Method 1 reduces the bled steam consumption of the HPH6 by 1.5 kg/s more than method 2. This is because the feedwater flow rate through the HPH6 in method 1 is 46.5 kg/s, which is much lower than the feedwater flow rate through the HPH6 in method 2, i.e. 232.2 kg/s.
2. Method 2 requires the boiler feedwater pump (BFP) to discharge an additional 40.7 kg/s of feedwater to the solar boiler, which increases the power consumption of the BFP by approximately 1.35 MW_e. As a result, the bled steam consumption of the BFPT is 1.8 kg/s more than plant operation using method 1.

6.1.2 HP feedwater heater 6: Power-boosting mode

During the 'Power-boosting' mode the boiler superheater outlet steam flow rate remains constant at full load, i.e. 491.2 kg/s. The saved bled steam mass flow rate adds to and increases the boiler reheater mass flow rate. A higher reheater pressure is now required for the increased reheater mass flow rate. The reheater pressure and mass flow rate during the 'Power-boosting mode' is higher than reheater pressure and mass flow rate during the 'Fuel-saving' mode.

The reheater spraywater flow has negligible change because the boiler load is essentially constant. The HP turbine power output is reduced although the boiler superheater outlet (HP turbine inlet flow) is at full load. The higher reheater pressure (HP turbine back pressure) is responsible for the reduction in the HP turbine power output. A reduced pressure drop across the HP turbine reduces the available energy[31] for the HP turbine. The changed reheater conditions have a consequential effect, as in the 'Fuel-saving' mode, of increasing the IP & LP turbine power output and the main steam condenser pressures.

The HPH6 feedwater heating solar heat integration option utilises either the PTC for methods 1 & 2, or the LFR technology for method 2. Method 1 and method 2 require 94.8 MW_t and 100.9 MW_t of solar heat to be delivered to the power plant respectively. However, it was noted from the VirtualPlant™ model simulation that method 1 increases the generator power output by 0.7 MW_e

[31] Available energy is the isentropic enthalpy difference between the inlet and exhaust pressures of the turbine [80].

more than method 2. The difference in the generator power output of methods 1 & 2 is explained as follows:

1. Method 1 reduces the bled steam consumption of the HPH6 by 3.5 kg/s more than method 2. This is because the feedwater flow rate through the HPH6 in method 1 is 53.8 kg/s, which is much lower than the feedwater flow rate through the HPH6 in method 2 i.e. 245.6 kg/s.
2. Method 2 requires the BFP to discharge an additional 41.3 kg/s of feedwater to the solar plant, which increases the power consumption of the BFP by approximately 1.4 MW_e. The bled steam consumption of the BFPT hence increases by 1.9 kg/s.
3. The IP turbine in method 1 produces approximately 1.9 MW_e more than in method 2. This power difference is because the IP turbine has a higher inlet mass flow rate, approximately 3.5 kg/s more than method 2, and a reduced 1st extraction bled steam consumption, to the BFPT. The IP & LP turbines have efficiencies of 91.4 % and 93 % in comparison to the HP turbine i.e. 90.9 %.

6.2 Research results

a) Land area and reflective area usage

It was found that the PTC and LFR fields have similar reflective area usages, as noted in Table 23. However, the land area usage of the PTC field is approximately twice the land area usage of the LFR field. This is because the PTC field requires large row-to-row spaces between the solar collector assemblies (SCAs), in order to reduce mutual shading between the SCAs which occurs in the morning and in the evening. The LFR field does not require large row-to-row spaces between the SCAs because of the planar ('flat') nature of the LFR assembly, hence the LFR field requires less land than the PTC field. [43]

The ST has the smallest reflective area usage, because the heliostat field has two axis of tracking and the heliostat field layout is optimised to reduce losses. However, the ST has the largest land area usage because the heliostats are required to be spaced adequately to reduce shadowing and blocking losses [87]. Shadowing and blocking losses are illustrated in Figure 42.

b) Integration effectiveness

As mentioned in section 5.5, the effectiveness of an integration option is its ability to reduce the solar-coal plant heat rate for a given amount of solar heat. It was found in this study that the Integration effectiveness (IE) of the HPH6 options was the highest amongst the feedwater heating options. The IE of the feedwater heating options was also found to decrease from the HPHs to the LPHs. A similar trend was found among the steam supply options, the IE of the steam supply options decreased from the HP turbine option to the LP turbine option. Thus, based on these results, it

illustrates that the IE of an integration option increases as the temperature/pressure of the steam produced or saved (in the case of M1 feedwater heating) by the integration option, increases.

A study by [24] which investigated the benefit[32] of solar aided feedwater heating in a coal-fired subcritical power plant, also found that there is a greater benefit in using solar heat at the high-temperature feedwater heaters than using solar heat at the low-temperature feedwater heaters. The reason for the greater benefit in using solar heat at the high-temperature feedwater heaters, as explained in the study by [24], is because the 'higher temperature corresponds to a higher quality of energy (exergy)'.

For example, the steam temperature supplied to the HP turbine by the ST is 535 ^{o}C, and the corresponding IE is 5.6 kJ/kWh$_e$.MW$_t$. In comparison, the HPH6 (M1, PTC) option which saves bled steam at a temperature 330 ^{o}C, has an IE of 4.3 kJ/kWh$_e$.MW$_t$.

c) Solar field size and solar electricity capacity

It was observed in section 5.4 that amongst all of the feedwater heating options, the HPHs could be supplied with the largest amount of solar heat. This is because the HPHs have the largest feedwater flow rates and they also produce the largest feedwater temperature rise. This can be noted from the operating conditions of the feedwater heaters, which are listed in Table 6. For example, the LPH3 produces a 19.4 ^{o}C temperature rise on a feedwater flow rate of 372.8 kg/s, whereas HPH6 produces a 58.6 ^{o}C temperature rise on a feedwater flow rate of 491.2 kg/s. The HPH6 integration options were also the only feedwater heating options that could achieve the 30 MW$_e$ of solar electricity during the 'Fuel-saving' mode, this is because of the 'thermal size' of the HPH6 and also because of the high IE associated with the HPH6 integration options.

Contrasting to the feedwater heaters, all of the steam supply options could achieve the 30 MW$_e$ of solar electricity (except for the steam supply to the BFPT) during the 'Fuel-saving' mode. The steam supply option to the LP turbine required the largest amount of solar heat because this option has a poor IE.

During the 'Power-boosting' mode it was found that the HPH6, HPH5 and all of the steam supply options (except for the steam supply to the BFPT) could achieve a solar electricity capacity > 30 MW$_e$, with the same amount of solar heat (or sometimes less) as during the 'Fuel-saving' mode. This is because the gross unit power and the heat rate reduction increases during the 'Power-boosting' mode.

[32] Benefit refers to the Energy Performance Index (EnPI) which is defined as the excess power generated over the design rated capacity divided by the energy input to the solar collector field [24].

The heat rate reduction increases during the 'Power-boosting' mode because the reference heat rate increases as the gross unit power increases.

The steam supply option to the BFPT was unable to achieve the 30 MW_e of solar electricity, although the steam to the BFPT was completely supplied by the solar plant. This is because the BFPT produces just 14.1 MW_e during normal plant operation.

d) Heat-cost and installed capacity cost

As noted in Table 33, each CSP technology has a different heat-cost. The LFR has the lowest heat-cost (approx. 8.3 Rm/MW_t), the PTC has the second lowest heat-cost (approx. 11.8 Rm/MW_t) and the ST has the highest heat-cost, 14.7 Rm/MW_t. The difference in heat-costs can be explained by analysing the CAPEX breakdown of each solar-coal plant option in Table 33. It was found that the reflective area[33] of the LFR influences 82 % of its CAPEX cost[34], and the reflective area of the PTC influences 75 % of its CAPEX cost. Also, the reflective area of the LFR contributes to its CAPEX at a rate of 265 \$/m^2, and the reflective area of the PTC contributes to its CAPEX a rate of 380 \$/m^2. Thus, the LFR heat-cost is significantly lower than the PTC heat-cost. The CAPEX of the ST is influenced by 40.4 % by the tower and receiver, which are expensive equipment items, hence the reason for the heat-cost of the ST being significantly more than the heat-cost of the LFR and PTC.

It can be observed from section 5.9 that the Installed capacity cost (ICC) of each integration option is driven by two factors i.e. the IE of the integration option and the heat-cost of the respective CSP technology. This is best illustrated with an example. The heat-cost of the ST is approximately 77 % more than the LFR. However, the ICC of the HP (ST) option is just 35 % greater than the ICC of the HPH6 (M2, LFR) option. The ICC of the HP (ST) option became comparable to the ICC of the HPH6 (M2, LFR) option, because the IE of the HP (ST) option is greater than the IE of the HPH6 (M2, LFR) option, i.e. the IE of the HP (ST) option is 5.6 and the IE of the HPH6 (M2,LFR) option is 4.1.

Thus, because the LFR has a significantly lower heat-cost than the PTC and ST, the integration options which use the LFR and produced a high IE, such as the HPH6 (M2, LFR) and the HPH5 (M2, LFR), have the lowest ICC in this study. The HPH6 (M2, LFR) option has an ICC of 28.1 kR/kW_e, which is the lowest ICC in this study.

[33] The reflective area was calculated by SAM, by using a loop conversion efficiency of 61.2 % for the LFR and 69.4% for the PTC, thus less reflective area is required by the PTC.

[34] 3 CAPEX cost categories, of both the LFR and the PTC, are calculated by using the reflective area. The cost categories are site preparations, solar collector field system and the heat transfer system, as per the CAPEX cost model in Table 15.

e) Economic life-cycle assessment

As explained in section 3.15, the LCA evaluates the costs against the benefits, to determine the economic feasibility of an integration option. The costs of an integration option are CAPEX, OPEX and income tax, and the economic benefits of an integration option are solar electricity, coal savings etc. Thus, the most economically feasible integration options would have the lowest CAPEX (in terms of heat-cost) and OPEX, and would have the best economic benefits.

As mentioned, the heat-cost of the LFR is significantly lower than its competitors i.e. the PTC and the ST, the LFR also has the lowest fixed OPEX amongst all the CSP technologies, as noted in Table 16. Based on the results in section 5.8 it was established that the best economic benefits are produced by the integration options which have high IEs.

Thus, it is no surprise that amongst the feedwater heating options the HPH6/5 (M2, LFR) options were the most economically feasible. The HPH6 (M2, LFR) and the HPH5 (M2, LFR) options produced an LCOE of 1.64 and 1.88 R/kWh$_e$, and have a DPB of 14.6 and 23.8 years respectively. The 3rd most economically feasible feedwater option is the HPH6 (M1, PTC) option, it has an LCOE of 1.92 R/kWh$_e$ and a DPB of 25.6 years. The HPH6 (M1, PTC) option has an IE of 4.3 which is greater than the IEs of the HPH6/5 (M2, LFR) options, however it is less economically feasible than the HPH6/5 (M2 LFR) options because the PTC has a higher heat-cost and OPEX cost than the LFR.

Amongst the steam supply options, the BFPT (LFR) option proved to be the most economically feasible option, because of the cost advantages associated with the LFR technology, and also because this option has a high IE of 3.1. The BFPT (LFR) option has a LCOE of 1.86 R/kWh$_e$ and a DPB of 22.9 years, i.e. the second most economically feasible option in this study. Thus, the HPH6 (M2, LFR) option is the most economically feasible integration option in this study, this option also produces electricity at the lowest carbon intensity i.e. 0.945 tCO_{2eq}/MWh$_e$.

It is worth mentioning that the HP (ST) option has the highest IE in this study, however this option was not economically feasible, because the ST has the highest heat-cost and OPEX cost amongst all the CSP technologies in this study.

6.3 Plant response to cloud cover

It was mentioned in section 2.12, that the effect of cloud cover on the solar field and on the power station should be assessed by transient heat modelling, however this investigation is beyond the scope of this study. During the duration of cloud cover it is expected that the coal-firing rate of the boiler should increase in order to maintain the generator output. The time required to re-establish load and system equilibrium is an important factor.

Thus, to approximate the response of the power station to the loss of solar heat, it was decided to observe the transient response of the power station, when high-pressure heaters (6) were put in-to-service, whilst the power station is operating at or near full load i.e. 600 MW_e. This scenario would closely resemble the feedwater heating option (HPH6) losing solar heat completely during full load plant operation. The Figure 49 and Table 37, based on actual plant data, illustrates the effect on generator power output and feedwater flow rate, when the HPH6 is put in-to-service.

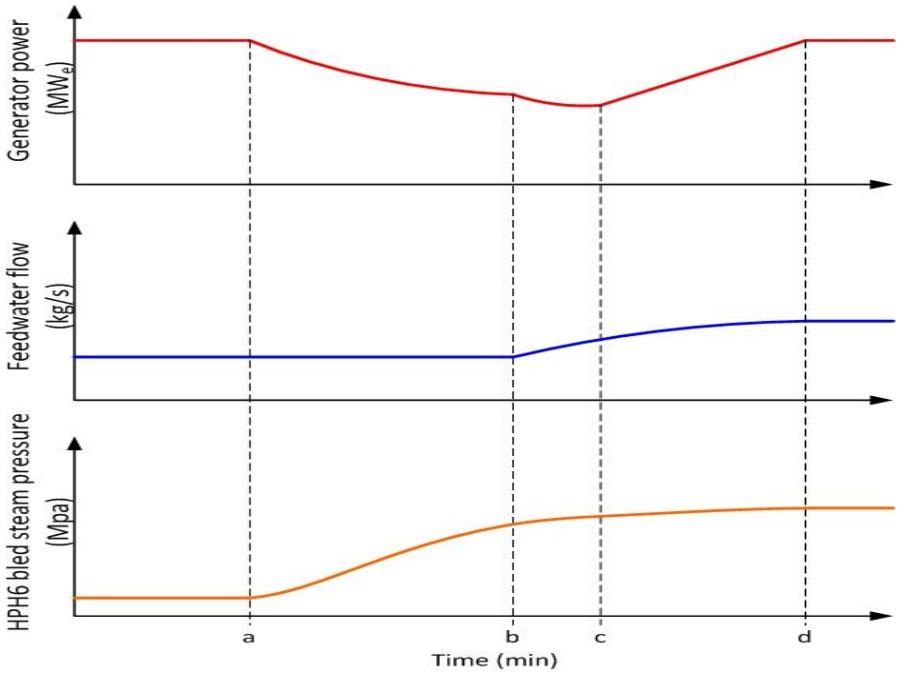

Figure 49: Boiler and turbine plant response to HPH6 put in-to-service during full load.

Table 37: HPH6 put in-to-service (15-01-2014)

Parameter	Units	Point a	Point b	Point c	Point d
Generator power	MW_e	583.5	567.1	557.9	583.5
Feedwater flow rate	Kg/s	396.2	397.2	411.5	432.3
Bled steam pressure	MPa	0.43	3.2	3.3	3.6
Time	h:min	13:08	13:18	13:20	13:25

Initially, at point *a*, the feedwater flow rate through the HPH6 is slowly increased from 0 %, which results in the bled steam pressure and bled steam mass flow rate of HPH6 increasing to point *b*. The generator power reduces to point *b* because of the increase in bled steam consumption whilst the feedwater flow rate remains relatively constant. The results in Table 37 show that the plant lost 16.4 MW_e in 10 minutes i.e. point *a* to point *b* loses 1.6 MW_e/min.

To recover the lost generator power, the boiler feedwater pump was then required to deliver more feedwater to the boiler (to compensate for the increased bled steam consumption), at point *b*. The initial increase in the feedwater flow rate results in a further reduction in the generator power, because a higher feedwater heater flow rate demands more bled steam to the feedwater heater. The generator power output is reduced by a further 9.2 MW_e in 2 minutes from points *b* to *c,* as illustrated in Figure 49.

After point *c*, the generator power increases proportionally to the increase in the boiler feedwater flow rate, until the generator power output is re-established at point *d*. The 25.6 (9.2 +16.4) MW_e loss is recovered in approximately 5 minutes i.e. point *c* to point *d* gains 5.2 MW_e/min.

This analysis illustrates that the total recovery time for the plant is approximately 17 minutes, when an HPH6 is put into service. The actual recovery time for the solar-coal plant (with the solar heat integration option) would be less than 17 minutes, because the system will have thermal inertia present from the solar piping, thermal oil etc, and also because the power station's boilers can safely re-establish load at a loading rate of 7 MW_e/min, if required.

Since the HPH6 is the largest of the feedwater heating integration options, 17 minutes is regarded as the longest recovery time expected for the feedwater heating options.

7. Conclusions and Recommendations

7.1 Conclusions

Eskom's coal-fired power stations are the largest single emitter of GHGs in South Africa [7]. The combustion of coal produces GHGs such as carbon dioxide, nitrous oxide etc. [65], and GHGs are responsible for global warming (climate change) [1] . One method of reducing the coal consumption (and hence GHG emissions) from a coal-fired power station is to add solar heat to the power station, this has been successfully demonstrated in countries such as Australia and the USA [25, 27] .

Thus, because the solar resource in SA is amongst the highest in the world [12], it was decided to conduct this study to investigate if the addition of solar heat to the power station (a coal-fired Eskom Power Station) is technically and economically feasible.

The first step that was taken in this study was to research the possible methods that can be used to integrate solar heat to the power station. The literature review revealed that the best possible methods to integrate solar heat to the power station, is by using solar heat to heat feedwater and to generate superheated steam. The next step in this study was to assess the available CSP technologies on the market to determine the maximum producible steam/water conditions from each CSP technology. It was found that 3 CSP technologies are applicable to this study i.e. the ST, LFR and PTC. The maximum producible steam conditions from the ST, LFR and PTC were found to be 535 ^{o}C/16 MPa, 500 ^{o}C/10 MPa and 380 ^{o}C/10 MPa respectively. Thereafter it was required to select a CSP technology (s) for each feedwater heating integration option and for each steam supply integration option. Essentially, all 3 CSP technologies were used for the steam supply options, however only the PTC and LFR were used for the feedwater heating options as the salt temperature (565 ^{o}C) from the ST was considered excessive for heating feedwater.

After selecting a CSP technology(s) for each integration option, it was required to determine the maximum amount of solar heat that can be supplied to the Rankine cycle of the power station, by each integration option. The maximum amount of solar heat that can be supplied by an integration option is such that none of the technical capabilities of the power station are exceeded during the addition of solar heat. Thus, a thermodynamic model of the Rankine cycle of the power station (referred to as the VirtualPlant^{TM} model) was used to predict the process flow conditions that are produced by each integration option. These process flow conditions were then compared to the technical capabilities of the power station to determine, through an iterative method, the maximum amount of solar heat for each integration option. The technical capabilities of the power station were sourced from OEM data sheets.

The annual benefits of each integration option were thereafter calculated i.e. solar electricity production, coal savings, GHG reduction etc. Essentially, each benefit was calculated for each hour of the year, by using the annual hourly solar field heat output (from SAM) and the heat rate reduction results from the VirtualPlant^{TM} model. The costs of each integration option, such as CAPEX and OPEX, were calculated by using cost models from SAM. The costs and benefits of each integration option were then used in a LCA to determine the economic feasibility of each integration option.

The results of the study indicated that the effectiveness of an integration option is related to the steam temperature and pressure that is produced or saved by the integration option. It was also observed from the results that the integration options which have a high effectiveness returned the best annual benefits. The LFR technology is found to be the most economically feasible CSP technology that can be used for feedwater heating or for supplying superheated steam. This is because the LFR can produce high steam temperatures and pressures, and it also has the lowest heat-cost and the lowest fixed OPEX cost amongst the 3 CSP technologies. The most economically feasible option in this study is the HPH6 (M2, LFR) option which has a LCOE of 1.64 R/kWh$_e$, and have a DPB of 14.6 years. This option reduces the carbon intensity of the power plant to 0.945 tCO$_{2eq}$/MWh$_e$ (i.e. the carbon intensity of the power plant is reduced by 1.6 %) and reduces the coal consumption of the power plant by 0.18t/MWh$_t$ of solar heat. Although there does not exist a bench mark DPB to compare to, the DPB of 14.6 years is less than half the expected plant life of 30 years.

Therefore, the answer to the question of this study, 'Is solar heat addition to the power station technically and economically feasible?' would be, yes, based on the assumptions made in the study. This result has a broader implication for Eskom. It would imply that subcritical and supercritical coal-fired power stations, which have an annual solar resource which is equivalent or greater than the solar resource at the power station, are also suitable to be supplied with solar heat.

7.1.1 Study limitations

a) As mentioned in section 5.10.2, the integration options mentioned were economically feasible because of the REFIT, based on the Homelight 60A tariff none of the integration options were economically feasible. The REFIT, as mentioned in 3.13.3, is only applicable to IPPs, thus at present moment this project would not be feasible to Eskom. Hence, a subsidy (e.g. from government) is required for solar-coal plants, in order to make this project a reality.

b) The tariff for the LFR was assumed to be equal to the PTC REFIT because there was no REFIT tariff specified for LFR. REFITs are calculated based on the technology CAPEX and on the fixed &

variable operating and maintenance costs [69], hence if a LFR REFIT was specified it would be expected to be lower than the PTC REFIT.

c) The LFR was found to be the most economically feasible CSP technology in this study, however unlike the PTC and ST, the LFR was not used to its full potential. For example, the LFR can produce steam of 500 ^{o}C/10 MPa, however in this study the highest steam temperature and pressure produced by the LFR was 330 ^{o}C /3.9 MPa. This is because steam temperatures of 500 ^{o}C only exist within the boiler, and hence steam cannot be supplied to these areas.

7.2 Recommendations

The following recommendations are provided for future work in this field:

a) It was illustrated in section 5.11, the effect of cooling water inlet temperature has a small impact on the outcome of this study. However, if it is required to achieve refined results, the effect of cooling water temperature should be addressed. It is suggested that the hourly CW inlet temperature be read of the cooling tower performance curves, by using the hourly dry bulb air temperature (which is obtained from the weather file). The hourly CW inlet temperature can then be used to determine the hourly condenser pressures and hourly plant heat rate.

b) As mentioned in section 4.1.2, the use of the OEM trend in Figure 25, to predict the reheater spray water flow in this study, is not entirely correct. However, the error associated with using the OEM trend would have little impact on the results. If it is required to produce refined results, a different approach should be used to predict the reheater spray flow. It is suggested that a heat transfer model of the reheater be developed, which can be used to determine the reheater spray flow for different flue gas and reheater steam flows.

c) It would also be advisable to investigate the transient effect of cloud cover on the heat output of the solar field, as this may create operational problems for some of the superheated steam supply options. The feedwater heating options are expected to cope with a scenario where solar heat is lost completely, as explained in section 6.3. It is suggested that a transient power plant model be developed to predict the dynamic power plant behaviour during fluctuating solar heat input.

It is advised that Eskom should not implement this project, based on the high-level of costing used in this study, but should rather perform a more detailed study before considering project implementation. The detailed study should be conducted according to the following steps:

a) Assess the DNI resource at other Eskom coal-fired power station sites, to determine the sites which have the highest DNI. The new build power stations such as Medupi and Kusile, should

also be included in this assessment because these power stations operate using supercritical Rankine cycles.

b) Once it has been determined which sites have the highest DNI resource, the economic feasibility for these sites should be calculated by using the methods of this study.

c) The LCA should then be repeated by using detailed cost estimates, only for the sites which are found to be the most economically feasible in point b. The detailed cost estimates are to include the shutdown cost of the plant, inflation costs of materials, 'tie-in' costs for the integration options etc.

d) Based on the outcome of the detailed LCA, Eskom should make a decision regarding project implementation.

8. List of References

[1] National Research Council, “REPORT IN BRIEF (America’s Climate Choices : Limiting the Magnitude of Future Climate Change),” National Academies Press, Washington, 2010.

[2] World Meteorological Organisation, “WMO GREENHOUSE GAS BULLETIN No.9,” Atmospheric Environment Research Division, Geneva, 2013.

[3] United States Environmental Protection Agency , “EPA,” 02 July 2014. [Online]. Available: http://www.epa.gov/climatechange/ghgemissions/gases/co2.html. [Accessed 13 November 2014].

[4] Intergovernmental Panel on Climate Change (IPCC), “Energy supply. In Climate Change 2007: Mitigation. Contribution of Working Group III to the Fourth Assessment Report of the Intergovernmental Panel on Climate Change,” Cambridge University Press, Cambridge, United Kingdom and New York, NY, USA., 2007.

[5] VGB PowerTech, *FACTS AND FIGURES, ELECTRICITY GENERATION 2012|2013,* Essen, Germany, 2012.

[6] International Energy Agency (IEA) Coal Industry Advisory Board , “Power Generation from Coal : Measuring and Reporting Efficiency Performance and CO2 Emissions,” International Energy Agency, Paris, 2010.

[7] National treasury: Republic of South Africa, “CARBON TAX POLICY PAPER: Reducing greenhouse gas emissions and facilitating the transition to a green economy,” National treasury of the Republic of South Africa, 2013.

[8] DEPARTMENT OF MINERALS AND ENERGY OF SOUTH AFRICA, “ELECTRICITY PRICING POLICY (EPP) OF THE SOUTH AFRICAN ELECTRICITY SUPPLY INDUSTRY,” 2008.

[9] Eskom, “Eskom Integrated Report 2011| Additional information -Tables,” Eskom, 2012. [Online]. Available: http://financialresults.co.za/2011/eskom_ar2011/add_info_tables.php. [Accessed 6 August 2014].

[10] The Department of Energy of South Africa, "INTEGRATED RESOURCE PLAN FOR ELECTRICITY (IRP) 2010-2030 UPDATE REPORT 2013," 2013.

[11] Eskom, "eskom," Eskom, [Online]. Available: http://www.eskom.co.za/Whatweredoing/NewBuild/Pages/Renewable_Energy.aspx. [Accessed 6 August 2014].

[12] DEPARTMENT OF MINERALS AND ENERGY :REPUBLIC OF SOUTH AFRICA , "WHITE PAPER ON RENEWABLE ENERGY," DEPARTMENT OF MINERALS AND ENERGY, 2003.

[13] Y. Yang, Q. Yan, R. Zhai, A. Kouzani and E. Hu, "An efficient way to use medium-or-low temperature solar heat for power generation-integration into conventional power plant," *Applied Thermal Engineering,* vol. 31, pp. 157-162, 2011.

[14] E. Hu, Y. Yang, A. Nishimura, F. Yilmaz and A. Kouzani, "Solar thermal aided power generation," *Applied Energy,* vol. 87, pp. 2881-2885, 2010.

[15] S. D. Bracher, "discoversiemensafrica," Siemens, 26 January 2012. [Online]. Available: http://www.discoversiemensafrica.com/topics/how-to-update-a-coal-fired-power-station/. [Accessed 12 August 2014].

[16] E. Hu, G. J. Nathan, D. Battye, G. Perignon and A. Nishimura, "AN EFFICIENT METHOD TO GENERATE POWER FROM LOW TO MEDIUM TEMPERATURE SOLAR AND GEOTHERMAL RESOURCES," in *Chemeca 2010*, Adelaide, 2010.

[17] D. Popov, "An option for solar thermal repowering of fossil fuel fired power plants," *Solar Energy,* vol. 85, pp. 344-349, 2011.

[18] J. H. Peterseim, S. White, A. Tadros and U. Hellwig, "INTEGRATED SOLAR COMBINED CYCLE PLANTS USING SOLAR POWER TOWERS TO OPTIMISE PLANT PERFORMANCE," in *SolarPACES 2012 conference* , Marrakech, 2012.

[19] AREVA solar, *Liddell Solar Thermal Station: Reliable solar steam for a clean power boost,* CA , 2009.

[20] "Enggcyclopedia," 2014. [Online]. Available: http://www.enggcyclopedia.com/2011/12/power-plant-efficiency/. [Accessed 20 September 2014].

[21] Eastern Mediterranean University : Department of Mechanical Engineering, "Eastern Mediterranean University : Department of Mechanical Engineering (Power plant engineering: Chapter 2 Power plant thermodynamics)," [Online]. Available: http://me.emu.edu.tr/haybar/me446/chapter2.pdf. [Accessed 24 November 2014].

[22] M. Steinhagen and H. M. Gottfried, "THERMOPEDIA," SEMANTIC GLOBE: THERMAL SCIENCES, 7 February 2011. [Online]. Available: http://www.thermopedia.com/content/1072/. [Accessed 24 November 2014].

[23] R. J. ZOSCHAK and S. F. WU, "STUDIES OF THE DIRECT INPUT OF SOLAR ENERGY TO A FOSSIL-FUELED CENTRAL STATION STEAM POWER PLANT," *Solar Energy,* vol. 17, pp. 297-305, 1975.

[24] M. R. K. a. K. A. Suresh, "4-E (Energy, Exergy, Environment and Economic) analysis of solar thermal aided coal-fired power plants," *Energy for Sustainable Development,* vol. 14, pp. 267-279, 2010.

[25] Electric Power Research Institute (EPRI), "Demonstration Development Project: Solar Augmentation at the Coal-Fired Cameo Generating Station," EPRI, Palo Alto, CA, 2011.

[26] M. R. K. a. K. A. Suresh, "4-E (Energy, Exergy, Environment and Economic) analysis of solar thermal aided coal-fired power plants," *Energy for Sustainable Development,* vol. 14, pp. 267-279, 2010.

[27] CSEnergy, "Kogan Creek Solar Boost Project," 2014. [Online]. Available: http://kogansolarboost.com.au/about/how-it-works/. [Accessed 18 August 2014].

[28] CS ENERGY , *World's largest solar integration with a coal-fired power station gets go ahead (MEDIA RELEASE),* 2011.

[29] B. Omar, K. Abdallah and M. Kamal, "A review of studies on central reciever solar thermal power plants," *Renewable and Sustainable Energy Reviews,* vol. 23, pp. 12-39, 2013.

[30] Z. E. L. P. M. Fernandez-Garcia A, "Parabolic-trough solar collectors and their applications," *Renewable and Sustainable Energy Reviews,* vol. 14, pp. 1695-1721, 2010.

[31] V. Quaschning, "Erneuerbare-Energien-und-Klimaschutz.de," [Online]. Available: http://www.volker-quaschning.de/articles/fundamentals2/index.php. [Accessed 18 August 2014].

[32] J. Ortega, J. Burgaleta and F. M. Tellez, "Central Reciever System Solar Power Plant Using Molten Salt as Heat Transfer Fluid," *Journal of Solar Energy Engineering,* vol. 130, pp. 024501-1-024501-6, 2008.

[33] Electric Power Research Institute (EPRI), Solar Power Fact Book, Palo Alto, California : EPRI, 2010.

[34] ATKEARNEY ,ESTELA, "Solar Thermal Electricity 2025 Clean electricity on demand: attractive STE cost stabilize energy production," 2010.

[35] Electric Power Research Institute (EPRI), "Solar Thermal Electric Technology :2008," EPRI, Palo Alto, 2008.

[36] P. Konstantin and J. Kretschmann , *Assessment of Technology Options for Development of Concentrating Solar Power in South Africa for The World Bank,* Johannesburg, 2010.

[37] D. Kearney , B. Kelly , R. Cable, N. Potrovitza , U. Herrmann, P. Nava , R. Mahoney, J. Pacheco, D. Blake and H. Price, "ASSESSMENT OF A MOLTEN SALT HEAT TRANSFER FLUID IN A PARABOLIC TROUGH SOLAR FIELD," 2002.

[38] U. Herrmann, M. Geyer and D. Kearney, *Overview on Thermal Storage Systems (Workshop on Thermal Storage for Trough Power Systems),* 2002.

[39] C. World, "CSP World," [Online]. Available: http://www.csp-world.com/resources/technology. [Accessed 8 August 2014].

[40] J. Glänzel, "pressebox," Novatec-solar, 20 April 2009. [Online]. Available: http://www.pressebox.de/presscorner/firma/novatec-solar/meldung/boxid/256435/iframe/779. [Accessed 25 september 2014].

[41] R. Abbas, J. Munoz-Anton, M. Valdes and J. Martinez-Val , "High concentration linear Fresnel reflectors," *Energy Conversion Management,* p. Article in press, 2013.

[42] M. J. Wagner, "Results and Comparison from the SAM Linear Fresnel Technology Performance Model," in *2012 World Renewable Energy Forum* , Denver, 2012.

[43] M. Gunther, "Chapter 6 Linear Fresnel Technology," in *Advanced CSP Teaching Materials*, 2012, pp. 1-42.

[44] Novatec Solar, *News Release: Novatec Solar's Fresnel collector generates superheated steam above 500°C,* Karlsruhe, 2011.

[45] Novatec Solar, *Turnkey Solar Boiler based on Fresnel Collector Technology, mass produced in industrial precision with performance guarantee (Product brochure),* Karlsruhe.

[46] AREVA SOLAR, *CLFR Molten Salt Storage for Reliable, Dispatchable CSP Generation,* Mountain View: AREVA SOLAR, 2012.

[47] D. Laing, C. Bahl, T. Bauer, D. Lehmann and W.-D. Steinmann, "Thermal energy storage for direct steam generation," *Solar Energy,* vol. 85, pp. 627-633, 2011.

[48] Eskom Holdings SOC Limited, "Eskom," Eskom, 2014. [Online]. Available: http://www.eskom.co.za/Whatweredoing/NewBuild/Pages/Renewable_Energy.aspx. [Accessed 20 August 2014].

[49] GeoModel SOLAR, "solargis," 2010. [Online]. Available: http://solargis.info/doc/free-solar-radiation-maps-DNI#S. [Accessed 12 August 2014].

[50] AfriGIS (PTY) Ltd,Google, "Google Maps Engine LITE," 2014. [Online]. Available: https://mapsengine.google.com/map/edit?hl=en&authuser=0&mid=zpyB-hvsSaRM.kSC4hqxHwEZk. [Accessed 21 August 2014].

[51] Xcel Energy Public Service Company of Colorado, "Final Report Innovative Clean Technology "The Colorado Integrated Solar Project"," 2011.

[52] C. Kutscher, M. Mehos, C. Turchi, G. Glatzmaier and T. Moss , "Line-Focus Solar Power Plant Cost Reduction Plan," NREL, Golden, 2010.

[53] National Renewable Energy Laboratory (NREL) and SolarPACES, “NREL,” NREL, 25 November 2013. [Online]. Available: http://www.nrel.gov/csp/solarpaces/. [Accessed 23 August 2014].

[54] J. Hinkley, B. Curtin, J. Hayward, A. Wonhas, R. Boyd, C. Grima, A. Tadros, R. Hall, K. Naicker and A. Mikhail, “Concentrating solar power – drivers and opportunities for cost-competitive electricity,” CSIRO, 2011.

[55] National Renewable Energy Laboratory (SolarPACES), “National Renewable Energy Laboratory (NREL),” NREL, 14 May 2014. [Online]. Available: http://www.nrel.gov/csp/solarpaces/power_tower.cfm. [Accessed 11 August 2014].

[56] N. R. E. L. (NREL), A Manual for the Economic Evaluation of Energy Eflciency and Renewable Energy Technologies, Golden: NREL, 1995.

[57] C. Turchi, “Parabolic Trough Reference Plant for Cost Modeling with the Solar Advisor Model (SAM) (Technical Report NREL/TP-550-47605),” National Renewable Energy Laboratory (NREL), Golden, 2010.

[58] C. S. Turchi and M. J. Wagner, “WREF 2012: POWER TOWER REFERENCE PLANT FOR COST MODELING WITH THE SYSTEM ADVISOR MODEL (SAM),” National Renewable Energy Laboratory (NREL), Golden, 2012.

[59] N. Blair, A. P. Dobos, J. Freeman , T. Neises, M. Wagner, T. Ferguson, P. Gilman and S. Janzou, “System Advisor Model, SAM 2014.1.14: General Description,” NREL, Golden, 2014.

[60] T. Fluri, *Solar Resource Mapping in South Africa,* Stellenbosch: Stellenbosch university, 2009.

[61] Legal and Policy Division, SOUTH AFRICAN REVENUE SERVICE (SARS), *TAXATION IN SOUTH AFRICA 2012/13,* 2013, p. 48.

[62] Eskom Holdings SOC Limited , “Interim Integrated Report for the six months ended 30 September 2013,” Eskom, 2013.

[63] A. Ruffini, “esi-africa,” WEB2WEB, 2 August 2013. [Online]. Available: http://www.esi-africa.com/coal-compact-necessary-for-sa-s-electricity-sector/. [Accessed 25 September 2014].

[64] S. Fakir, “The South African Civil Society Information Service (SACSIS),” SACSIS, 2 October 2013. [Online]. Available: http://sacsis.org.za/site/article/1803. [Accessed 25 September 2014].

[65] EPA, “Bituminous And Subbituminous Coal Combustion,” 2014. [Online]. Available: http://www.epa.gov/ttnchie1/ap42/ch01/final/c01s01.pdf. [Accessed 21 september 2014].

[66] M. EDKINS, A. MARQUARD and H. WINKLER, “South Africa’s renewable energy policy roadmaps,” Cape Town , 2010.

[67] INTERGOVERNMENTAL PANEL ON CLIMATE CHANGE (IPCC), “IPCC,” 15 June 2012. [Online]. Available: http://www.ipcc.ch/publications_and_data/publications_ipcc_fourth_assessment_report_wg1_report_the_physical_science_basis.htm. [Accessed 14 August 2014].

[68] ESKOM, *Homelight Brochure Small Power Users,* 2013.

[69] NATIONAL ENERGY REGULATOR OF SOUTH AFRICA (NERSA), *NERSA Consultation Paper:Review of Renewable Energy Feed - In Tariffs,* NERSA, 2011, p. 25.

[70] H. von Blottnitz, “A comparison of air emissions of thermal power plants in South Africa and 15 European countries,” *Journal of Energy in Southern Africa,* vol. 17, no. 1, pp. 72-81, 2006.

[71] National Renewable Energy Laboratory (NREL), “System Advisor Model (SAM) Help guide,” 2013.

[72] J.-B. Styan, “Fin24,” News24, 28 October 2011. [Online]. Available: http://www.fin24.com/Companies/Industrial/World-Bank-grants-second-loan-to-Eskom-20111028. [Accessed 12 August 2014].

[73] The World Bank (IBRD.IDA), “worldbank,” The World Bank, [Online]. Available: http://data.worldbank.org/indicator/FR.INR.LEND. [Accessed 12 August 2014].

[74] R. P. Charles, K. W. Davis and J. L. Smith, “ASSESSMENT OF CONCENTRATING SOLAR POWER TECHNOLOGY COSTS AND PERFORMANCE FORECASTS,” in *Electric Power*, Chicago, 2005.

[75] G. Morin , J. Dersch, W. Platzer, M. Eck and A. Haberle, "Comparison of Linear Fresnel and Parabolic Trough Collector power plants," *Solar Energy,* vol. 86, pp. 1-12, 2012.

[76] Investopedia US, "INVESTOPEDIA," 2014. [Online]. Available: http://www.investopedia.com/terms/n/npv.asp. [Accessed 03 September 2014].

[77] Department of Energy of South Africa, *IRP INPUT PARAMETERS S3: Discount rate - IRP 2010 Input Parameter,* 2010.

[78] General Physics Corporation, *EtaPRO:VirtualPlant USER GUIDE,* New York , 2011.

[79] STEINMULLER, [redacted] *SPRAYWATER FLOW VERSUS BOILER LOAD,* 1977.

[80] R. C. SPENCER, K. C. COTTON and C. N. CANNON, "A Method for Prediciting the Performance of Steam Turbine-Generators.... 16,500kW and Larger," *Journal of Engineering for Power ,* pp. 249-298, 1963.

[81] Google, "Google," 2014. [Online]. Available: https://www.google.co.za/maps/place/[redacted]+Power+Station/@-25.968496,29.3356014,2510m/data=!3m1!1e3!4m2!3m1!1s0x1eeaf72a64d4e783:0x2fec59887abf49. [Accessed 12 August 2014].

[82] meteonorm, "meteonorm," [Online]. Available: http://meteonorm.com/. [Accessed 20 September 2014].

[83] NREL, "Solar and Wind Energy Resource Assessment (SWERA)," OpenEI, [Online]. Available: http://en.openei.org/apps/SWERA/. [Accessed 13 August 2014].

[84] M. J. Wagner and P. Gilman, "Technical Manual for the SAM Physical Trough Model," NREL, Golden, 2011.

[85] A. M. PATNODE, "Simulation and Performance Evaluation of Parabolic Trough Solar Power Plants," WISCONSIN-MADISON, 2006.

[86] M. J. Wagner and G. Zhu, "A DIRECT-STEAM LINEAR FRESNEL PERFORMANCE MODEL FOR NREL'S," in *ASME 2012 6th International Conference on Energy Sustainability & 10th Fuel Cell Science, Engineering and Technology Conference* , San Diego, 2012.

[87] M. J. WAGNER , “Simulation and Predictive Performance Modeling of Utility-Scale Central Receiver System Power Plants,” MADISON , 2008.

[88] P. K. Falcone, A HANDBOOK FOR SOLAR CENTRAL RECEIVER DESIGN, Livermore: Sandia National Laboratories, 1986, pp. 2.3-3.

[89] Sargent & Lundy LLC Consulting Group , “Assessment of Parabolic Trough and Power Tower Solar Technology Cost and Performance Forecasts,” NREL, Golden, 2003.

[90] Statistics South Africa, “Statistics South Africa,” Statistics South Africa, 24 June 2014. [Online]. Available: http://beta2.statssa.gov.za/?page_id=1854&PPN=P0277&SCH=5849. [Accessed 10 September 2014].

[91] U.S. Bureau of Labor Statistics, “United States Department of Labour bureau of Labor Statistics,” 1 April 2014. [Online]. Available: http://www.bls.gov/oes/current/oes518013.htm. [Accessed 10 September 2014].

[92] R. K. Kapooria, S. Kumar and K. S. Kasana , “Technological investigations and efficiency analysis of a steam heat exchange condenser: conceptual design of a hybrid steam condenser,” *Journal of Energy in Southern Africa ,* vol. 19, no. 3, pp. 35-45, 2008.

[93] EPA : United States Environmental Protection Agency, “EPA,” 9 September 2013. [Online]. Available: http://www.epa.gov/climatechange/glossary.html. [Accessed 14 August 2014].

[94] SULZER, *Calculated characteristics of a HPT pak 43-35.st and 302 HZB 580,* 1976.

[95] C. S. T. a. G. A. Heath, “Molten Salt Power Tower Cost Model for the System Advisor Model (SAM),” Golden, 2013.

[96] property24 , “property24,” 2014. [Online]. Available: http://www.property24.com/vacant-land-for-sale/witbank/mpumalanga/44. [Accessed 21 September 2013].

[97] Next Era Energy Resources, *Solar Electric Generating Systems.*

[98] M. Geyer, E. Lupfert, R. Osuna, A. Esteban, W. Schiel , A. Schweitzer, E. Zarza, . P. Nava , J. Langenkamp and E. Mandelberg, “EUROTROUGH - Parabolic Trough Collector Developed

for Cost Efficient Solar Power Generation," in *11th SolarPACES International Symposium on Concentrated Solar Power and Chemical Energy Technologies*, Zurich, 2002.

[99] National Renewable Energy Laboratory (SolarPACES), "National Renewable Energy Laboratory," NREL, 3 December 2013. [Online]. Available: http://www.nrel.gov/csp/solarpaces/project_detail.cfm/projectID=36. [Accessed 10 August 2014].

[100] Instalaciones Inabensa, S.A. , "EUROTROUGH II : Extension,Test and Qualification of EUROTROUGH from 4 to 6 Segments at Plataforma Solar de Almeria," 2003.

[101] J. Kötter, "Heliotrough," Flagsol GmbH, 2013. [Online]. Available: http://www.heliotrough.com/legalinfo.html. [Accessed 11 August 2014].

[102] M. Günther , M. Joemann and S. Csambor, " Chapter 5 Parabolic Trough Technology," in *Advanced CSP Teaching Materials* , Kassel , 2012, p. 39.

[103] B. F, K. C and NREL, "Heat Loss Testing of Schott's 2008 PTR70 Parabolic Trough Receiver," National Renewable Energy Laboratory (NREL), Golden, 2009.

[104] B. F, K. C and NREL, "Heat-Loss Testing of Solel's UVAC3 Parabolic Trough Receiver," National Renewable Energy Laboratory (NREL), Golden, 2008.

[105] . H. Price, "A Parabolic Trough Solar Power Plant Simulation Model," in *International Solar Energy Conference*, Hawaii Island, 2003.

[106] G. J. Kolb, S. A. Jones, M. W. Donnelly, D. Gorman, R. Thomas, R. Davenport and R. Lumia, "Heliostat Cost Reduction Study," Sandia National Laboratories, Livermore, 2007.

[107] C. . K. Hon and B. D. Iverson, "Review of high-temperature central receiver designs for concentrating solar power," *Renewable and Sustainable Energy Reviews,* vol. 29, pp. 835-846, 2014.

[108] solarreserve, "SOLARRESERVE," 28 July 2014. [Online]. Available: http://www.solarreserve.com/newsroom/photo-video-library/. [Accessed 12 August 2014].

[109] R. OsunaGonzalez-Aguilar , *NREL CSP Technology Workshop : Panel 1 –Central Receivers PS 10 andPS 20 Power Towers in Seville, Spain,* 2007.

[110] National Renewable Energy Laboratory (NREL), "System Advisor Model (SAM) Case Study: Gemasolar," NREL, 2013.

[111] P. KIAMEH, POWER GENERATION HANDBOOK:SELECTION,APPLICATIONS,OPERATION AND MAINTENANCE, McGraw-Hill , 2004.

[112] J. D. Kramer and C. Jacky, "How to write biblos," vol. 1, no. 1, 2006.

[113] Myself, The best of the best, Home, 2005.

[114] Dummy, "www.dummy.ac.za," 1 2 2014. [Online].

[115] Intergovernmental Panel on Climate Change (IPCC), "Climate Change 2001: Mitigation - Contribution of Working Group III to the Third Assessment Report of the Intergovernmental Panel on Climate Change (IPCC)," Cambridge University Press, Cambridge, 2001.

[116] Y. Y. a. A. N. Eric Hu, "Solar Aided Power Generation: Generating "Green" Power from Conventional Fossil Fuelled Power Stations, Thermal Power Plants," in *Thermal Power Plants*, Shanghai, InTech, 2012, pp. 3-18.

[117] The Department of Minerals and Energy :Republic of South Africa, *Application Form for Subsidy Contract,* Pretoria.

[118] Eskom Holdings SOC Limited , "Eskom," Eskom, 2014. [Online]. Available: http://www.eskom.co.za/Whatweredoing/ElectricityGeneration/PowerStations/Pages/[redacted]_Power_Station.aspx. [Accessed 11 August 2014].

[119] Bloomberg NEW ENERGY FINANCE, *RESEARCH NOTE-CLEAN ENERGY , South Africa decides to give wind PV a tender embrace,* 2011.

[120] ABB, *Making solar energy affordable and reliable Turnkey solar power plants from ABB (Product brochure),* Zürich, 2012.

[121] AREVA SOLAR, *Solar Simplified (Product brochure),* CA , 2012.

[122] Electric Power Research Institute (EPRI), “Solar Thermal Electric Technology: 2006,” EPRI, CA, 2006.

[123] T. a. Q. A. Palm, Private and Public Investment Analysis, Cincinnati : South- Western Publishing Co. , 1985.

[124] W. Stine and M. Geyer, “POWER From The SUN.net,” 2014. [Online]. Available: http://www.powerfromthesun.net/Book/chapter08/chapter08.html. [Accessed 20 August 2014].

Appendix A. Mathematical derivation

A.1) Coal savings

The hourly coal savings, for a given generator output power, is calculated by subtracting the coal consumption of the solar-coal power plant from the coal consumption of the coal power plant. The result below follows from the above definition.

$$CS = C_c - C_{sc}$$

Where,

CS = Hourly coal savings, [tonnes / hour]
C_c = Coal consumption of the coal power plant, [tonnes / hour]
C_{sc} = Coal consumption of the solar - coal power plant, [tonnes / hour]

Coal consumption

By the definition of heat rate, which is the amount of energy required from coal per unit of electricity generated [20], the result below is established:

$$HR\,(\text{Heat rate}) = \frac{CE\ (\text{Coal energy})}{E\,(\text{Electricity generated})}$$

Where, CE & E are expressed in Mega Joule and MegaWatt-hour respectively.

Rearranging:

$$CE = HR \times E$$

Dividing this result by hours and expressing the coal energy flow as the net calorific value of coal multiplied by the coal consumption rate.

$$HR \times \dot{E} = \dot{C}E$$

$$HR \times \dot{E} = 1000 \times NCV \times C_c$$

Therefore:

$$C_c = \frac{HR \times \dot{E}}{1000 \times NCV}$$

The factor of 1000 is used to convert the coal consumption which is expressed in tons/hour, to kg/hr. Taking into account boiler efficiency:

$$C_c = \frac{HR \times \dot{E}}{1000 \times NCV \times \eta_b}$$

By applying the result for calculating coal consumption to the formula for calculating coal savings, equation (A1) is derived:

$$CS = \frac{\dot{E} \times \Delta HR}{1000 \times NCV \times \eta_b} \quad \text{(A1)}$$

Where,

CS = Hourly coal savings, [tonnes / hour]
$\dot{E}$ = Hourly electricity power output of a single unit, i.e. $\geq 600\ MW_e$
E = Hourly electricity production of a single unit, i.e. $\geq 600\ MWh_e$
ΔHR = Heat rate reduction of the Power Station, $[kJ / kWh]_e$
NCV = Net calorific value of coal, 22.35, [MJ / kg]
η_b = Coal boiler thermal efficiency, 95, [%]

A.2) Greenhouse gas emission reduction

The hourly greenhouse gas (GHG) emission reduction produced by an integration option, for a given generator output, is calculated by subtracting the hourly GHG production of the solar-coal power plant from the hourly GHG production of the coal power plant. The result below follows from the above statement:

$$ER = \dot{GHG}_c - \dot{GHG}_{sc}$$

Where,

ER = Hourly GHG emission reduction, $[tCO_{2eq}$ / hour]
$\dot{GHG}_c$ = Hourly GHG production of the coal power plant, $[tCO_{2eq}$ / hour]
$\dot{GHG}_{sc}$ = Hourly GHG production of the solar - coal power plant, $[tCO_{2eq}$ / hour]

GHG production

An emission factor expresses the amount of a particular GHG that is emitted per the energy content of coal i.e. emission factors have the units kg/GJ [93].Thus, the amount of a particular GHG emitted from a given amount of coal energy can be calculated as:

$$GHG = \varepsilon \times CE$$

Where

$$\begin{aligned} GHG &= \text{Greenhouse gas emitted, [tonnes]} \\ \varepsilon &= \text{GHG emission factor, [kg / GJ]} \\ CE &= \text{Coal energy, [MJ]} \end{aligned}$$

Dividing this result by hours and expressing the coal energy flow as the net calorific value of coal multiplied by the coal consumption rate, an expression is derived to calculate the hourly production of a particular GHG.

$$\dot{GHG} = \varepsilon \times \dot{CE}$$

$$\dot{GHG} = \frac{\varepsilon \times NCV \times C_c}{1000}$$

Carbon dioxide equivalence of GHG's

The CO_2 equivalence of a GHG gas is estimated by multiplying the quantity of the GHG gas by its Global Warming Potential (GWP) [93]. The GWP of a GHG is a measure of the total energy that the GHG absorbs, over 100 years, relative to CO_2 [93]. By applying the result of hourly GHG production to the formula to calculate GHG emission reduction, hourly GHG emission reduction can be expressed as equation (A2), i.e. carbon dioxide, methane and nitrous oxide are the GHGs examined in this study.

$$ER = \frac{(\varepsilon_{CO_2} + \varepsilon_{CH_4} \times GWP_{CH_4} + \varepsilon_{N_2O} \times GWP_{N_2O}) \times NCV \times CS}{1000} \qquad (A2)$$

Where,

$$\begin{aligned} ER &= \text{Hourly GHG emission reduction, [t}CO_{2eq}\text{ / hour]} \\ \varepsilon_{CO_2} &= \text{Carbon dioxide emission factor, 96.25, [kg / GJ]} \\ \varepsilon_{CH_4} &= \text{Methane emission factor, 0.001, [kg / GJ]} \\ GWP_{CH_4} &= \text{Global Warming Potential of } CH_4\text{, 25} \\ \varepsilon_{N_2O} &= \text{Nitrous oxide emission factor, 0.0014, [kg / GJ]} \\ GWP_{N_2O} &= \text{Global Warming Potential of } N_2O\text{, 298} \\ NCV &= \text{Net calorific value of coal, 22.35, [MJ / kg]} \\ CS &= \text{Hourly coal savings, [tonnes / hour]} \end{aligned}$$

A.3) Solar electricity production

The hourly solar electricity production of the solar field is defined as the amount of electricity that would be produced by the coal-power plant by combusting the hourly saved coal. By applying the definition of heat rate the following result is obtained:

$$\mathrm{HR\,(Heat\ rate)} = \frac{\mathrm{CE\ (Coal\ energy)}}{\mathrm{E\,(Electricity\ generated)}}$$

Thus,

$$\frac{HR_{ref}}{\eta_b} = \frac{\text{Saved coal energy}}{\text{Solar electricity}}$$

By rearranging the above expression, a formula is derived to calculate the hourly solar electricity production i.e. equation (A3)

$$E_s = \frac{CS \times NCV \times \eta_b}{HR_{ref}} \qquad \text{(A3)}$$

Where,

E_s = Hourly electricity production of the solar field, $[GWh_e]$
HR_{ref} = Reference heat rate of the coal power plant, $[kJ / kWh_e]$
CS = Hourly coal savings, [tonnes / hour]
NCV = Net calorific value of coal, 22.35, [MJ / kg]
η_b = Coal boiler thermal efficiency, 95, [%]

A.4) Carbon tax savings

Carbon tax is calculated by applying a rate (R/tCO_{2eq}) to the annual GHG emissions of the power station. An allowance in terms of a tax-free threshold (%) is granted to reduce the annual carbon tax. Carbon tax savings is the difference in the payable carbon taxes of the coal power plant and the solar-coal power plant. Carbon tax savings is thus calculated as follows:

$$CT_{saved} = CT_c - CT_{sc}$$

Where,

CT_c = Annual carbon taxes of the coal power plant, [Rm]

CT_{sc} = Annual carbon taxes of the solar - coal power plant, [Rm]

Carbon tax is calculated, as explained in the Carbon Tax Policy Paper [7] as:

$$CT = \left[G \times \left(1 - \frac{60}{100} \times \left(\frac{BI}{AI} \right) \right) \right] \times \frac{CT_R}{10^6}$$

By applying the above formula to the definition of carbon tax savings, we arrive at equation (A4):

$$CT_{saved} = \left[G_c \times \left(1 - \frac{60}{100} \times \left(\frac{BI}{AI} \right)_c \right) - G_{sc} \times \left(1 - \frac{60}{100} \times \left(\frac{BI}{AI} \right)_{sc} \right) \right] \times \frac{CT_R}{10^6} \quad \text{(A4)}$$

Where,

CT_{saved} = Annual carbon tax savings, [Rm]

G_c = Annual GHG emissions of the coal power plant, [tCO_{2eq} /year]

G_{sc} = Annual GHG emissions of the solar - coal power plant , [tCO_{2eq} /year]

AI = Power plant actual carbon intensity, [tCO_{2eq} /MWh_e]

BI = Power plant benchmark carbon intensity, [tCO_{2eq} /MWh_e]

CT_R = Carbon tax rate, [R / tCO_{2eq}]

A.5) Net present value (NPV)

Net present value (NPV): The NPV of the project is the difference between the present value of cash inflows and the present value of cash outflows (costs), during the life of the project [76]. The formula for calculating NPV is as follows [56]:

$$NPV = \sum_{n=0}^{N} \frac{F_n}{(1 + d_r)^n}$$

Where,

NPV = Net present value, [Rm]

F_n = Net cash flow in year n, [Rm]

N = Analysis period, [years]

d_r = Annual real discount rate, [%]

The net cash flow in year n can be expressed as:

$$F_n = \text{cash inflows - cash outflows}$$

$$F_n = (R_g + CT_{saved} + CS_A) - (T_A + L_r + O\&M_F + O\&M_V)$$

Where,

R_g = Annual gross revenue, [Rm]
CT_{saved} = Annual carbon tax savings, [Rm]
CS_A = Annual coal savings, [Rm]
T_A = Annual income tax, [Rm]
L_r = Annual loan repayment, [Rm]
$O\&M_F$ = Annual fixed OPEX cost, [Rm]
$O\&M_V$ = Annual variable OPEX cost, [Rm]

Hence, by applying the result of F_n to the formula for NPV, we arrive at equation (A5):

$$NPV = \sum_{n=0}^{n=30} \frac{(R_g + CT_{saved} + CS_A) - (T_A + L_r + O\&M_F + O\&M_V)_n}{(1 + d_r)^n} \quad \text{(A5)}$$

A.6) Total Life-Cycle cost (TLCC)

Total life-cycle cost (TLCC): The TLCC of the project is the sum of all costs during the life of the project. These costs are then discounted to the 1st year of the project. TLCC is calculated by using the following formula. [56]

$$TLCC = \sum_{n=0}^{N} \frac{C_n}{(1 + d_r)^n}$$

Where,

TLCC = Present value of the TLCC, [Rm]
C_n = Cost in period n, [Rm]
N = Analysis period, [years]
d_r = Annual real discount rate, [%]

The cost in period n of the project can be expressed as:

$$C_n = (T_A + L_r + O\&M_F + O\&M_V)$$

Where,

T_A = Annual income tax, [Rm]
L_r = Annual loan repayment, [Rm]
$O\&M_F$ = Annual fixed OPEX cost, [Rm]
$O\&M_V$ = Annual variable OPEX cost, [Rm]

Hence, by applying the result for C_n to the formula for TLCC, we arrive at equation (A6):

$$TLCC = \sum_{n=0}^{n=30} \frac{(T_A + L_r + O\&M_F + O\&M_V)_n}{(1 + d_r)^n} \quad (A6)$$

A.7) Income tax

Income tax, as demonstrated in the NREL economic handbook [56] is calculated as follows:

$$T_A = T_r \times TI$$

Where,

T_A = Income tax, [Rm]
T_r = Income tax rate, [%]
TI = Taxable income, [Rm]

Taxable income is the revenues less project costs, less depreciation, less loan interest payment [56] i.e.:

$$TI = (R_g + CT_{saved} + CS_A) - (D_A + L_i + O\&M_F + O\&M_V)$$

Where,

R_g = Annual gross revenue, [Rm]
CT_{saved} = Annual carbon tax savings, [Rm]
CS_A = Annual coal savings, [Rm]
D_A = Annual depreciation allowance, [Rm]
L_i = Annual loan interest repayment, [Rm]
$O\&M_F$ = Annual fixed OPEX cost, [Rm]
$O\&M_V$ = Annual variable OPEX cost, [Rm]

Hence, by applying the result of taxable income to the formula for calculating income tax, we arrive at equation (A7):

$$T_A = T_r \times (R_g + CT_{saved} + CS_A - D_A - L_i - O\&M_F - O\&M_V) \quad (A7)$$

Appendix B. Power plant technical data

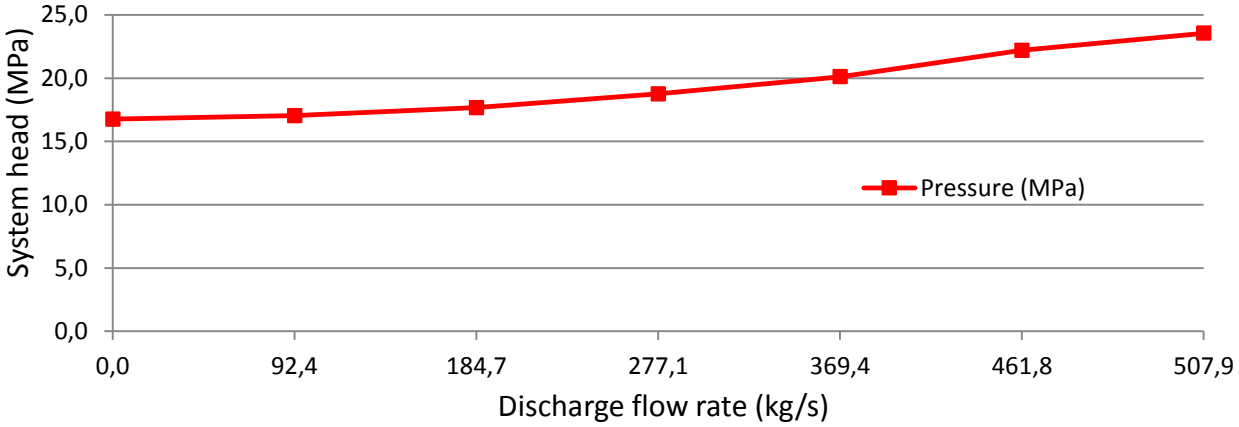

Figure 50: System resistance curve versus flow rate [94].

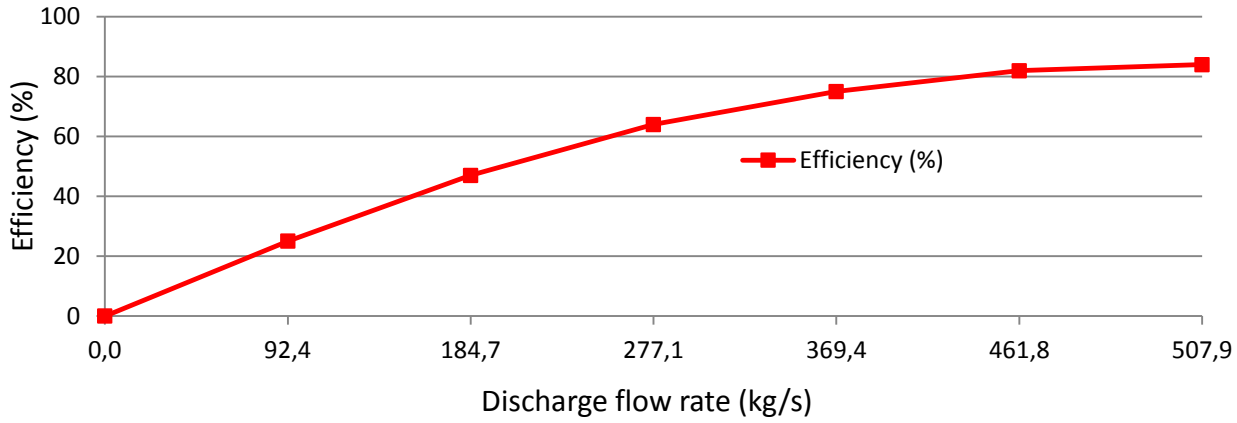

Figure 51: Boiler feedwater pump efficiency versus flow rate [94].

Appendix C. Validation results

Table 38: Turbine power and Boiler heat load

Load (%)	HP Turbine (MW_e)		IP Turbine (MW_e)		LP Turbine (MW_e)		Total turbine power (MW_e)		Error (%)	Boiler Load (MW_t)	
	HBD	VP	HBD	VP	HBD	VP	HBD	VP		HBD	VP
110	154.9	155.3	273.9	272.2	250.3	251.3	679.1	678.9	-2.E-4	1592.5	1596.1
105	161.0	161.8	257.4	256.4	226.1	227.2	644.5	645.4	1.E-3	1484.7	1485.9
100	169.9	168.8	240.8	240.5	202.3	203.2	613.0	612.6	-6.E-4	1378.5	1376.7
80	135.5	134.3	192.5	192.5	162.5	161.9	490.5	488.7	-3.E-3	1113.3	1109.4
Average error									-7.E-4		

Table 39: Generator output

Load (%)	Generator output (MW_e)	
	HBD	**VP**
110	665.2	665.1
105	631.1	631.9
100	600.0	599.6
80	479.1	477.4

Table 40: Condenser pressures

Load (%)	Cold condenser pressure (kPa)		Hot condenser pressure (kPa)	
	HBD	**VP**	**HBD**	**VP**
110	6.60	6.21	10.00	9.97
105	6.27	5.83	9.78	8.92
100	5.81	5.45	8.76	8.45
80	5.00	4.73	7.00	6.60

Table 41: Gross unit heat rate

Load (%)	Gross unit heat rate (kJ/kWh_e)		Error (%)
	HBD	**VP**	
110	8618,4	8640,1	0,25
105	8469,6	8464,2	-0,06
100	8270,7	8265,4	-0,06
80	8365,4	8366,1	0,01
Average error			0.03

Appendix D. Project costs

D.1) Steam generation system cost

The 'Balance of Plant' category in SAM's cost page refers to the cost of the steam generator [95]. The 'Balance of Plant' reference cost from SAM (which is provided as $/kW$_e$), is converted to $/kW$_t$ by using the power cycle efficiency of the PTC or ST stand-alone solar plant (the LFR plant does not require a steam generator).The change of the units of the 'Balance of Plant' reference cost was done because, the size of the solar field (MW$_t$) should reflect the cost of the steam generator i.e. the Integration effectiveness differs between integration options. The 'Balance of Plant' costs for the PTC or ST technology are presented in Table 42.

Table 42: Steam generation system costs

Solar technology	**'Balance of Plant' cost ($/kW$_e$)**	**Power cycle efficiency (%)**	**'Balance of Plant' cost ($/kW$_t$)**
PTC	110	37.74	41.15
ST	350	41.2	144.2

D.2) Land costs

The reference land cost for the CAPEX reference plant, was estimated by noting the cost of vacant land (farms) near the power station, and thereafter calculating the average land cost in R/m^2. The land costs were retrieved from [96].

Table 43: Typical land costs near the power station [96].

Farm location (Mpumalanga)	**Area (km^2)**	**Selling price (Rm)**	**R/m^2**
Blancheville	0.04	1.95	48.8
Naauport	0.0232	1.75	75.4
Naauport	0.11	6.5	59.1
Naauport	0.28	21.4	76.4
Average			65

D.2) OPEX costs

The fixed and variable reference OPEX costs in SAM's cost page (which are provided as $/kW$_e$ and $/MWh$_e$) are converted to $/kW$_t$ and $/MWh$_t$ respectively, by using the power cycle efficiency of the PTC, ST or LFR stand-alone solar plant. The units of the OPEX reference costs was changed because, the size of the solar field (MW$_t$) and the heat production of the solar field should reflect the OPEX costs i.e. the Integration effectiveness differs between integration options. The fixed and variable OPEX costs for the ST, PTC and LFR technology are presented in Table 44.

Table 44: Fixed and variable OPEX costs

Solar technology	Power cycle efficiency (%)	Fixed OPEX ($/kW$_e$)	Variable OPEX ($/MWh$_e$)	Fixed OPEX ($/kW$_t$)	Variable OPEX ($/MWh$_t$)
PTC	37.74	65	4	24.53	1.51
ST	41.2	65	4	26.8	1.65
LFR	38	55	4	20.9	1.52

Appendix E. CSP technologies

E.1) The Parabolic Trough Collector

The field of parabolic trough collectors are modelled by using the *empirical trough* model in SAM. The *empirical trough* model uses a set of equations which are derived from measured operational data of the SEGS (Solar Energy Generating Systems) plants [71], which is one of the largest solar energy installations in the world [97]. The *empirical trough* model in SAM requires the following inputs:

a) Solar collector assembly (SCA) geometry:

The EuroTrough ET150 is used in this study. It has a length of 150 m and a reflective surface area of 817.5 m^2 [98]. The EuroTrough ET150 collector was selected for this study because its size is typical of PTCs that are used for commercial scale applications. For example, the SEGS IX plant in the United States of America, which is an 80 MW_e installation, uses the LS3 collector [99]. The EuroTrough ET150 SCA is compared to other commercial SCAs in Table 45. The EuroTrough ET150 is also available in the SAM SCA library. An illustration of the EuroTrough ET150 is presented in Figure 52.

Figure 52: The ET150 collector in operation at the Plataforma Solar de Almeria. [100]

Table 45: Commercial PTC assemblies. [98] [99] [101] [102]

SCA type	Aperture width (m)	Length (m)
HelioTrough	6.78	191
LS3	5.7	99
EuroTrough ET150	5.77	150

b) Reference weather conditions and a weather file:

A weather file which contains annual hourly weather data of the location of the power station, is used by the *empirical trough* model in SAM model. The weather file was obtained from Meteonorm, which is a meteorological database. The reference weather conditions which were obtained from the weather file, are summarized in Table 46. The reference weather conditions are used together with the 'design point solar heat' to size the PTC solar field, of the integration option.

Table 46: Reference weather conditions (annual average)

Weather condition	**Unit**	**Value**
Daily peak DNI	W/m^2	651
Wind speed	m/s	3.1
Dry-bulb air temperature	^oC	15.9

c) Heat collection element (HCE) type

The two best performing HCEs with regard to heat loss, which are available in SAM, are the Schott and Solel HCEs. The Schott PTR70 HCE is selected for this study, because it has a lower heat loss value than the Solel UVAC3 HCE. At an average absorber tube temperature of 400 ^oC (oil operating temperature used in this study is 390 ^oC) the Schott PTR70 HCE loses 222.2 W/m [103] in comparison to the Solel UVAC3 HCE which loses 318.7 W/m [104].

d) Design cycle thermal input

The design cycle thermal input is entered as the amount of solar heat required by the integration option at the design point. This corresponds to the 'design point solar heat' of an integration option, as explained in section 3.8.

Model outputs

The *empirical trough* model in SAM calculates the required reflective area of the solar field and the total land area required by the solar field, by using the reference weather conditions and the design cycle thermal input. The model thereafter performs a calculation for each of the 8760 hours of the year, to determine the heat output of the solar field for each hour of the year.

Model verification

The NREL trough model was validated against 1999 performance data of the SEGS VI plant [105].

E.2) The Central Receiver

The *molten salt power tower* model in SAM is used to model the performance of the Central receiver system. The following inputs are required for the *molten salt power tower* model:

a) Heliostat geometry:

A heliostat geometry was selected which has an area of 140 m^2 and a mirror reflectance of 90 % (including soiling effects).A large area heliostat was selected as these heliostats lower life-cycle costs [106]. This heliostat size is typical of heliostats that are used in commercial scale CR power plants, as presented in Table 47.

Table 47: Heliostat sizes used in commercial central receiver power plants. [55]

Project name (Country)	**Construction year**	**Capacity (MW_e)**	**Heliostat manufacturer (Area, m^2)**
Gemasolar (Spain)	2009	19.9	Sener (120)
PS20 (Spain)	2006	20	Abengoa (120)
Khi Solar one (South Africa)	2012	50	Abengoa (140)
Planta Solar (Chile)	2014	110	Abengoa (140)

b) Receiver type:

Two types of receivers are available in SAM i.e. a cavity tube receiver and an external receiver, which are illustrated in Figure 53.A cavity tube receiver was selected for this study rather than an external tube receiver, because of the following reasons. A cavity receiver requires a field span angle of less than 180^o, and the external receiver requires a field span angle of 360^o [71], this is illustrated in Figure 54 .A solar field with a span angle less than 180^o would be more easily accommodated by the available land plot for the solar field at the power station, see Figure 35. A taller tower will be required for the cavity receiver; however the cavity receiver has a lower radiation and reflection heat loss than the external receiver [88]. The aperture of the cavity receiver as illustrated in Figure 53, is assumed by SAM, to face south which is typical of heliostat fields located in the southern hemisphere [71].

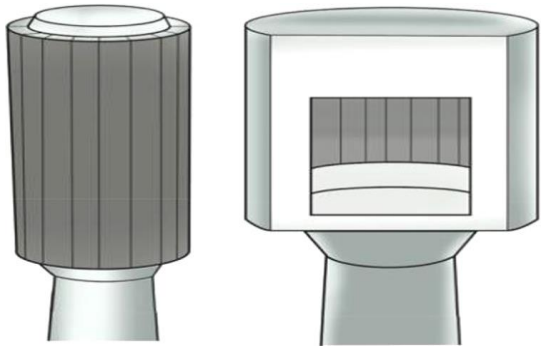

Figure 53: An external receiver (left) and a cavity receiver. [107]

Figure 54: The 110 MW_e Cresent Dunes Solar energy project with an external receiver [108] (left), and the 11 MW_e PS10 Power tower with a cavity receiver [109].

c) Reference weather conditions and a weather file:

The reference weather conditions and weather file that are used for the *empirical trough* model, are also used for the *molten salt power tower* model.

d) Design thermal power :

The design thermal power is specified as the amount of heat required by the solar heat integration option at the design point. This corresponds to the 'design point solar heat' of an integration option, as explained in section 3.8.

Model outputs

The *molten salt power tower* model calculates the required number of heliostats, the heliostat field layout and the land area, by the use of an optimisation tool. The model thereafter performs a calculation for each of the 8760 hours of the year to determine the receiver thermal power output for each hour of the year.

Model verification

The *molten salt power tower* model was validated against performance data of the Gemasolar power tower plant [110].

E.3) The Linear Fresnel Reflector

The *linear Fresnel* model in SAM is used to model the performance of the linear Fresnel reflector (LFR) field. The Novatec LFR assembly is used in this study because a 'Linear Fresnel Novatec Solar Boiler' sample file, which uses Novatec's guaranteed Key Performance Indicators, is available in SAM. The following inputs are required by the *Linear Fresnel* model:

a) Collector geometry:

The Novatec LFR assembly has a length of 44.8 m and a reflective aperture area of 513.6 m^2.

b) Loop flow configuration:

There are two types of loop flow configuration that are applicable to the linear Fresnel solar boiler in SAM i.e. the recirculated boiler and the once-through boiler which are illustrated in Figure 55.

The recirculated boiler operates by separating the liquid and vapour phase of water from the boiler outlet, then recirculating the saturated liquid portion to the boiler inlet, and superheating the saturated vapour portion. The once-through design heats the boiler inlet water flow to a superheated state without any recirculation. The once-through boiler design has advantages over the recirculated boiler design, such as it eliminates the need for a recirculation loop and a water/steam separator. The outlet steam temperature from the once-through design is also more controlled than the outlet steam temperature from the recirculation design. However, the recirculation design will only be considered in this study because the once-through design has not yet been commercially demonstrated. [42]

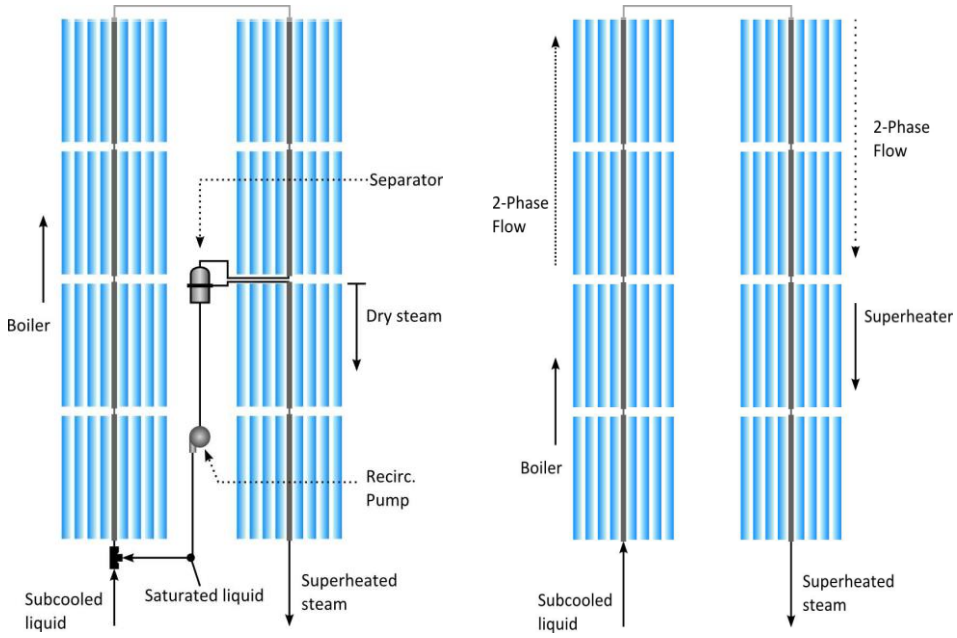

Figure 55: The recirculated linear Fresnel boiler (left) and the once-through linear Fresnel boiler. [42]

c) Reference weather conditions and weather file:

The reference weather conditions and the weather file that are used for the *empirical trough* model, are also used for the *Linear Fresnel* model.

d) Design thermal input power:

The design thermal input power is specified as the amount of heat required by the solar heat integration option at the design point. This corresponds to the 'design point solar heat' of an integration option, as explained in section 3.8.

e) Solar field inlet and outlet temperature and pressure:

The required solar field inlet and outlet temperature and pressure are dependent on the integration option. These parameters are obtained from Table 6 and Table 7, for the feedwater heating and superheated steam supply integration options respectively.

Model outputs

The *Linear Fresnel* model calculates the required reflective area and the total land area of the solar field. The model thereafter performs a calculation for each of the 8760 hours of the year to determine the heat output of the solar field for each hour of the year.

Model verification

The technical review and validation of the *Linear Fresnel* model was performed by Novatec Solar of Germany [86].

Appendix F. Land assessment

As illustrated in Figure 35, the power station is surrounded by an ash dam, a coal stockpile, a waste water dam, a raw (untreated) water reservoir, a high-voltage yard, a farm and three vacant land areas. The selection process of a suitable land area(s) for the solar field took into consideration the following aspects of the land areas: Environmental conditions

- The distance from the power station
- Accessibility

The land assessment revealed that:

a) The land areas near the ash dam will experience a higher level of ash dust. The dust particles from the ash dam will soil the reflective mirror surfaces of the solar collectors more frequently (hence reducing plant performance), and resulting in higher operation and maintenance costs through increased mirror washing. Thus, site 1 is better suited for the installation of the solar field because it is not located in the close vicinity of the ash dam.

b) Site 3 has drainage systems for storm water (V-ditches etc.) which will be required to be rerouted (an additional expense and complication).

c) The topography of all three vacant land areas are fairly flat, and will require moderate site preparations.

d) Site 1 is located adjacent to the access road to the power station and is thus the most easily accessible land area.

e) Site 1 and site 3 are the closest land areas to the power station, and would thus require the least amount of solar field header piping, although overhead piping for the access road will be required for site 1.

Based on the results from the land assessment, site 1 is thus selected as the land area for the solar field, because it has the cleanest environmental conditions, is located the closest to the power station and is easily accessible via road. The available land area of site 1, was estimated by using Google Earth, is approximately 2.85 km^2.

The Units 1, 2 and 3 of the power station are located closest to site 1, and will thus be investigated for the addition of solar heat. The Units 1, 2 and 3 have a smaller cooling water system than Units 4, 5 and 6 of the power station, this is accounted for in the VirtualPlant^{TM} model.

Appendix G. Process flow changes

G.1) HP feedwater heater 5: Fuel-saving mode

During the Fuel-saving mode the boiler superheater outlet flow is lower than full load conditions. The HP turbine exhaust flow is thus also reduced (i.e. there are no steam extractions on HP cylinder). The reheater mass flow rate and pressure are consequently also reduced.

The reheater spraywater flow rate reduces by 0.9-1 kg/s, because of the reduction in boiler load. The HP and IP turbine power output are both reduced due to the reduction in the superheater and reheater flow rates respectively. The HPH5 extraction steam (the 1st steam extraction point on the IP cylinder) is reduced because of the solar heat addition to HPH5.The effect of saving bled steam does increase the IP turbine power; however, the effect of a reduced IP turbine inlet mass flow rate and pressure creates a larger reduction in IP turbine power.

The saved IP turbine extraction steam increases the IP turbine exhaust flow rate and pressure. The LP turbine power output increases due to the higher steam inlet flow rate and pressure, whilst all of the LP turbine steam extraction flows are relatively unchanged. The LP turbine efficiency increases by 1% due to the higher inlet pressure and reduced exhaust loss. The increased steam flow rate to the main condenser increases the condenser pressures. The condenser pressures increase because the cooling water flow to the condenser is constant whilst the heat load of the condenser increases.

The HPH5 feedwater heating solar heat integration option utilises either the PTC, for methods 1 & 2, or the LFR technology for method 2. Method 1 and method 2 require (99.8 MW_t and 85.5 MW_t) of solar heat to be delivered to the power plant respectively. It was noted that method 2 and method 1 both have the same integration effectiveness of 3.18 $kJ/kWh_e.MW_t$.

The difference noted between the two methods is as follows:

1. Method 2 requires the BFP to discharge an additional 33 kg/s of feedwater, which increases the power consumption of the BFP by approximately 1.2 MW_e.
2. Method 2 increases the IP turbine's 1st bled steam extraction flow rate by 1.6 kg/s more than method 1, to account for the power increase of the BFPT.
3. Method 1 requires 5.4 kg/s less bled steam to the deaerator, because the deaerator receives a higher enthalpy drain from HPH5 (894 kJ/kg) in comparison to method 2 (610 kJ/kg).
4. Method 2 requires 0.1 kg/s more of reheater spray water than method 1.

Although method 2 has the above mentioned disadvantages over method 1, its integration effectiveness is improved, equal to that of method 1, because the heating of feedwater in HPH5 is

assisted by the cascaded drains from HPH6. Plant thermal efficiency is improved by cascaded feedwater heater drains [111].

G.2) HP feedwater heater 5: Power-boosting mode

During the Power-boosting mode the boiler superheater outlet steam flow rate is maintained at full load i.e. 491.2 kg/s. The boiler reheater flows and pressure increase slightly, thus the HP turbine power output is reduced by 0.8-1.1 MW_e. The IP turbine power output increases by 0.9- 2.6 MW_e because of the reduction in the 1st steam extraction point flow rate. The saved extraction steam also increases the IP turbine exhaust flow and pressure. The reheater spraywater flow rate has negligible change because the boiler load is essentially constant.

The LP turbine power output is effected the most and increases by 19.4-24.2 MW_e, due to the higher mass flow rate and pressure from the IP turbine exhaust. The reduced exhaust loss[35] and the higher LP turbine inlet mass flow rate and pressure increase the LP turbine efficiency by 1 %. The main steam condenser pressures are increased by 0.7-0.9 kPa_a because of the higher LP turbine exhaust flow rates.

The HPH5 feedwater heating solar heat integration option utilises either the PTC, for methods 1 & 2, or the LFR technology for method 2. Method 1 and method 2 require (99.8 MW_t and 85.5 MW_t) of solar heat to be delivered to the power plant respectively. It was noted from the VirtualPlant^{TM} simulation that method 1 produces 3.2 MW_e more than method 2. The difference in the generator output is explained as follows:

1. The BFP in method 2 requires 1.1 MW_e more than in method 1, to supply 33 kg/s of feedwater to the solar field. Hence the BFPT consumes 1.5 kg/s more bled steam.
2. The Deaerator in method 2 consumes 5.7 kg/s more bled steam than in method 1, this is because of the lower drain inlet enthalpy in method 2 (615 kJ/kg) in comparison to method 1 which has a drain enthalpy of (900 kJ/kg).

[35] The efficiency of the LP turbine is primarily a function of the annulus velocity of the last stage [80]. An increase in the LP turbine exhaust flow produces a larger annulus velocity. The increase in the annulus velocity, in this case, reduces exhaust loss.

G.3) HP turbine steam supply: Fuel-saving mode

During the fuel-saving mode the boiler superheater outlet flow rate is reduced because some feedwater flow from the BFP discharge is heated by the solar boiler, in parallel with the coal boiler. The HP turbine inlet flow rate is thus unchanged. The reheater spraywater flow rate reduces by 1.3 kg/s because of the reduction in boiler load.

The reheater inlet and outlet flow rates are increased slightly because of the lower HPH 6 steam extraction flow rates. The HPH6 steam extraction flow rates are reduced by the lower feedwater flow rate to the boiler. The HPH5 steam extraction flow rates are also slightly reduced for the same reason. The HP turbine power is thus reduced by 1.8 MW_e.

The IP and LP turbines power outputs are increased by 0.5 MW_e and 1.3 MW_e respectively, due to the higher reheater outlet pressure and flow rate. The LP turbine exhaust flow rate is unchanged; hence the main condenser pressures are unchanged. The BFP power is reduced by 0.1 MW_e because the BFP discharge flow rate is reduced by 2.3 kg/s. The BFPT bled steam consumption is thus reduced by 0.2 kg/s, which assists in increasing the IP turbine power.

G.4) HP turbine steam supply: Power-boosting mode

During the power-boosting mode the boiler superheater outlet flow rate is unchanged at 491.2 kg/s but the HP turbine inlet flow rate increases by 20.2 kg/s. The additional 20.2 kg/s of steam, supplied by the solar boiler, drives the HP turbine to operate at maximum capacity i.e. 175 MW_e. The reheater spraywater flow rate has negligible change because the boiler load is essentially constant.

The higher HP turbine exhaust flow increases the reheater pressure by 0.19 MPa. The power output of the IP turbine and the LP turbine increases by 10.7 MW_e and 9.8 MW_e respectively, due to the additional steam flow rate. The steam flow rate to the main condenser increases slightly, producing a small change in condenser pressure. The BFP power requirement increases by 0.65 MW_e, to pump the additional 20.2 kg/s of feedwater flow. The BFPT consumes 0.8 kg/s more bled steam to provide the increase in the BFP power.

G.5) IP turbine steam supply: Fuel-saving mode

During the fuel-saving mode the boiler superheater outlet steam flow rate is reduced by 19.3 kg/s, which consequentially reduces the HP turbine power output and efficiency. The HP turbine efficiency is reduced by 2.3 % because of the increase in the throttling losses across the governing control valves.

A reduced superheater outlet steam flow rate also reduces the reheater steam flow rates (the HPH 6 extraction steam flow rates are slightly reduced). The reheater spray water flow rate decreases by 1.3 kg/s, because of the reduction in boiler load. Although the reheater flow rate is reduced, the reheater inlet pressure increases by 0.12 MPa because the 32 kg/s of steam that is supplied to the IP turbine inlet (by the solar boiler) has an effect on the upstream reheater pressure. The increased reheater pressure, along with a reduced HP turbine inlet mass flow rate, reduces the HP turbine power output by 14 MW_e. A higher exhaust pressure reduces the pressure difference across the HP cylinder, thus the available energy across the turbine is reduced.

The additional reheater steam flow and higher reheater outlet pressure increases the IP turbine and the LP turbine power output by approximately 7 MW_e each. The steam flow rate to the main condenser increases, producing a rise in condenser pressures. The BFP power requirement increases by 0.4 MW_e, to pump the additional 12.7 kg/s of feedwater flow. The BFPT steam consumption increases by 0.5 kg/s to provide the increase in BFP power.

G.6) IP turbine steam supply: Power-boosting mode

During the Power-boosting mode the boiler superheater outlet steam flow rate is maintained at 491.2 kg/s, however the HP turbine power output is reduced by 7.6 MW_e. This is because the 31.9 kg/s solar steam that is supplied to the IP turbine inlet increases the reheater upstream pressure by 0.25 MPa i.e. the HP turbine exhaust pressure. The reheater spraywater flow rate has negligible change because the boiler load is essentially constant.

The higher IP turbine inlet steam mass flow rate and pressure increases the IP turbine and the LP turbine power outputs by 16.1 MW_e and 14.6 MW_e respectively. The steam flow rate to the main condenser increases, producing a moderate rise in condenser pressures. The BFP power requirement increases by 1.1 MW_e, to pump the additional 31.9 kg/s of feedwater flow. The BFPT steam consumption increases by 1.2 kg/s to provide the increase in the BFP power.